AD659146

RESEARCH and

TECHNOLOGY

DEVELOPMENT

INCORPORATED

LIFE SCIENCES DIVISION

RESEARCH ON OCULAR EFFECTS PRODUCED BY THERMAL RADIATION

RALPH G. ALLEN, JR.
WILLIAM R. BRUCE
KENNETH R. KAY
LARRY K. MORRISON
ROBERT A. NEISH
CHARLES A. POLASKI
RANSOM A. RICHARDS

JULY 1967

TECHNOLOGY INCORPORATED, Final Report
Contract AF41(609)-3099, prepared for:
USAF School of Aerospace Medicine
Aerospace Medical Division (AFSC)
Brooks Air Force Base, Texas

for public release and sale; its distribution is unlimited.

Reproduced by the
CLEARINGHOUSE
for Federal Scientific & Technical
Information Springfield Va 22151

8531 N. NEW BRAUNFELS AVE. • SAN ANTONIO, TEXAS 78217

Best
Available
Copy

RESEARCH ON OCULAR EFFECTS PRODUCED BY THERMAL RADIATION

RALPH G. ALLEN, JR.

WILLIAM R. BRUCE

KENNETH R. KAY

LARRY K. MORRISON

ROBERT A. NEISH

CHARLES A. POLASKI

RANSOM A. RICHARDS

JULY 1967

TECHNOLOGY INCORPORATED, Final Report
Contract AF41(609)-3099, prepared for:
USAF School of Aerospace Medicine
Aerospace Medical Division (AFSC)
Brooks Air Force Base, Texas

FOREWORD

This report was prepared by the Life Sciences Division of Technology Incorporated for the USAF School of Aerospace Medicine under Contract AF41(609)-3099 and covers the period from 1 July 1966 to 30 June 1967. Research was performed under Project 6301, Task 630103, Work Unit 6301 03 023 and was partially funded by the Defense Atomic Support Agency under Program Element 6.16.46.01.D, Project 5710, Subtask 03.003. Mr. Everett O. Richey Ophthalmology Branch, USAF School of Aerospace Medicine was the Contract Monitor and Dr. Ralph G. Allen, Jr., was the principal investigator.

Grateful acknowledgement is hereby made of the assistance provided by the following personnel of the School of Aerospace Medicine: Mr. Everett O. Richey, Lt. Col. Thomas J. Tredici, Lt. Col. Albert V. Adler, Major Donald J. Pitts and Capt. William A. Newsom of the Ophthalmology Branch, and Lt. Col. Dale D. Boyd of the Veterinary Sciences Division. Acknowledgement is also made of the assistance of Mrs. Norma D. Miller, of the Life Sciences Division of Technology Incorporated, who assisted in the writing and editing of this report.

A portion of the work described in this report covers the study of chorioretinal burns in rabbits and is a continuation of earlier work (1, 2) carried out by the Life Sciences Division of Technology Incorporated.

Additional threshold burn studies are reported on primate eyes using the Zeiss coagulator, and a pilot study of fluorescence angiography for the sensitive detection of minimal retinal damage from thermal irradiation is described.

The primary efforts and results obtained during the contract period are documented in detail in the series of five reports as listed below:

PART I

A study of the production of chorioretinal lesions in rabbits by thermal radiation.

PART II

A preliminary study of the production of chorioretinal lesions by thermal radiation in the rhesus monkey.

PART III

Fluorescence angiography of chorioretinal lesions produced by thermal radiation.

PART IV

Development of a ruby laser system for the production of chorioretinal burns.

PART V

Construction of a flashblindness testing apparatus.

Research performed as reported was conducted according to the

Principles of Laboratory Animal Care as promulgated by the National Society for Medical Research.

Publication of this report does not constitute Air Force approval of the report's findings or conclusions. It is published only for the exchange and stimulation of ideas.

ABSTRACT

Chorioretinal burn thresholds for rabbits have been determined for 66 various combinations of exposure durations and retinal image diameters. The criterion for burn damage was the appearance of an ophthalmoscopically visible lesion 5 minutes after the flash exposure. Exposure durations ranged from 165 μsec to 100 sec and the range of image diameters was from 0.053 mm to 1.08 mm. The thresholds were based on an average of 9 eyes per condition.

The same Zeiss photocoagulator that was used in the rabbit burn study was used for determining burn thresholds for rhesus monkeys. Exposure durations from 4 to 250 msec and image diameters from 0.11 to 1.30 mm were employed for the threshold determinations. Fluorescein angiographs were investigated as a means for the detection of chorioretinal damage below the level of the ophthalmoscopically visible lesion. In an area of moderate damage there is rapid fluorescence which was interpreted to be the result of an increase in capillary permeability.

Two new pieces of apparatus were constructed for research on the ocular effects from high intensity visible radiation. A ruby laser was adapted for further studies on chorioretinal burns in rabbits and primates. And a flashblindness testing apparatus for measuring visual recovery times for human subjects has been constructed and tested.

TABLE OF CONTENTS

TABLE OF CONTENTS (continued)

TABLE OF CONTENTS (continued)

LIST OF ILLUSTRATIONS

LIST OF ILLUSTRATIONS (continued)

LIST OF ILLUSTRATIONS (continued)

LIST OF TABLES

LIST OF TABLES (continued)

LIST OF TABLES (continued)

I. A STUDY OF THE PRODUCTION OF CHORIORETINAL LESIONS IN RABBITS BY THERMAL RADIATION

by

R. G. Allen, Jr., K. R. Kay, W. R. Bruce, and R. A. Neish

1. INTRODUCTION

With increased application of high intensity light sources, such as Xenon and mercury high pressure lamps, nuclear weapons, solar simulators, and lasers, a basic necessity for predicting threshold levels for the production of chorioretinal lesions by thermal radiation has developed. The prediction of chorioretinal burns still depends basically upon threshold data collected in the laboratory using rabbits as subjects. Acquisition of reliable and complete threshold data for rabbits was the objective for this study.

Threshold data were obtained for the production of five-minute minimal retinal lesions in rabbits for seven image diameters from 0.053 to 1.08 mm with exposure times ranging from 165 microseconds to 100 seconds. Sixty-six combinations of exposure time and retinal image diameters were used for determining the effects of these variables upon retinal irradiance thresholds and the values of the thresholds.

The incident energy, primarily in the visible region of the electromagnetic spectrum, was generated with a Meyer-Schwickerath

photocoagulator which had been modified for controlled pulsed operation. (Modifications are discussed later in this report.)

The criteria used to define a five-minute minimal retinal lesion were as follows: (a) appearance of an area of disturbance with a gray or white center within five minutes after the end of exposure, and (b) appearance of a similar lesion after five minutes at an irradiance level approximately two to five percent lower.

The threshold irradiance level for producing a five-minute minimal lesion was arbitrarily taken as the average between the lowest, obtainable irradiance level that produced a lesion in five minutes and the highest, obtainable irradiance level that would not produce such a lesion in five minutes--where the difference between the two levels was typically one to five percent.

2. DESCRIPTION OF APPARATUS

A number of modifications were made to the basic Zeiss Coagulator light source for precise control of the beam energy and exposure duration. The xenon arc lamp of the coagulator was pulsed by external power components for exposures less than 10 seconds. Additional field apertures were made to provide a greater range of cone angles of the emerging light.

2.1 Control of Exposure Duration

The Zeiss coagulator may be pulsed from an aircraft battery source for pulse durations of 2 milliseconds through 10 seconds, from a capacitor bank for pulse durations of 165 microseconds to 1 millisecond, or from the internal power supply of the coagulator for pulse duration of 10 seconds to 100 seconds. The components are shown in the block diagram of Figure 1.

When the DC contactor is energized, the capacitor bank is in parallel with the batteries. When de-energized, the capacitor bank is charged from the Kepco power supply.

Pulsing is accomplished by closing a push button switch on the ophthalmoscope handle. This energizes a relay in the sequential control (Figure 2) which energizes the shutter relay in the Zeiss coagulator which in turn starts the operation of the waveform generator. The output of the waveform generator triggers the "on" and "off" pulse generators. A composite of the outputs of the pulse generators is shown in Figure 3. The "on" pulse (Figure 4) furnished a square wave which triggers the silicon control rectifiers, which in turn causes the capacitor bank to be discharged through the Xenon lamp of the coagulator. The "off" pulse (Figure 5) furnished a bias to turn off the silicon control rectifiers at the preset time of the waveform generator. The Eput Timer is triggered by the on-off pulse to give a visual display of pulse durations.

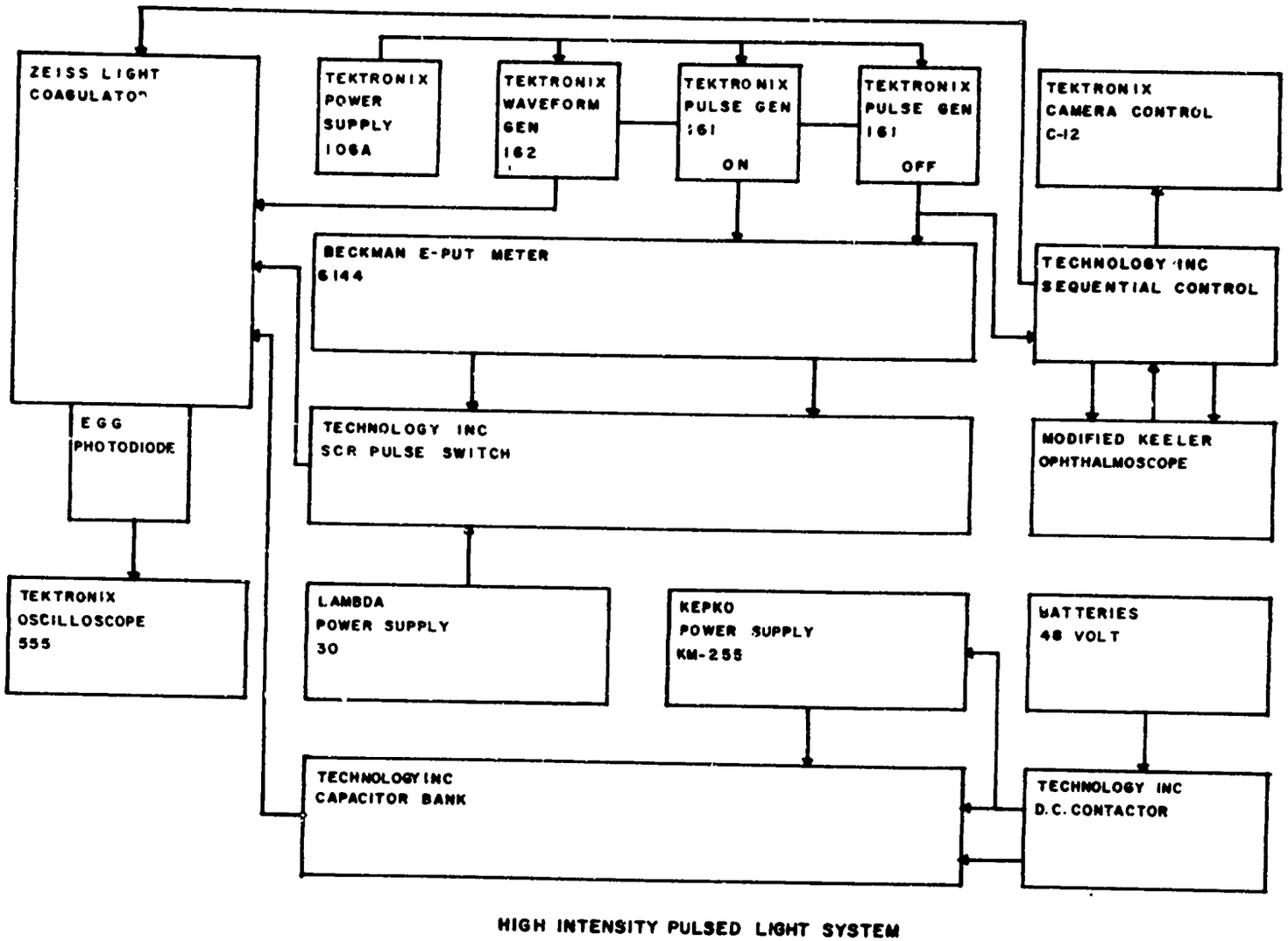

Figure 1 - High intensity pulsed light system, block diagram

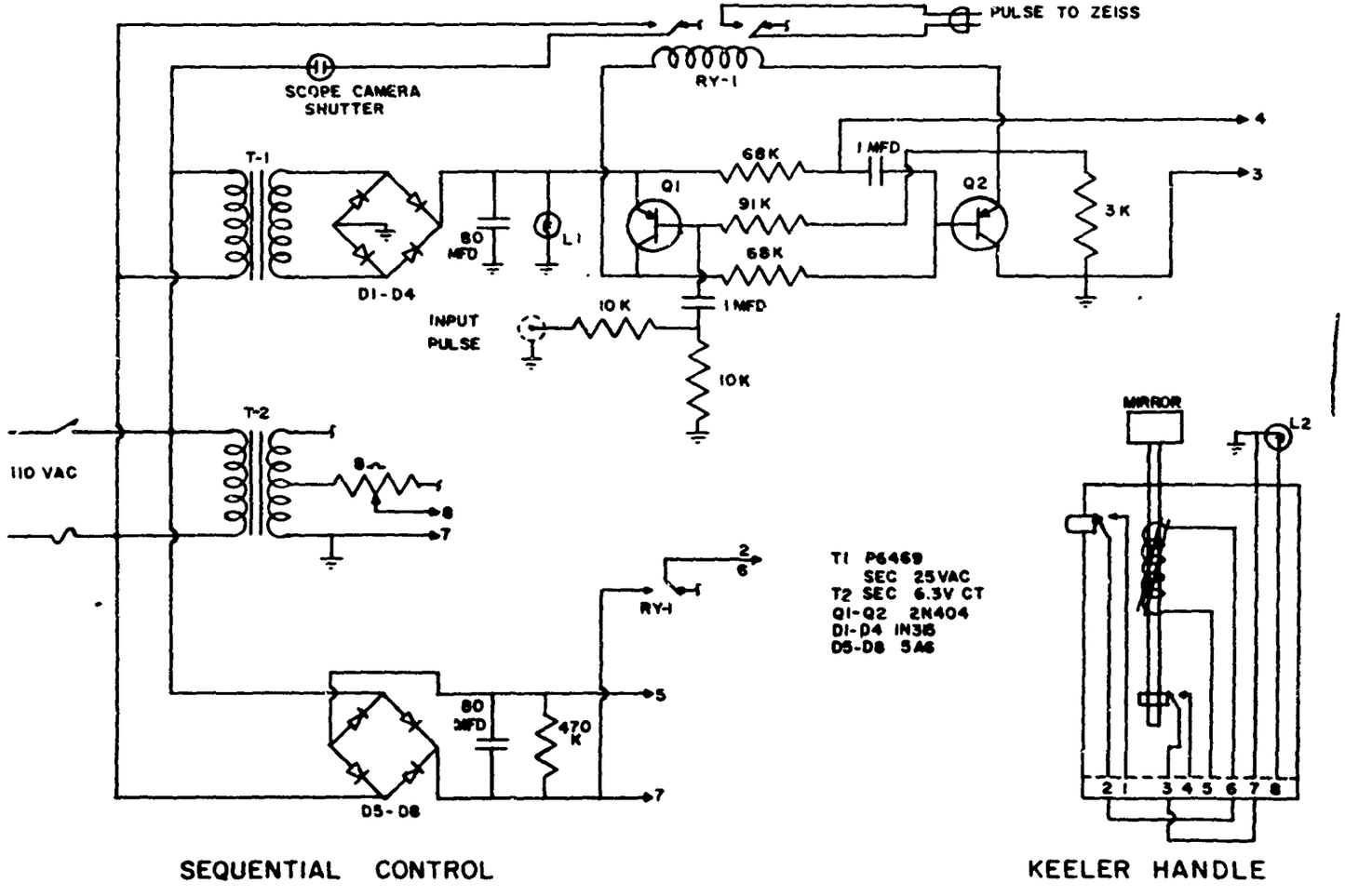

Figure 2 - Sequential control and Keeler handle circuit diagram

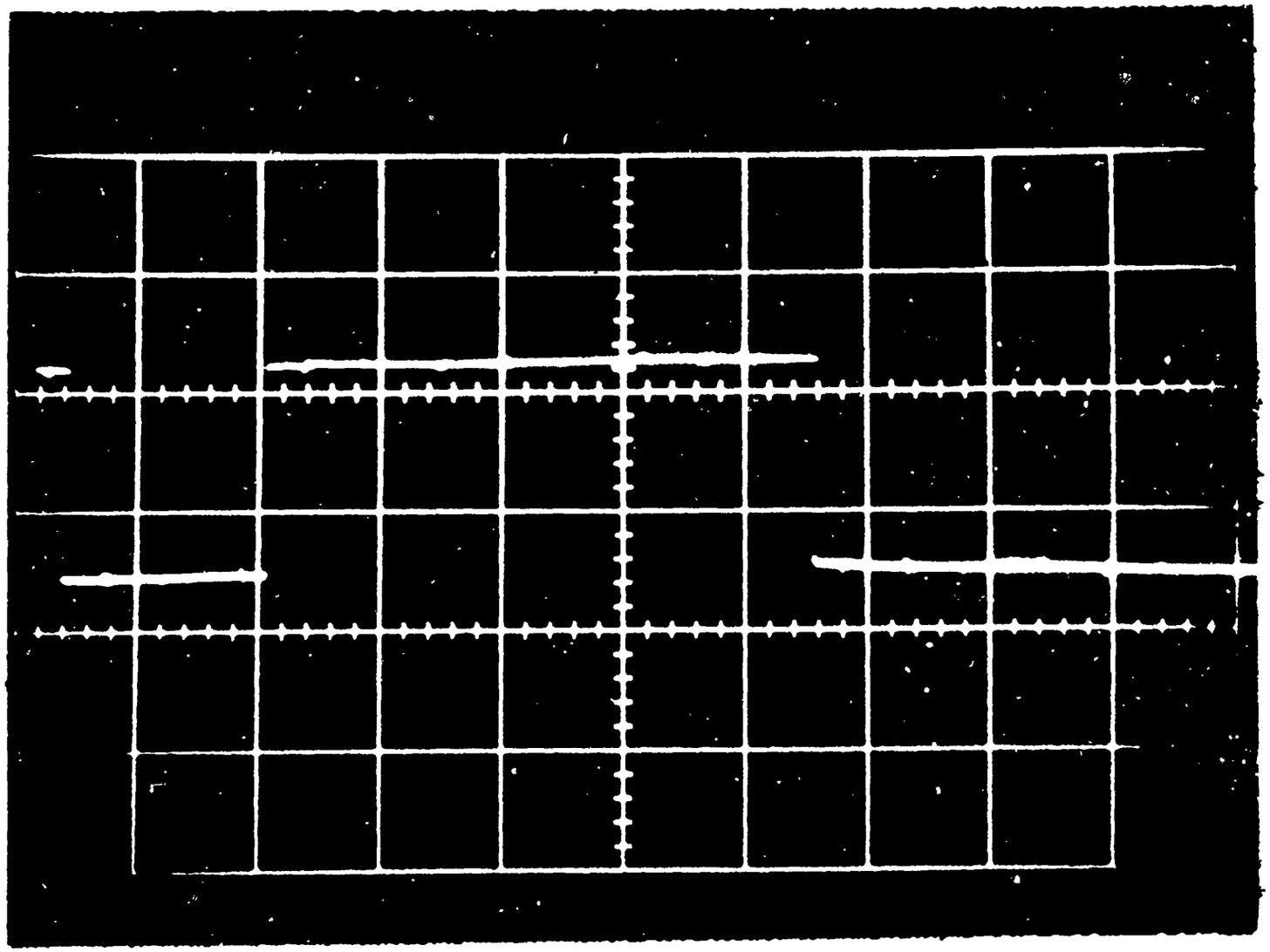

Figure 3 - Composite turn "on" and "off" pulse. Oscilloscope set at 5 msec/cm and 10 v/cm.

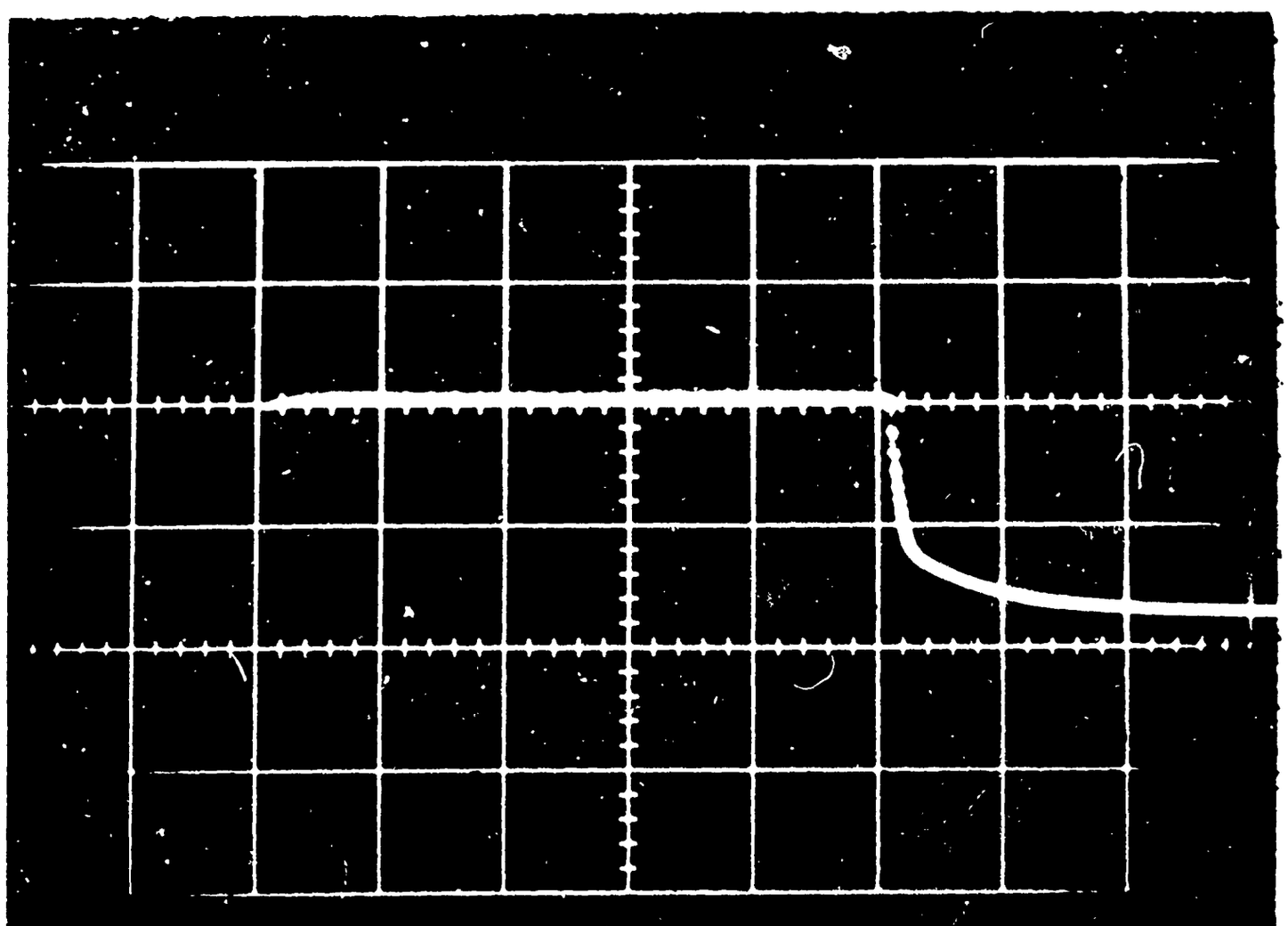

Figure 4. - Turn on pulse. Oscilloscope set at 2 microsec/cm and 10 v/cm

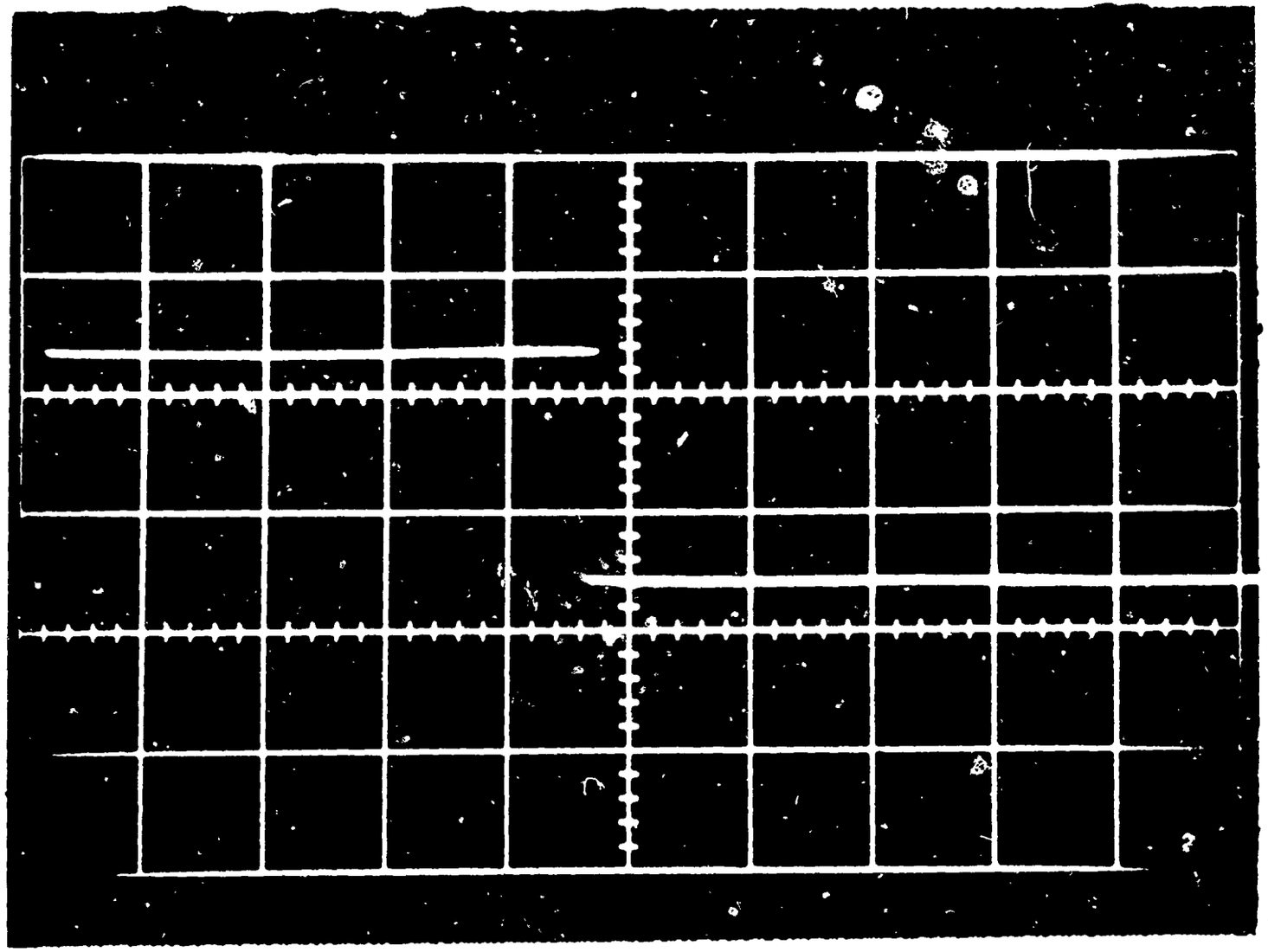

Figure 5 - Turn off pulse. Oscilloscope set at 5 msec/cm and 10 v/cm

The Kepco power supply furnished a D. C. potential to charge the capacitor bank during capacitor bank operation. It also provided a trickle charge to the batteries during battery operation.

The Lambda power supply furnished a D. C. potential for commutation of the SCR pulse switch to turn off the Xenon lamp.

2.2 Light Source

The light source used was a Meyer-Schwickerath Coagulator. For the purpose of studying chorioretinal burns, this machine was modified as follows: a) additional field diaphragm apertures were made and installed in the coagulator allowing the use of 0.32°, 0.45°, 11.93°, and 22.70° cone angles, (b) the iris control mechanism was replaced by a steel rule with a vernier in order to obtain a more accurate intensity control of the beam in 88 graded steps, and (c) previous work done in this laboratory (1, 2, 3, 4). The modified coagulator with the auxiliary equipment is presented in Figure 6 and the iris control mechanism is presented in Figure 7.

Spectral measurements were made on the light produced by the modified Zeiss coagulator and reported previously (5). The irradiance output of the light source (Xenon 2500W lamp) approximates a 5800° black body in the visible portion of the electromagnetic spectrum. The light output of the modified coagulator is in the 400 nm to 900 nm spectral

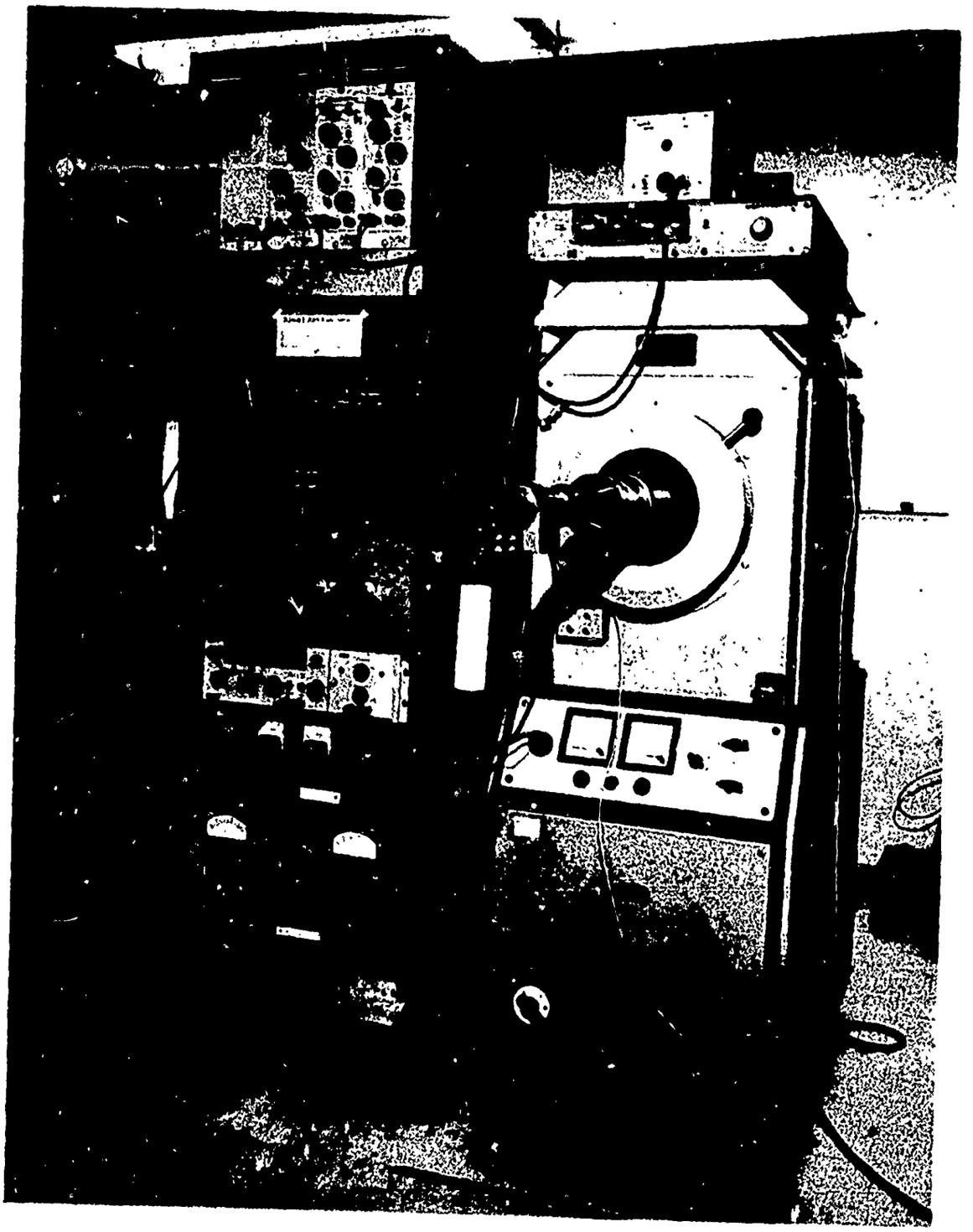

Figure 6 - Modified light coagulator with auxiliary equipment

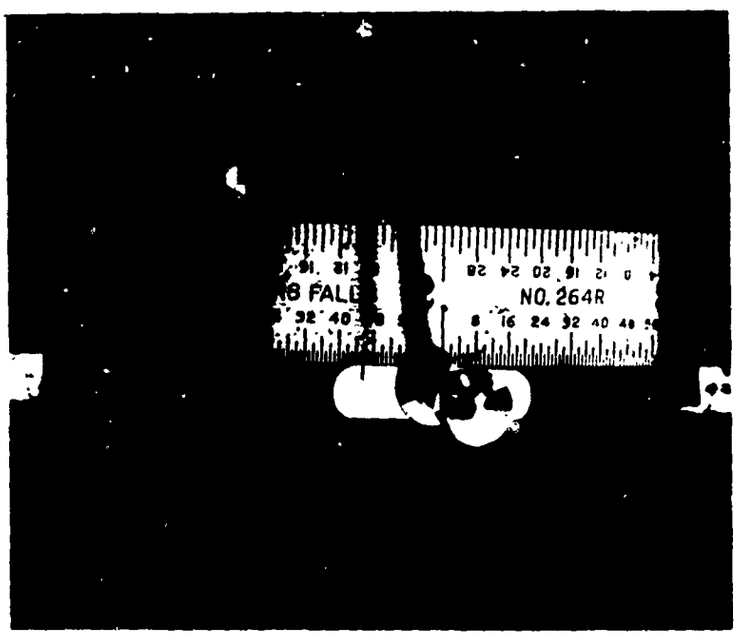

Figure 7

Modified Iris Control Mechanism

The Iris Control Mechanism allows the intensity of the Beam to be reduced in 88 graduated steps.

band with peaks at 500 nm to 550 nm.

2.2.1 Divergence of the Coagulating Beam

Before modifications could be made to the mechanism by which the divergence of the photocoagulating beam was varied, it was necessary to understand the optical principles of the photocoagulator.

The luminous plasma 3 (Figure 8) of the xenon high pressure lamp X BO 2001, 2, is reflected back to the lamp by means of a concave mirror in order to increase the luminous density. The following are interposed successively in the beam path: perforation diaphragm 4, condenser 5, KG-3 filter 6, iris diaphragm 7, filter disc 8, image field diaphragm 9, objective lens 10 and eye mirror 11.

The condenser 5 forms the image of the luminous plasma 3 in the plane of the field diaphragm 9. The image of the field diaphragm is formed at infinity by the objective lens 10. The beam is reflected into the patient's eye by the mirror 11. An image of the condenser is formed in the pupil of the patient. The exit pupil of the photocoagulator optical system is the image of the condenser 5 in the subject's pupil. The diameter of the condenser image is varied by the iris diaphragm 7. Finally, the image of the field diaphragm 9 is formed on the retina of the patient.

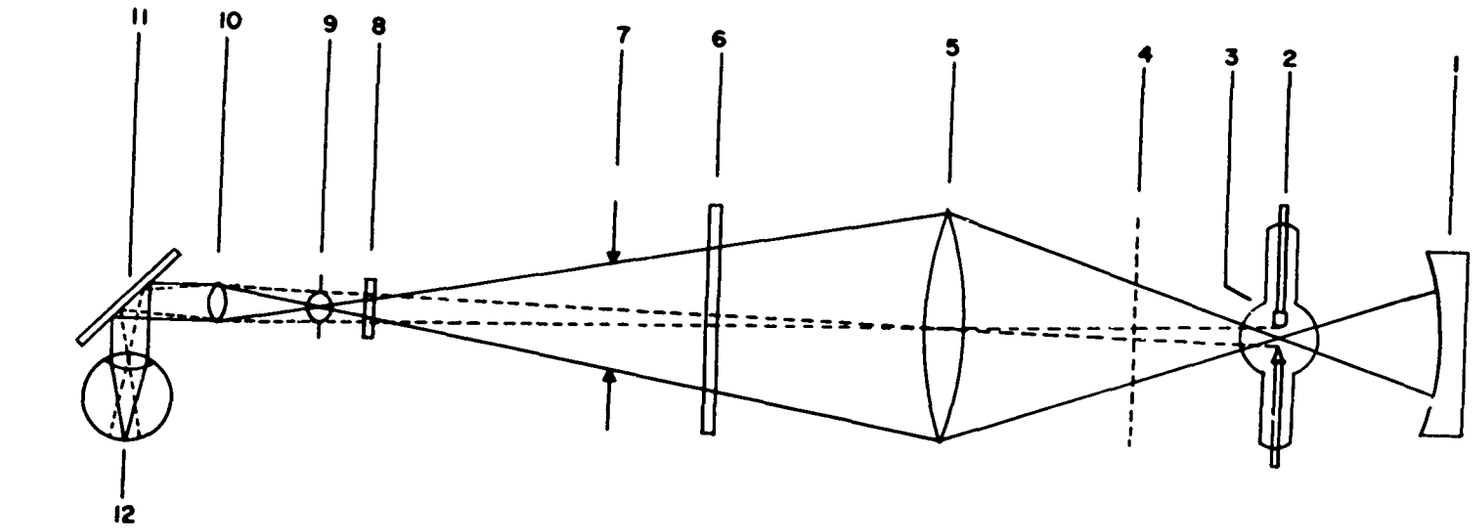

Figure 8 - Zeiss optical schematic

From the foregoing statements, it is recognized that the beam divergence is controlled by the field diaphragm 9 and the objective lens 10. From Figure 9, and the following definitions, an expression for the beam divergence can be derived:

θ = cone angle (divergence) (radians)

α = cone half angle

f = focal length of the objective lens (mm)

β = diameter of the field diaphragm (mm)

y = radius of the field diaphragm (mm)

$$\beta = 2y \qquad \theta = 2\alpha \qquad \tan \alpha = y/f$$

hence, $$\tan \frac{\theta}{2} = \frac{\beta}{2f}. \tag{7}$$

$\therefore$ The beam divergence is given by:

$$\theta = 2 \arctan \frac{\beta}{2f} \tag{8}$$

From equation (8) it can be seen that varying β and/or f will cause a change in the divergence and that the divergence θ can be determined theoretically by knowing β and f. The focal lengths of the objective lenses and the diameters of the field diaphragms used to vary the divergence in the modified photocoagulator were determined experimentally. From this data, the divergence of the light beam could be predicted, using equation (8). The data are presented in Table I with a prediction of the divergence values of the light beam.

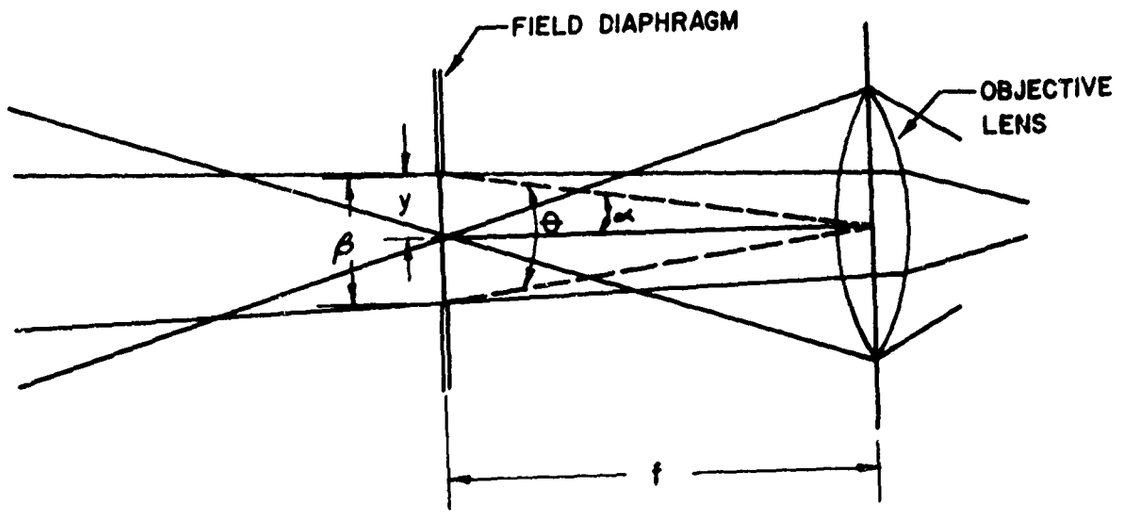

β = field diagram diameter

y = field diameter radius

θ = beam divergence angle

α = beam divergence half-angle

f = focal length of objective lens

Figure 9

Beam divergence schematic

TABLE I

THEORETICAL DIVERGENCE VALUES

β (mm)	f (mm)	θ
16.00	40.0	22.62°
16.00	80.5	11.35°
8.20	80.5	5.83°
4.25	80.5	3.02°
2.07	80.5	1.47°
1.40	80.5	1.00°
0.80	80.5	0.57°
0.60	80.5	0.43°
0.45	80.5	0.39°

3. MAINTENANCE AND CALIBRATION OF THE APPARATUS

3.1 Maintenance

The instruction manual of the individual components were followed for operation, maintenance and calibration (6). The Xenon bulb and high voltage connectors were checked for security of mounting once each month. When corrosion appeared on the knife switch pivot, it was cleaned and lubricated. The carbon granules in the ozone filter were replaced when ozone was detected. The mounting and shutter microswitch in the coagulator were checked and all points on the D. C. contactor burnished every six months.

3.2 Calibration and Monoriting of the Light Source

An Eppley thermopile, calibrated by the National Bureau of Standards, was used to determine the total irradiance output of the Zeiss Coagulator. The thermopile and an E. G. & G. SD-100 photodiode are used simultaneously to record the irradiance output of the coagulator for a ten second pulse. The 1/e time constant of the thermopile is approximately six to seven seconds, so a ten second measurement was taken so that the thermopile could reach output equilibrium.

The output of the thermopile was displayed by a Hewlitt-Packard VTVM and the output of the photodiode was displayed on a Tektronix 551 Oscilloscope. The output of the thermopile was recorded with the peak

reading of the photodiode output which had been photographed on the oscilloscope by a Tektronix C-12 polaroid camera. Once the ten second baseline was established, the output of the photodiode was recorded for pulsewidths less than ten seconds and cross calibrated against the thermopile.

3.2.1 Calibration of Beam Divergence

The calculations of the beam divergence for the various field apertures were experimentally verified. The diameter of the light beam at two distinct distances from the objective lens 10, and the distance between these planes of measurement were measured and recorded. With these data, the schematic of Figure 10, and the following derivation, the beam divergence was determined experimentally.

Definitions:

$\theta = 2\alpha$

d_1 = diameter of beam at first plane of measurement (mm)

d_2 = diameter of beam at second plane of measurement (mm)

a = distance between planes (mm)

From Figure 10, $d_2 = d_1 + 2c$

$$\frac{d_2 - d_1}{2} = c$$

$$\tan \alpha = \frac{c}{a} = \frac{d_2 - d_1}{2a}$$

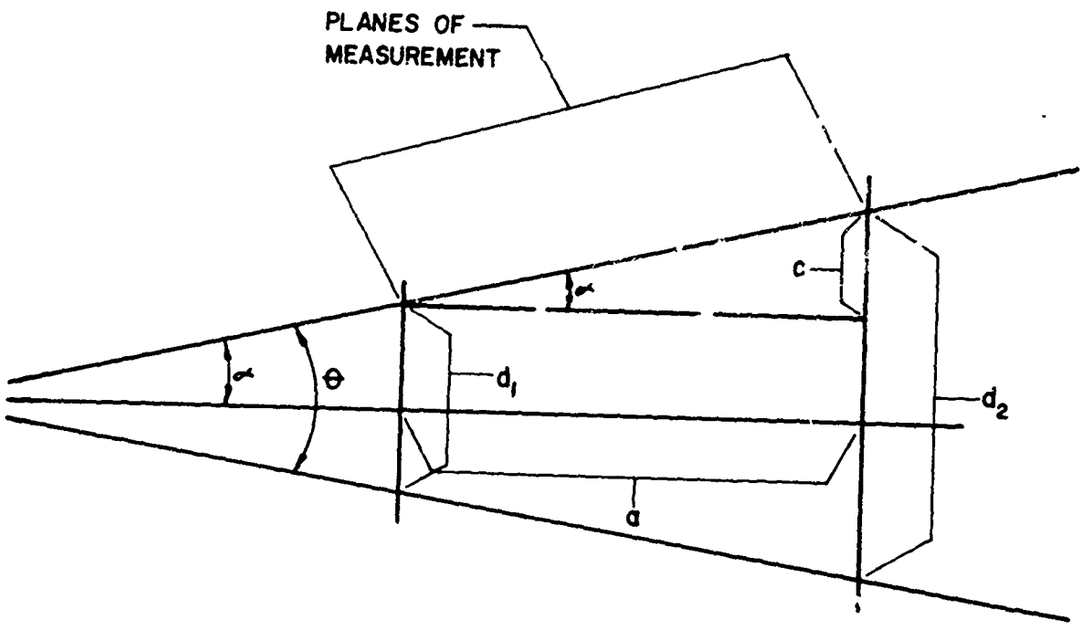

Figure 10

Schematic of beam divergence measurements

$$\tan \frac{\theta}{2} = \frac{d_2 - d_1}{2a}$$

$$\left[\text{ divergence }\right] \quad \theta = 2 \text{ arc } \theta \tan \frac{d_2 - d_1}{2a} \qquad (9)$$

The data are presented in Table II with the determined divergence values for the photocoagulator beam. The two sets of results are presented in Table III for comparison. The theoretical and experimental values of the beam divergence agree quite well.

3.2.2 Homogeneity of the Photocoagulator Beam

The homogeneity of the light beam was determined using a SD-100 photodiode. The photocoagulator was set on 80 amps and operated continuously with the dummy shutter plug inserted. An optical chopper was placed in the beam to keep the photodiode output from drifting due to temperature effects.

The photodiode was moved in steps along a horizontal and vertical diameter of the light beam. The voltage output of the photodiode was measured by recording the signal from a Tektronix oscilloscope with a C-12 camera for each increment of the two diameters. The 6.20° cone and 3.07° cone were the only two measured in this manner. The normalized data is recorded in Table I-B and II-B in the appendix. The curves for irradiance, H (relative to the center of the beam) versus the distance from the center of the beam are shown in Figures 11 and 12.

TABLE II

Experimental Divergence Values

d_1 (mm)	α(mm)	d_2 (mm)	θ
568	1000	986	22.70°
629	1000	838	11.93°
405	3000	730	6.20°
309	3000	470	3.07°
172	6000	325	1.47°
119	6000	229	1.05°
68	6000	122	0.52°
56	6000	96	0.45°
43	6000	75	0.33°

TABLE III

Comparison of Experimental and Theoretical Divergence Values

Experimental	Theoretical
θ	θ
22.70°	22.62°
11.93°	11.35°
6.20°	5.83°
3.07°	3.02°
1.47°	1.47°
1.05°	1.00°
0.52°	0.57°
0.45°	0.43°
0.33°	0.39°

θ = beam divergence

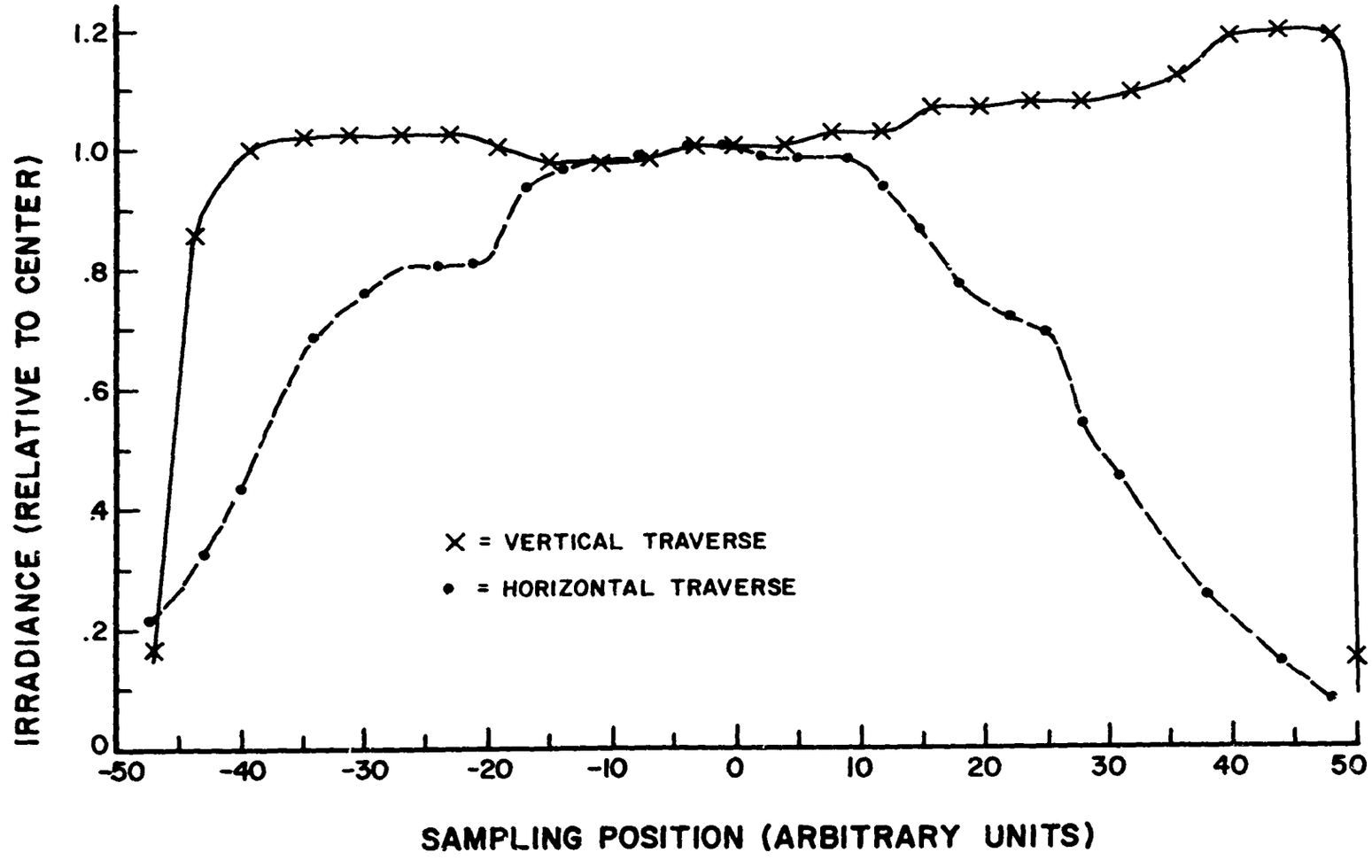

Figure 11 - Beam Homogeneity Curve for 3.07° Cone

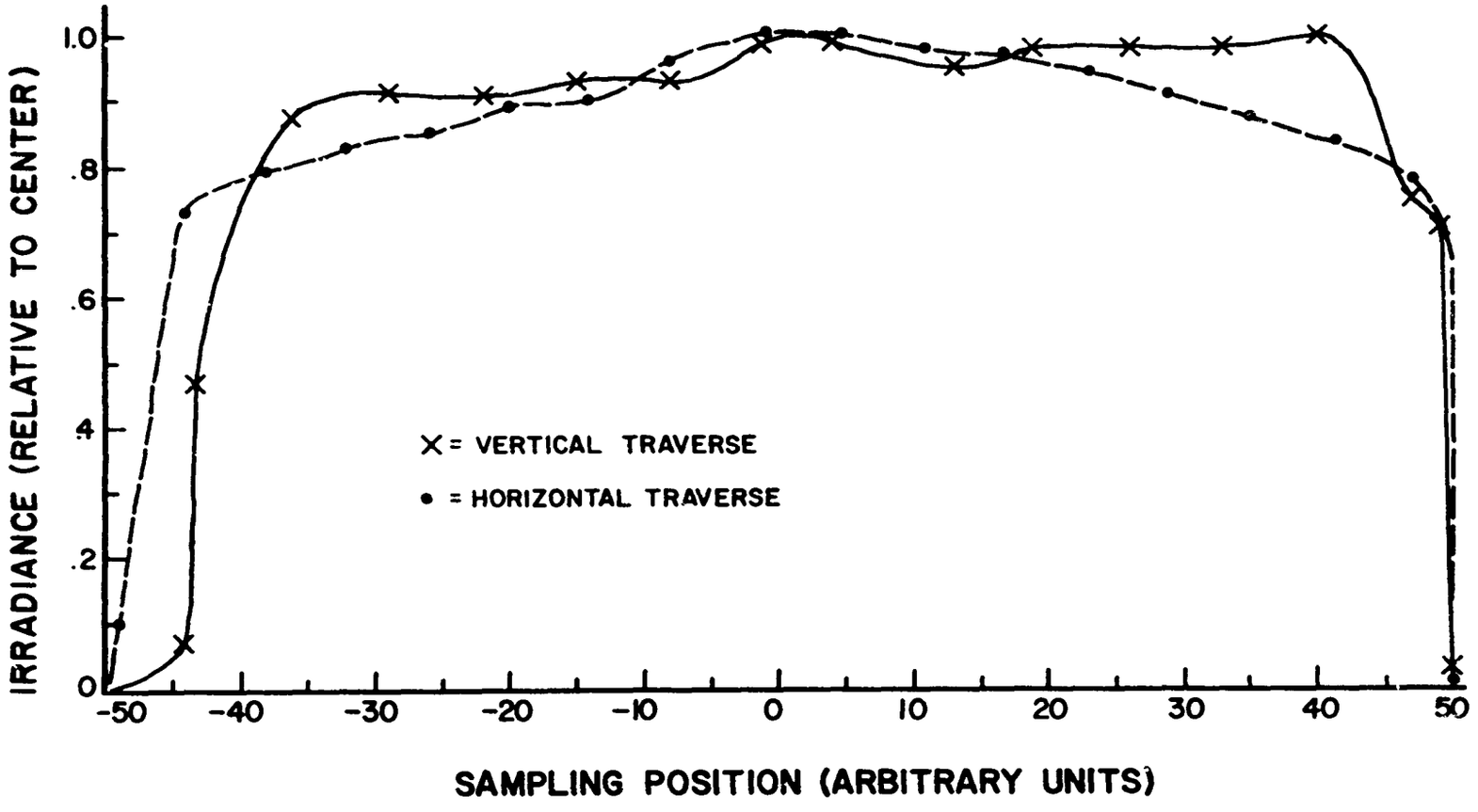

Figure 12 - Beam Homogeneity Curve for 6, 20° Cone

The cone angles less than 3.07° were not measured as the smaller cone angles consist of only the center portion of the 3.07° (Figure 11) which is homogeneous.

One can see from Figure 12, that in the 6.20° cone, the irradiance diminished as the outer edge of the beam is approached along the horizontal diameter, but it is reasonably homogeneous along its vertical diameter. The 3.07° cone (Figure 11) shows good homogeneity except along the edge of the light beam.

After determining the inhomogeneity of the light beam of steady state operation, it was decided to investigate the beam under pulsed conditions. An attempt to obtain quantitative results was unsuccessful; but, pictures of the reflected light beam were obtained for subjective interpretation. (See Figure 13). Some inhomogeneity is indicated in the photographs. A picture of the reflected light beam indicating the relative inhomogeneity of the 11.93° light beam is shown in Figure 14. The results of this picture are similar to those found by using the 22.70° light beam.

From the results obtained in the two reported investigations, it was decided not to use the 11.93° and 22.70° light beams for experimentation because of marked inhomogeneity. It was also decided to conduct more research at a later date using a Jarrel Ash Traveling Microden-

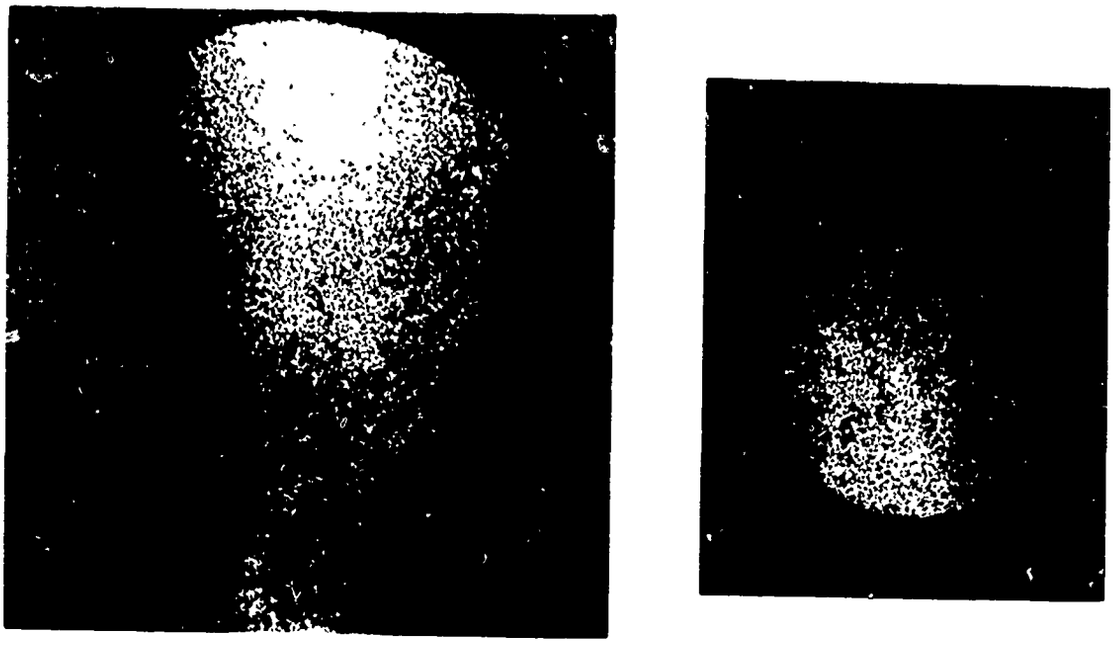

A. 6.20° light beam with areas of inhomogeneity.

B. 3.07° light beam with areas of inhomogeneity.

Figure 13

Typical beam pictures of the 6.20° and 3.07° cones

Beam pictures of 100 msec pulse at 34.9% maximum intensity

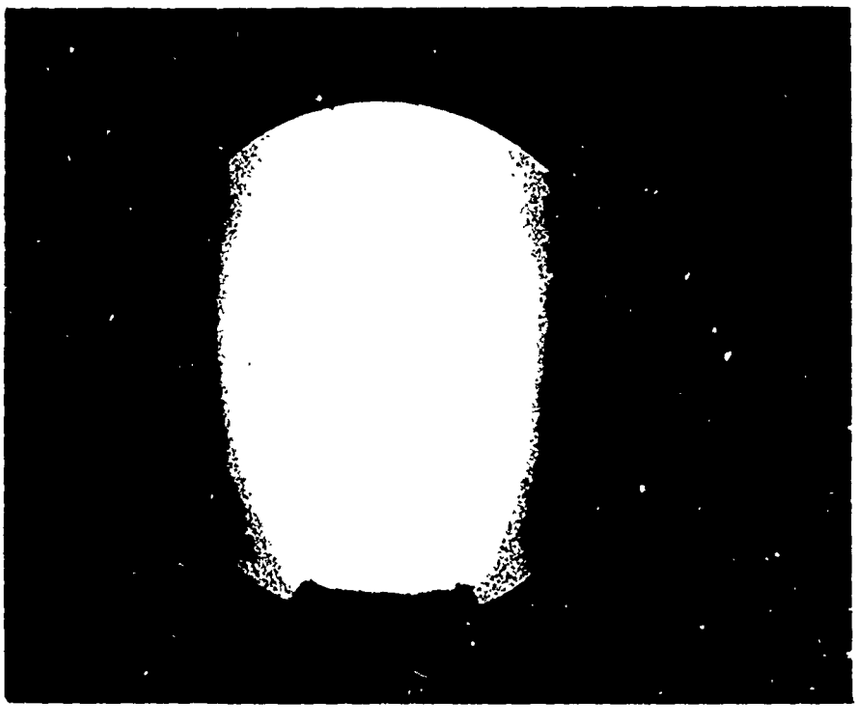

Figure 14

Typical inhomogeneity of the 22.70° and 11.93° cones

sitometer and radiographic photography to interpret the beam pictures quantitatively.

3.3 Determination of Irradiance

3.3.1 Determination of Retinal Image Diameter

The experimental values for the beam divergence in Table II can be used to determine the retinal image diameter for various subjects. A schematic eye of the subject is presented in Figure 15. The light beam of the photocoagulator (focused at infinity) enters the subjects eye and passes through the nodal point N at the angle α, and passes undeviated to the retina. Using the notation of Figure 15, the equation for the retinal image diameter of the subject can be derived:

Definitions:

d = retinal image diameter

$f = \overline{NF}$ = effective focal length of the eye

θ = beam divergence

α = half cone angle

$$\tan \frac{\theta}{2} = \frac{d}{2f}$$

$$d = 2f \tan \frac{\theta}{2} \qquad (10)$$

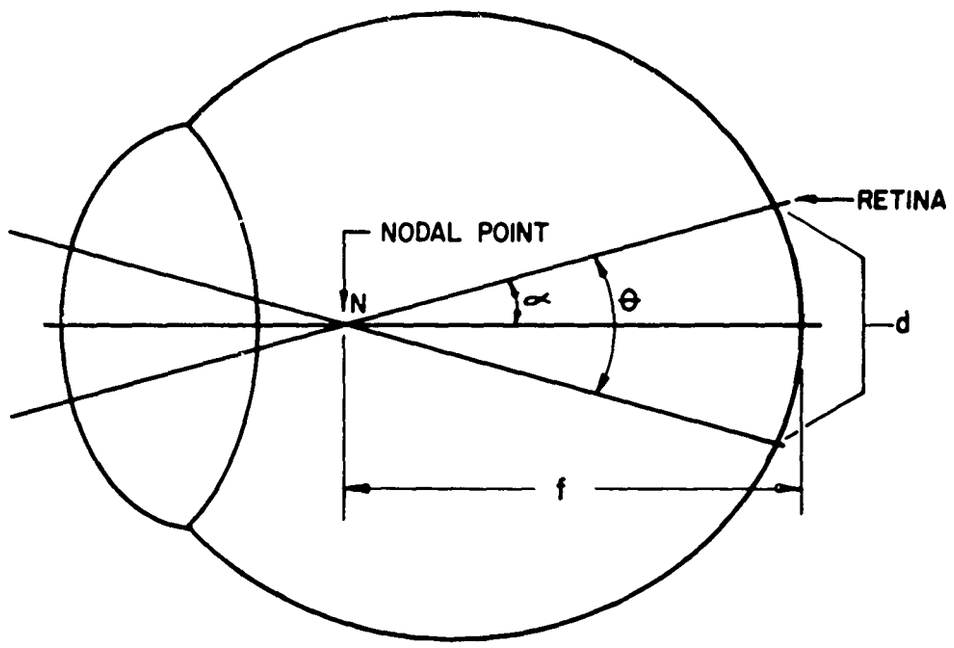

Figure 15

Schematic eye of subject

Using the equation (10), the value of the focal length, and the values of θ from Table II, the theoretical values of the retinal image diameter for various subjects can be calculated. The data and calculated image diameters are presented in Table IV.

3.3.2 Retinal Irradiance Equation

Determination of the retinal irradiance at time t, $H_r(t)$, is given by equation 1, (2) for battery discharge.

$$H_r(t) = ICSG\bar{T}_e G'V_{pd} \qquad (1)$$

The various factors of equation 1 are defined as follows:

$$I = \frac{V_E}{V'_E} \qquad G = \left(\frac{D}{F}\right)^2 \qquad S = \frac{V'_E}{V'_{pd}}$$

$H_r(t)$ = retinal irradiance

V'_E = equilibrium value of thermopile (millivolts). Iris fully open.

V_E = response of thermopile (millivolts) with iris at any setting.

C = thermopile calibration constant ($= 1.15 \times 10^{-3}$) cal/cm^2-sec-mv for present thermopile.

D = distance between light source and thermopile (cm). (300 cm at present)

F = effective focal length of subject's eye e.g., (rabbit, primate, or man).

$\bar{T}_e$ = transmission factor for the eye media.

V'_{pd} = corresponding voltage response of photodiode (millitolts) to V'_E.

V_{pd} = voltage response of photodiode (millivolts) at any pulsewidth t.

$G' = \frac{A_p}{A_B} = \frac{d_p^2}{d_B^2}$ (when $d_B \leq d_p$, $\frac{d_p^2}{d_B^2} \equiv 1$ by definition)

A_p = area (mm^2) of the subjects apparent pupil.

A_B = area (mm^2) of the photocoagulating beam at the exit pupil (see Figure 8).

d_p = diameter (mm) of the subjects apparent pupil.

d_B = diameter (mm) of the photocoagulating beam at the exit pupil.

The beam diameter d_B is determined by the iris diaphragm. The beam diameter as a function of the iris control setting was calibrated over the total range used. Therefore, equation 1 may be written:

$$H_r(t) = \frac{ICV'_E}{V'_{pd}} \left(\frac{D}{F}\right)^2 \bar{T}_e \left(\frac{d_p^2}{D_B^2}\right) V_{pd} \qquad (2)$$

The quantity $I = \frac{V_E}{V'_E}$ was determined experimentally and the results were tabulated to provide a calibration chart of the attenuation factors versus iris control settings.

For non-square, symmetrical or semi-symmetrical pulses, (the case for relatively short pulses <2 msec), using a capacitor bank discharge, the average retinal irradiance is given by:

$$H_r(t) = IC \frac{V'_E}{V'_{pd}} \left(\frac{D}{F}\right)^2 \bar{T}_e \left(\frac{d_p^2}{d_B^2}\right) V_{pd} \left(\frac{T_m}{T_{1/2}}\right) \qquad (3)$$

$t_{1/2}$ = light pulsewidth at half maximum.

TABLE IV

Calculated Retinal Image Diameters

Rabbit f = 10 mm		Rhesus Monkey f = 12 mm		Man f = 17 mm	
θ	d (mm)	θ	d (mm)	θ	d (mm)
22.70°	4.18	22.70°	5.02	22.70°	7.12
11.93°	2.11	11.93°	2.54	11.93°	3.59
6.20°	1.08	6.20°	1.30	6.20°	1.84
3.07°	0.54	3.07°	0.64	3.07°	0.91
1.47°	0.26	1.47°	0.31	1.47°	0.43
1.05°	0.18	1.05°	0.22	1.05°	0.31
0.52°	0.09	0.52°	0.11	0.52°	0.15
0.45°	0.067	0.45°	0.079	0.45°	0.11
0.33°	0.053	0.33°	0.064	0.33°	0.09

f = focal length

θ = Beam Divergence

d = retinal image diameter

The ratio $t_m / t_{1/2}$ was determined experimentally for various conditions and the following values obtained:

$t_m / t_{1/2}$	pulsewidth
1.00	> 1 msec
0.99	1 msec
0.96	400 μsec
0.90	145 μsec

With the above values of $t_m / t_{1/2}$, equation (3) can be adapted for use for a battery of capacitor bank discharge.

3.3.3 Retinal Irradiance Calculations

The retinal irradiance for any experimental exposure can be calculated from equation (3) using the calibration data and the various constants for the thermopile and for the eye of the subject animal. The following example will illustrate the procedure:

Subject: Rabbit

$\bar{T}_e = 0.89$ $F = 1.0$ cm $d_p = 1.2$ cm

From the calibration charts for the beam diameters and attenuation factors, the values for the given iris control setting:

$d_B = 1.2$ cm $I = .995$

The calibration constant for the thermopile:

$C = 1.15 \times 10^{-3}$ cal/cm^2-sec-mv $D = 300$ cm

From the comparison of the photodiode and the thermopile for a 10 sec exposure with the iris fully open:

$$V'_E = 5.00 \text{ mv} \qquad V'_{pd} = 1200 \text{ mv}$$

Pulsewidth = 165 μsec

$$V_{pd} = 3600 \text{ mv} \qquad t_m / t_{1/2} = 0.906$$

∴ Retinal irradiance from (3):

$$H_r(t) = \frac{0.995 \times 1.15 \times 10^{-3} \times 5.0}{1200} \left(\frac{300}{1.0}\right)^2 0.89 \left(\frac{1.2}{1.2}\right)^2 3600 \times 0.906 \quad \frac{\text{Cal}}{\text{cm}^2\text{-sec}}$$

$$= 1245.7 \text{ cal/cm}^2\text{-sec for 165 } \mu\text{sec.}$$

This result can be converted to the total energy per unit area received by the retina by multiplying by the pulsewidth:

$$Q_r = 0.206 \text{ cal/cm}^2$$

4. EXPERIMENTAL PROCEDURES

Dutch and Checker rabbits were used throughout the study. Many animals were found to have clumpy and striated pigmentation of the fundus, but only those with medium, brown, homogeneous pigmentation of the fundus and with clear media were utilized.

For exposure times less than 250 milliseconds the animal was tranquilized with 2 cc demerol, IM. For longer exposure times, it was necessary to sedate the animal with sodium thiopental (sodium pentothal), and gallamine triethiodide (Flaxedil), by using a No. 19 intracath, intro-

duced in an ear vein. Respiration was maintained via a tracheotomy and a Bird Mark VII respirator. Maximum pupillary dilation was obtained by the use of Atropine, Ophthalmic solution, 1%. The animal was placed in a restraining box, and positioned in front of the Zeiss beam director (Figure 8), where the eye was examined using the modified Keeler ophthalmoscope.

The cone was set corresponding to the retinal image diameter and the electronic pulse control for the pulse width desired. Using the irradiance obtained from the calibration procedure for the pulse duration being investigated, and the results of pilot studies, the iris diaphram was set to give an $\bar{H}_r$ of approximately twice the energy calculated to give a minimal burn to provide a marker burn for a reference point on the retina. The marker burn was placed in the central region of the fundus about 5 mm below the medullated nerve fibers.

After determining that the marker burn had been produced, the modified Keeler ophthalmoscope was positioned to bring an adjacent area of the fundus into view, the iris diaphram reset to decrease the irradiance, and another exposure made. This process was continued, with exposures placed in horizontal rows (Figure 16), until the threshold irradiance for a 5 minute, minimal burn was determined. This procedure was repeated for various exposure durations, retinal image diameters, and subjects, until approximately 10 or more threshold levels were obtained

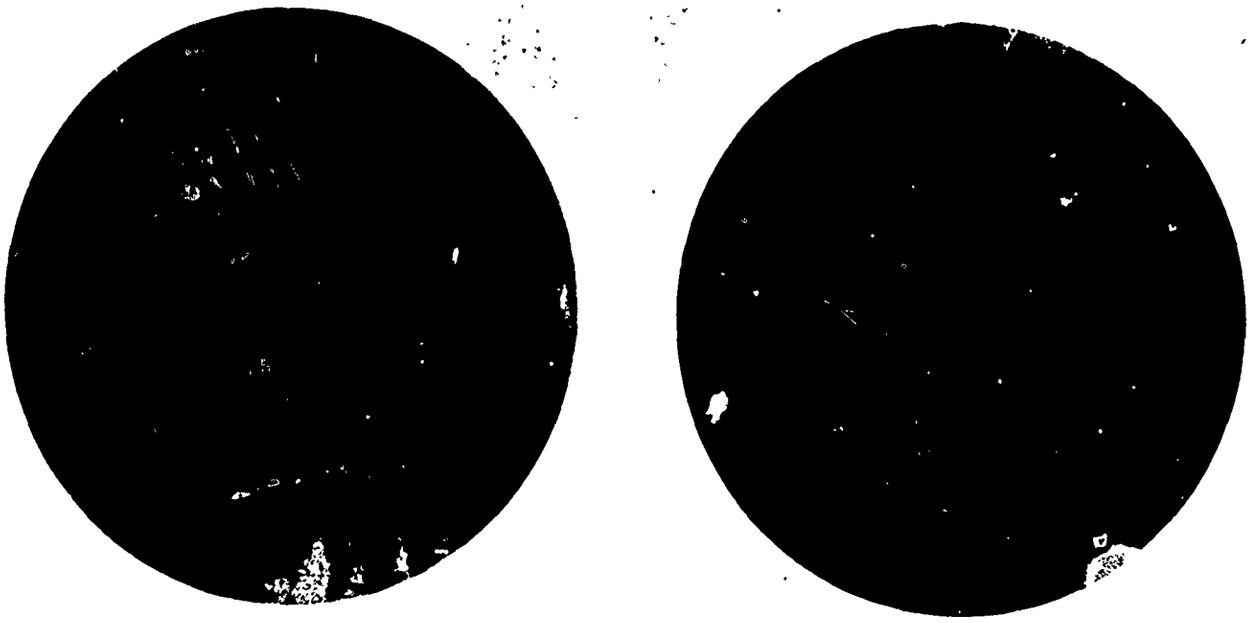

A. Horizontal placement

B. Vertical placement

Figure 16

Placement of retinal burns

at each of the retinal image diameters and exposure duration combinations selected for investigation. Ordinarily, a sufficient number of exposures could be placed in a single eye to establish several points on a threshold irradiance versus time curve; however, the number of exposures actually placed in one eye depended upon the retinal image diameter. The average number of exposures per eye was approximately twenty-five to prevent the possibility of over-lapping adjacent irradiated areas.

5. DISCUSSION OF EXPERIMENTAL RESULTS

The average threshold irradiance, $\bar{H}_r$, standard deviation σ, and the number of rabbit eyes per threshold point are summarized in Table V. The values of individual threshold irradiances for various image diameters are given in Tables III-B through XII - B of the appendix. The average threshold irradiance, $\bar{H}_r$, standard deviation σ, and average retinal exposure $\bar{Q}_r$, are also given.

Figure 17 presents the average, measured, threshold irradiance, $\bar{H}_r$, along curves of "best fit"--obtained through consideration of the entire set of data. To obtain these "best fit" curves, the average values of threshold irradiance were graphed versus retinal image diameter--for a fixed value of exposure time. Smooth curves were fitted to these points by eye. Values of $\bar{H}_r$ corresponding to the exposure times actually used were taken from these curves and used to determine the curves which

TABLE V

Average Retinal Irradiance (cal/cm^2-sec) (For 5-Minute Burn)

Image Diameter (mm)	Exposure Time (sec)													
	165×10^{-6}	400×10^{-6}	1×10^{-3}	4×10^{-3}	10×10^{-3}	20×10^{-3}	40×10^{-3}	100×10^{-3}	250×10^{-3}	1	4	10	30	100
1.08	799	330	210		36.8		13.8	8.33	5.17	3.91	3.10	2.49		
	210 [3]	34.6 [6]	27.0 [4]		3.19 [7]		1.75 [6]	0.96 [11]	0.47 [12]	0.42 [12]	0.38 [11]	0.31 [11]		
0.54	815	436	231		50.2		15.8	10.5	7.51	6.77	5.64	4.93		
	77.1 [2]	74.6 [6]	53.5 [4]		10.8 [7]		3.8 [3]	2.02 [10]	1.11 [11]	0.73 [12]	0.79 [12]	0.82 [12]		
0.26	738	503	333		57.4		31.8	23.3	17.0	16.1	14.3	13.4		
	168.5 [4]	190.3 [11]	137 [5]		12.6 [11]		9.54 [11]	6.74 [16]	4.64 [13]	1.28 [12]	1.51 [12]	1.77 [12]		
0.18	880	691	382		75.4		36.4	30.5	29.1	22.4	19.8	18.9	17.9	17.9
	297 [2]	169 [7]	273 [3]		17.0 [7]		7.19 [7]	9.22 [8]	14.3 [9]	1.42 [11]	1.63 [11]	2.00 [11]	1.55 [6]	1.55 [6]
0.09	1321	1100	645	432	237.6		129	96	79	68.4	64.1	62.1		
	219.6 [7]	125.8 [9]	87.8 [7]	23.0 [7]	63.7 [12]		42.5 [16]	25.5 [16]	21.8 [17]	1.34 [10]	3.83 [10]	4.85 [10]		
0.067				425.3	257.2	180.9	126.2	97.4	87.9					
				3.56 [10]	3.56 [10]	5.92 [10]	3.99 [11]	4.64 [11]	3.50 [11]					
0.05			1250	442	292	259	187	132	110					
			23.1 [4]	11.9 [11]	20.2 [12]	15.9 [12]	7.95 [12]	3.49 [12]	7.54 [12]					

NOTE: The numbers in the small boxes give the number of rabbit eyes used in obtaining the average retinal irradiance listed.

The numbers in the medium size boxes give the absolute value of the standard deviation (σ).

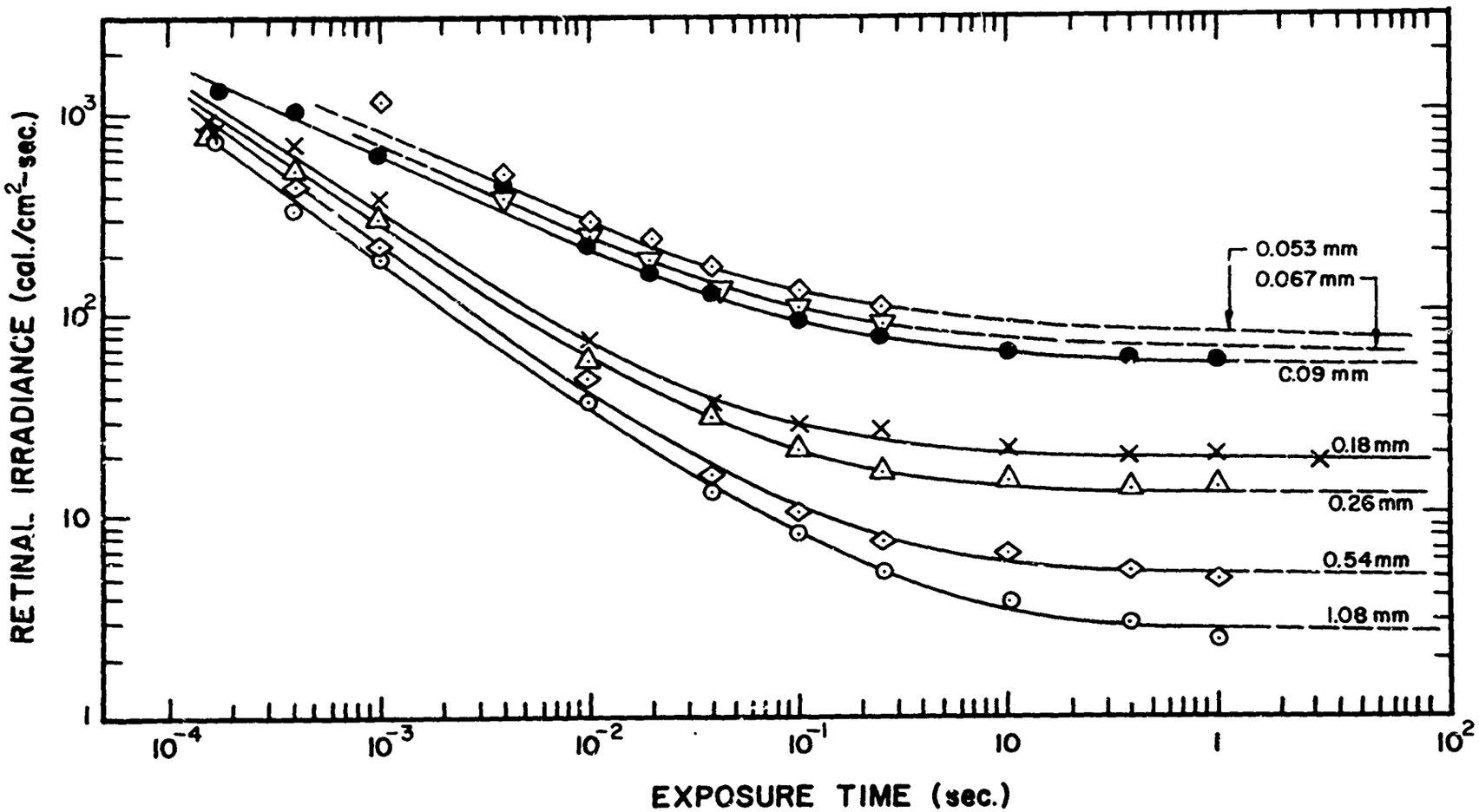

Figure 17 - Average threshold irradiance ($\bar{H}_r$) versus time for seven image sizes

best fit the expression $\bar{H}_r = At^B+C$, where A, B, and C are constants and t is expressed in seconds. The smooth fitted data was then run on a Philco 2000 computer using the Regula Falsi iteration technique, and the method of least squares, to yield constants for the theoretical retinal irradiance equation $\bar{H}_r = At^B+C$. The computed values of the constants are shown in Table XIII-B in the appendix. Comparisons of theoretical threshold retinal irradiance values and the experimental results are listed in Tables VI to XII. The theoretical values of irradiance agree quite well with the average values determined in the laboratory.

From Figure 17, several important conclusions can be drawn. There is no reciprocity relationship between $\bar{H}_r$ and t at exposure times greater than one second. However, there is a definite asymptote associated with each curve. This asymptote is represented by the constant C in the equation $\bar{H}_r = At^B+C$. Values of C are shown in Table XIII-B and agree favorably with the experimental data. The change in C with respect to retinal image diameter approximates a change proportional to burn area but only for large burns. For exposure durations less than one second there is a trend toward reciprocity for $\bar{H}_r$ and t. This becomes very evident at short times (less than one millisecond)--the curves of Figure 17 show a tendency to converge, indicating less variation of threshold with image diameter and show a definite reciprocity effect.

TABLE VI

Comparison of Experimental and Theoretical Threshold Retinal Irradiance

6.20° Cone - 1.08 mm Calculated Image Diameter

Exposure Duration	Experimental $\bar{H}_r$ (cal/cm^2-sec)	Theoretical H_r (cal/cm^2-sec)
0.17 msec	799	802.2
0.4 "	330	378.2
1.0 "	210	188.3
10.0 "	36.8	34.21
40.0 "	13.8	13.53
100.0 "	8.33	8.041
250.0 "	5.17	4.983
1.0 sec	3.91	3.594
4.0 "	3.10	2.997
10.0 "	2.49	2.839

TABLE VII

Comparison of Experimental and Theoretical Threshold Retinal Irradiance

3.07° Cone - 0.54 mm Calculated Image Diameter

Exposure Duration	Experimental $\bar{H}_r$ (cal/cm^2-sec)	Theoretical $\bar{H}_r$ (cal/cm^2-sec)
0.17 msec	815	954.6
0.4 "	436	445.4
1.0 "	231	219.9
10.0 "	50.2	40.40
40.0 "	15.8	16.95
100.00 "	10.5	10.83
250.00 "	7.51	7.850
1.0 sec	6.77	5.966
4.0 "	5.64	5.330
10.0 "	4.93	5.164

TABLE VIII

Comparison of Experimental and Theoretical Threshold Retinal Irradiance

1.47° Cone - 0.26 mm Calculated Image Diameter

Exposure Duration	Experimental $\bar{H}_r$ (cal/cm^2-sec)	Theoretical $\bar{H}_r$ (cal/cm^2-sec)
0.17 msec	738	1079
0.4 "	503	532.2
1.0 "	333	278.1
10.0 "	57.4	61.85
40.0 "	31.8	30.55
100.0 "	23.3	21.86
250.0 "	17.0	17.42
1.0 sec	16.1	14.77
4.0 "	14.3	13.40
10.0 "	13.4	13.10

TABLE IX

Comparison of Experimental and Theoretical Threshold Retinal Irradiance

1.05° Cone - 0.18 mm Calculated Image Diameter

Exposure Duration	Experimental $\bar{H}_r$ (cal/cm^2-sec)	Theoretical $\bar{H}_r$ (cal/cm^2-sec)
0.17 msec	880	1306
0.4 "	691	644.5
4.0 "	382	133.6
10.0 "	75.4	77.19
40.0 "	36.4	39.71
100.0 "	30.5	29.34
250.0 "	29.1	24.06
1.0 sec	22.4	20.55
4.0 "	19.8	19.28
10.0 "	18.9	18.93
30.0 "	17.9	18.73
100.0 "	17.9	18.64

TABLE X

Comparison of Experimental and Theoretical Threshold Retinal Irradiance

0.52° Cone - 0.09 mm Calculated Image Diameter

Exposure Duration	Experimental $\bar{H}_r$ (cal/cm^2-sec)	Theoretical $\bar{H}_r$ (cal/cm^2-sec)
0.17 msec	1321	1747
0.4 "	1100	1027
1.0 "	645	633.5
4.0 "	432	319.1
10.0 "	238	212.3
40.0 "	129	126.9
100.0 "	96	97.91
250.0 "	79	80.64
1.0 sec	68.4	66.83
4.0 "	64.1	60.53
10.0 "	62.1	58.39

TABLE XI

Comparison of Experimental and Theoretical Threshold Retinal Irradiance

0.45° Cone - 0.067 mm Calculated Image Diameter

Exposure Duration	Experimental $\bar{H}_e$ (cal/cm^2-sec)	Theoretical $\bar{H}_r$ (cal/cm^2-sec)
4.0 msec	425.25	384.2
10.0 "	257.19	250.0
20.0 "	180.89	187.3
40.0 "	126.19	145.6
100.0 "	97.35	111.2
250.0 "	87.90	88.37

TABLE XII

Comparison of Experimental and Theoretical Threshold Retinal Irradiance

0.33° Cone - 0.053 mm Calculated Image Diameter

Exposure Duration	Experimental $\bar{H}_r$ (cal/cm^2-sec)	Theoretical $\bar{H}_r$ (cal/cm^2-sec)
1.0 msec	1250	918.1
4.0 "	442	462.8
10.0 "	292	306.9
20.0 "	259	232.0
40.0 "	187	181.2
100.0 "	132	138.2
250.0 "	110	108.7

Average values of retinal exposure $\bar{Q}_r$ and the number of eyes per threshold point for the various exposure times are listed in Table XIII. The curves for $\bar{Q}_r$ (cal/cm^2) versus time are presented in Figure 18 for seven image sizes. This information is presented because the problem of threshold predictions can often be simplified by using $\bar{Q}_r$ rather than $\bar{H}_r$. The values of $\bar{Q}_r$ were found from the relationship--$\bar{Q}_r = \bar{H}_r \times t$.

Several trends can also be seen in Figure 18. For exposure times less than one millisecond, the curves converge toward a value for $\bar{Q}_r \simeq 0.13$ cal/cm^2--quite independent of burn area. For exposure durations greater than one second, there is a reciprocal relationship between $\bar{Q}_r$ and t.

On several occasions, attempts were made to determine whether ophthalmoscopically visible lesions might develop at a later time even though no lesion could be detected five minutes after the exposure. Some animals were examined 24 and 48 hours after exposure and were found to have developed the typical burn lesion in areas that received sub-minimal irradiance for the production of "5-minute burns". Summarizing the results in general, it was found that the 24 and 48 hour thresholds were lower by a factor of 2 to 4. So adequate compensation should be given for predictions involving subthreshold exposures based on the five-minute criterion. The 24 and 48 hour thresholds will be investigated thoroughly at a later date using primates.

TABLE XIII

Summary of Average Retinal Exposure ($\bar{Q}r$) (cal/cm^2) (Using 5-minute criterion)

Image Diameter (mm) \ Exposure Time (sec)	165×10^{-6}	400×10^{-6}	1×10^{-3}	4×10^{-3}	10×10^{-3}	20×10^{-3}	40×10^{-3}	100×10^{-3}	250×10^{-3}	1	4	10	30	100
0.053			1.25 [4]	1.77 [11]	2.92 [12]	5.18 [12]	7.52 [12]	13.2 [12]	27.5 [12]					
0.067	0			1.70 [10]	2.57 [10]	3.62 [10]	5.05 [11]	9.74 [11]	21.8 [11]					
0.09	0.22 [7]	0.44 [9]	0.65 [7]	1.75 [7]	2.39 [12]		5.16 [16]	9.60 [16]	19.8 [17]	68.4 [10]	256 [10]	621 [10]		
0.18	0.15 [2]	0.28 [7]		0.38 [3]	0.75 [7]		1.46 [7]	3.05 [8]	7.28 [9]	22.4 [11]	79.2 [11]	189 [11]	537 [6]	1790 [6]
0.26	0.12 [4]	0.20 [11]	0.33 [5]		0.57 [11]		1.28 [11]	2.33 [16]	4.25 [13]	16.1 [12]	57.2 [12]	134 [12]		
0.54	0.13 [2]	0.17 [6]	0.23 [4]		0.50 [7]		0.63 [3]	1.05 [10]	1.88 [11]	6.77 [12]	22.6 [12]	49.3 [12]		
1.08	0.13 [3]	0.13 [6]	0.21 [4]		0.37 [7]		0.55 [6]	0.83 [11]	1.29 [12]	3.91 [11]	12.4 [11]	24.9 [11]		

NOTE: The numbers in the small boxes give the number of rabbit eyes used in obtaining the average retinal exposure ($\bar{Q}r$) listed.

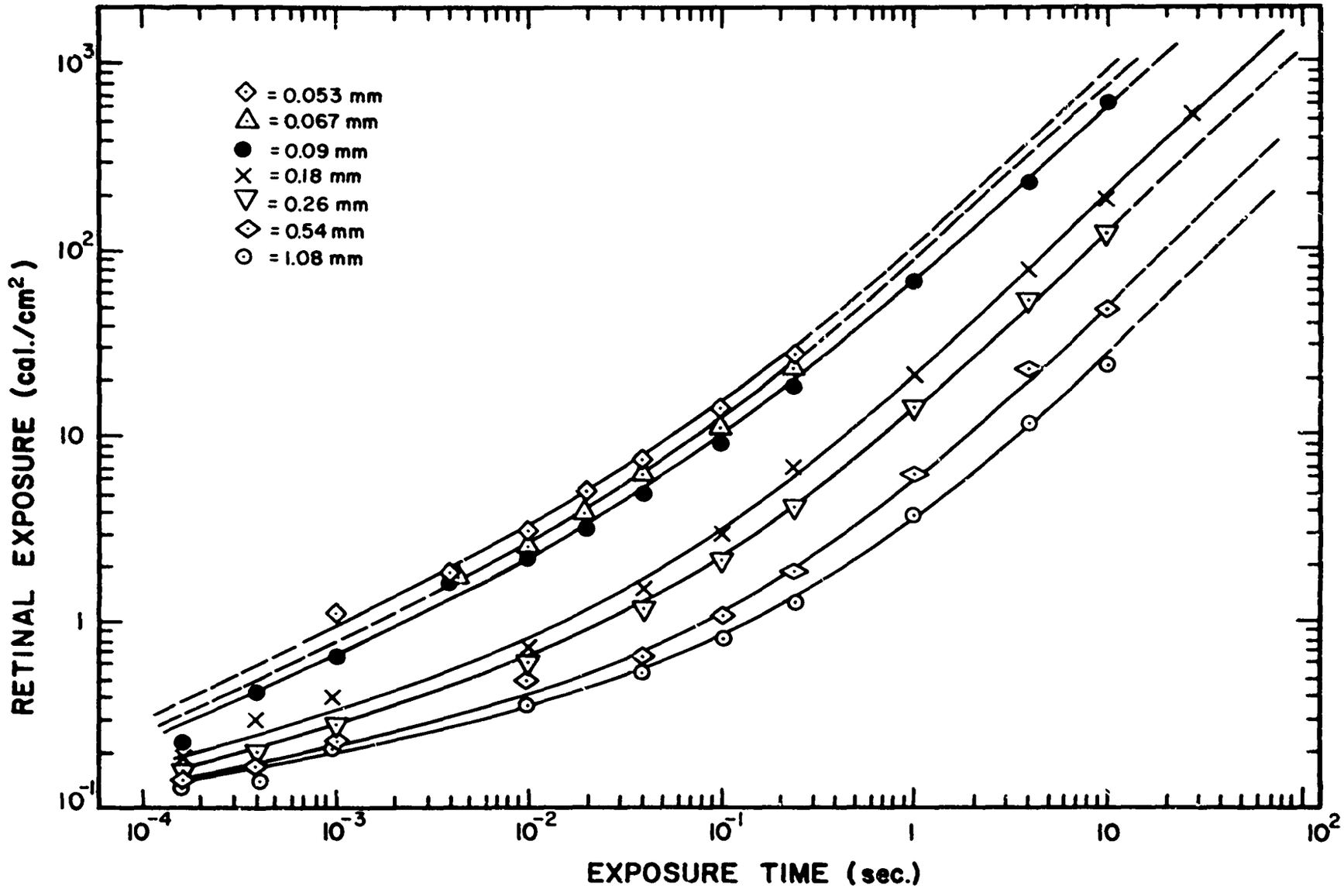

Figure 18 - Average threshold Exposure ($\bar{Q}_r$) versus time for seven image sizes

6. REFERENCES

1. Alexander, T. A., E. R. Lawler, Jr., P. W. Wilson, Jr., and R. I. McDonald. High D. C. Power, Solid-State Switch for Pulsing an Arc Lamp. Review of Sci. Illus., 36 pp. 1707-1709. December 1965.

2. Bessey, R. L., and R. G. Allen, Jr. Calibration of Zeiss Photocoagulator. Final Report of Contract AF41(609)-2906. July 1966.

3. Lawler, E. F., Jr., and W. R. Bruce. Operating Instructions for Modified Zeiss Photocoagulator. Final Report of Contract AF41(609)-2906. July 1966.

4. Alexander, T. A., R. L. Bessey, E. R. Lawler, Jr., W. R. Bruce, and R. G. Allen, Jr. A Study of the Production of Chorioretinal Lesions by Thermal Radiation. Final Report on Contract AF41(609)-2906. July 1966.

5. Alexander, T. A., R. L. Bessey, and E. R. Lawler, Jr. Research for Ocular Effects of Thermal Radiation. Final Report of Contract AF41(609)-2464. Task No. 630103. December 1965.

6. Operating and Service Manuals for:

Hewlitt-Packard - 412A Vacuum Tube Voltmeter

Tektronix - 160 Series Equipment

Zeiss Light Coagulator

Lambda - Model 50 Regulated Power Supply

Kepco - Model KM-255 Power Supply

Beckman - Model 6144 Eput / Timer

Tektronix - Type 551 Dual Beam Oscilloscope and Power Supply

Tektronix - Type C-12 Oscilloscope Camera

II. A PRELIMINARY STUDY OF THE PRODUCTION OF CHORIORETINAL LESIONS BY THERMAL RADIATION IN THE RHESUS MONKEY

by

R. G. Allen, Jr., W. R. Bruce, K. R. Kay, and R. A. Neish

1. INTRODUCTION

The prediction of safe separation distances for the prevention of ocular injury from nuclear detonations depends upon the availibility of a suitable theoretical model of the effect of thermal radiation on the eye. Precise experimental data on burn thresholds are required for the development of a reasonable model. Extensive experimental work has been completed using rabbit eyes for determining the minimum white light irradiance resulting in threshold burns for various exposure parameters. The resulting data provide a sound basis for the general theoretical approach for developing the mathematical model, but leave much to be desired in the realm of predicting damage to human eyes. The present study was undertaken to refine the burn threshold data by using primate eyes which are more similar to human eyes. The rhesus monkey (Macaca mulatta) was chosen for the study.

Threshold data were obtained on the production of 5-minute minimal retinal lesions in monkeys for image sizes of 1.30, 0.64, 0.30, 0.22, and 0.11 mm; with exposure times ranging from 2.5×10^{-1} to 4.0×10^{-3} seconds.

Thermal energy primarily in the visible, was generated with a modified Meyer-Schwickerath photocoagulator (1, 2).

The criteria used to define five-minute minimal retinal lesions were as follows: (1) appearance of an irradiated area with a grey or white center within five minutes after exposure, (2) edema, pigment bleaching or non-appearance of a similar lesion within five minutes at an irradiance of approximately two percent lower.

2. EQUIPMENT

The modified Meyer-Schwickerath photocoagulator (1, 2) was the instrument used for producing chorioretinal lesions. Further modifications were included to have an iris capability of 174 possible positions. A Nikon portable camera and a Zeiss fundus camera were used to photograph the internal eye.

3. EXPERIMENTAL PROCEDURES

The cycloplegic agent employed was cyclopentolate hydrochloride, 1% ophthalmic solution. Three different anesthetics were used for preparation of the monkeys. One anesthetic was thorazine hydrochloride; and another was Sernylan* (3), administered intramuscularly. These were found to be effective tranquilizers and the eyes were self-lubricating

*Park Davis Co., Detroit, Michigan.

but eye movement was not arrested. The third anesthetic was thiopental sodium and normal saline intravenously until the monkey was completely anethetized, but the eyes were not self-lubricating and irrigation with normal saline was necessary. There was less eye movement under deep anesthesia but further investigation is necessary for elimination of eye movement by an anesthetic or a combination of anesthetics.

When anesthetized and with maximum pupillary dilation, the monkey was placed in a restraining chair (Figure 19) for irradiation. A sketch of the retina was made and all irradiated areas recorded. The image field diaphram was set for a record specific image size and a pulse width selected. The iris diaphram was set for an appropriate attenuation factor. If a lesion was observed within five minutes it was noted and the attenuation factor increased in steps of 2% until no lesion appeared within that period. Some animals were observed for eight hours and others monitored at twenty-four and forty-eight hour intervals. Threshold lesions were found in the long term observations which were at significantly lower values than those found in the normal five-minute observation period.

4. EXPERIMENTAL RESULTS

The data collected are listed in Tables XIV-XVIII and are shown plotted in Figure 20 as average threshold irradiance ($\bar{H}_r$) versus exposure duration time. The curves in Figure 20 are merely a tentative attempt

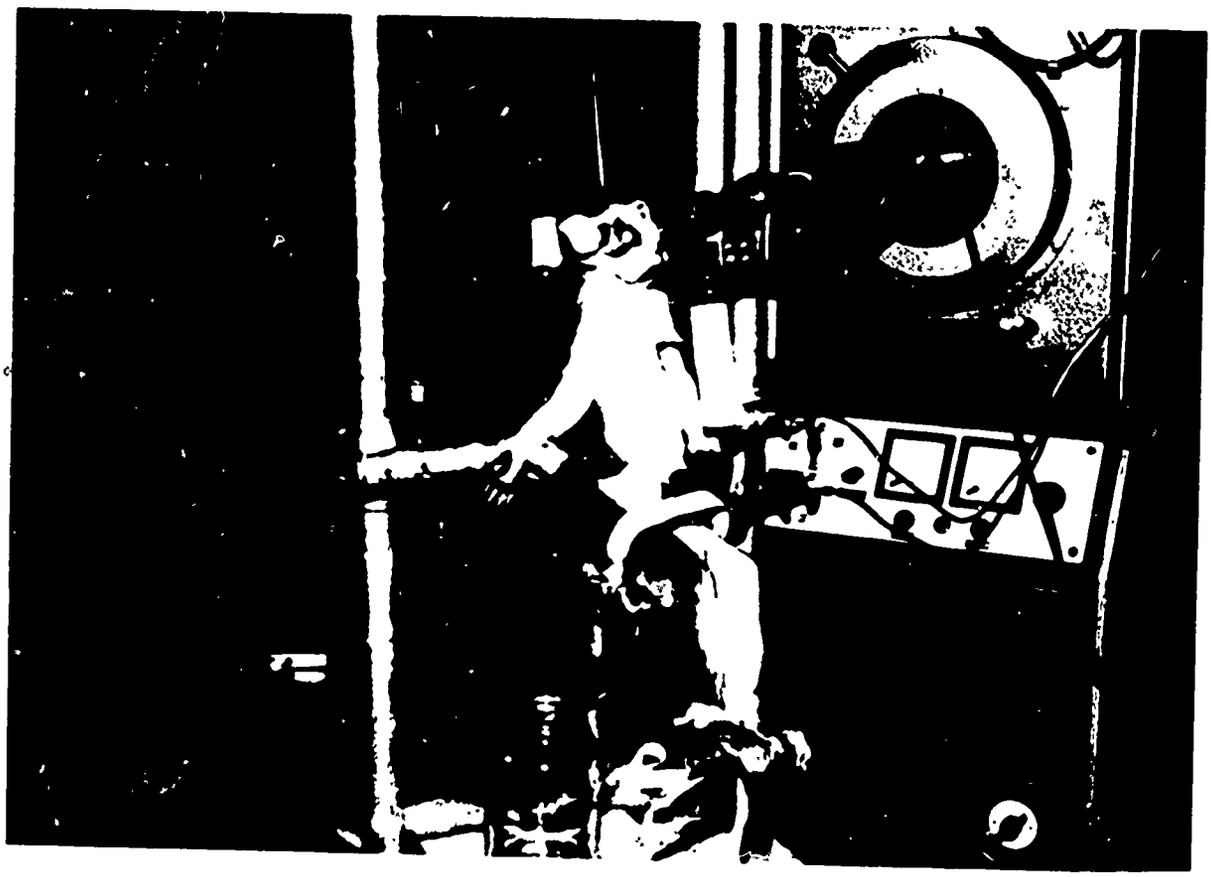

Figure 19

Monkey restraining apparatus

TABLE XIV - Retinal Irradiance for the Production of 5 Minute Minimal Burns in Rhesus Monkeys

A. 1.30 mm Image Diameter (Nominal 6.20° Light Cone from Zeiss Coagulator)

$\bar{H}_r$ (cal/cm^2-sec)

MONKEY NO.	EXPOSURE TIME 2.5×10^{-1}	1.0×10^{-1}	4.0×10^{-2}	2.0×10^{-2}
2 P7 R	13.56	21.88	49.65	71.38
2 P7 L	12.19	21.88		
4 P1 R	12.93	23.19	50.37	69.89
4 P1 L	14.42	19.42	42.64	69.89
AVERAGE $\bar{H}_r$	13.28	21.59	47.55	70.38
AVERAGE $\bar{Q}_r$	3.32	2.16	1.88	1.41

TABLE XV - Retinal Irradiance for the Production of 5 Minute Minimal Burns in Rhesus Monkeys

A. 0.64 mm Image Diameter (Nominal 3.07° Light Cone from Zeiss Coagulator)

$\bar{H}_r$ (cal/cm^2-sec)

	EXPOSURE TIME					
MONKEY NO.	2.5×10^{-1}	1.0×10^{-1}	4.0×10^{-2}	2.0×10^{-2}	1.0×10^{-2}	4.0×10^{-3}
9M8 R		26.49				
9M8 L		21.63				
0A7 R		23.65	43.08			
0A7 L		26.49	40.18			
0P5 R	17.84				107.71	
0P5 L	19.89	21.43	45.53	82.71		
5P3 R	20.19	20.19	38.77	80.00	111.08	121.66
5P3 L			38.77			
6P3 R	18.34	22.22	41.40	78.06	104.89	
6P3 L		19.43	39.42			
7P3 R	15.69	19.70	39.97	76.21	109.56	118.64
AVERAGE $\bar{H}_r$	18.39	22.35	40.89	79.24	108.31	120.15
AVERAGE $\bar{Q}_r$	4.60	2.24	1.64	1.58	1.08	0.48

TABLE XVI - Retinal Irradiance for the Production of 5 Minute Minimal Burns in Rhesus Monkeys

A. 0.31 mm Image Diameter (Nominal 1.47° Light Cone from Zeiss Coagulator)

$\bar{H}_r$ (cal/cm^2-sec)

	EXPOSURE TIME					
MONKEY NO.	2.5×10^{-1}	1.0×10^{-1}	4.0×10^{-2}	2.0×10^{-2}	1.0×10^{-2}	4.0×10^{-3}
0P3 R	14.98	31.61	29.80	57.23	52.42	
0P3 L	14.98	27.91	33.75	52.42	47.24	
1P9 R	14.37	31.44	33.32	53.89	53.89	
1P9 L	14.37	31.44	33.32	53.89	57.14	
5P5 R	19.19	29.81	33.30	55.41	62.92	83.00
5P5 L				55.41		
6P3 R	19.01	30.31	35.93	58.92	66.1	80.91
6P3 L		28.21	33.61			
AVERAGE $\bar{H}_r$	16.15	30.10	33.29	55.31	56.63	81.95
AVERAGE $\bar{Q}_r$	4.04	3.01	1.33	1.11	0.57	0.33

TABLE XVII- Retinal Irradiance for the Production of 5 Minute Minimal Burns in Rhesus Monkeys

A. 0.22 mm Image Diameter (Nominal 1.05° Light Cone from Zeiss Coagulator)

$\bar{H}_r$ (cal/cm^2-sec)

	EXPOSURE TIME					
MONKEY NO.	2.5×10^{-1}	1.0×10^{-1}	4.0×10^{-2}	2.0×10^{-2}	1.0×10^{-2}	4.0×10^{-3}
6N9 R	32.40	47.79	57.24	84.98	97.06	115.54
4P7 R	31.00	40.33	60.35	86.62	96.99	106.67
7P1 L	33.01	39.13	62.37	86.60	95.81	109.39
AVERAGE $\bar{H}_r$	32.14	42.41	59.98	86.06	96.62	110.53
AVERAGE $\bar{Q}_r$	8.04	4.24	2.40	1.72	0.97	0.44

TABLE XVIII- Retinal Irradiance for the Production of 5 Minute Minimal Burns in Rhesus Monkeys

A. 0.11 mm Image Diameter (Nominal 0.52° Light Cone from Zeiss Coagulator)

$\bar{H}_r$ (cal/cm^2-sec)

	EXPOSURE TIME				
MONKEY NO.	2.5×10^{-1}	1.0×10^{-1}	4.0×10^{-2}	2.0×10^{-2}	1.0×10^{-2}
8M3 R		96.09	99.34	190.54	
6N7 R		118.12			
7N3 R	100.10	109.54	104.11	189.15	249.37
7N3 L	100.10	115.28	109.53	189.15	249.37
8P1 R	106.41	110.08	115.82	181.32	242.00
8P1 L	95.64	104.67	104.67	169.50	227.97
AVERAGE $\bar{H}_r$	100.56	108.96	106.69	183.93	242.17
AVERAGE $\bar{Q}_r$	25.14	10.90	4.27	3.80	2.42

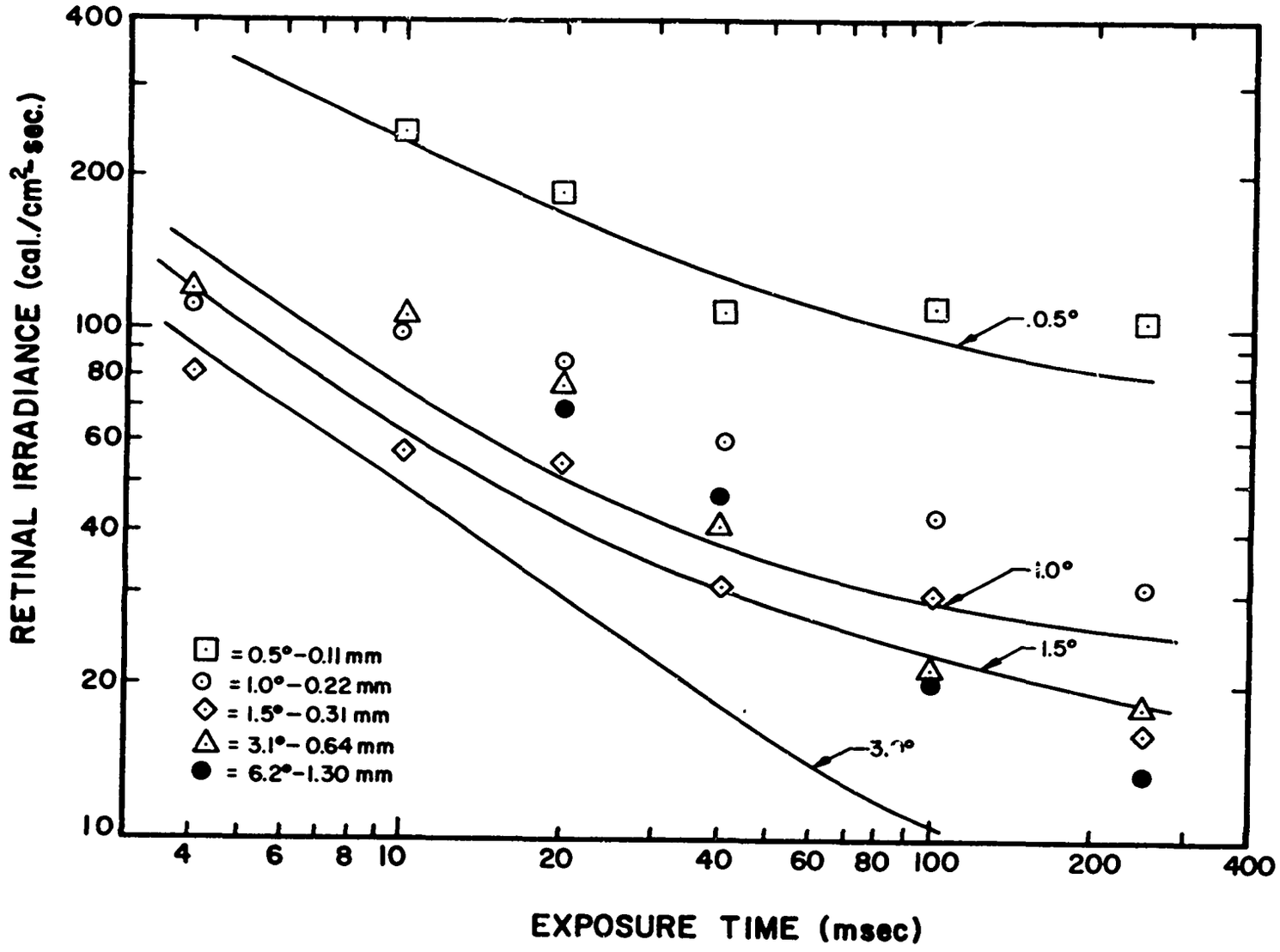

Figure 20 - Average threshold irradiance ($\bar{H}_r$) versus time for four image sizes

to realize an orientation of the pilot data. The data for the 6.20° cone are shown as marked points only. The points were too variable to be connected by a curve. The data are inconsistent with the rabbit data in Part I of this report.but, additional experimental work will be needed before specific comparisons can be made.

The preliminary data on the 48 hour observations are inconclusive at this time. At a later date, experiments will be conducted to determine the minimal detectable threshold for retinal lesions, thereby eliminating the present five-minute observation period.

The foveas of two monkeys were exposed and burns were detected for energy levels considerably lower than the threshold level for the paramacular area. It was determined that (at least for these two animals) the foveal threshold was 2-3 times lower than the paramacular area of the retina.

It must be noted that the data and results presented in this report are of a preliminary nature and are not to be interpreted as conclusive at this time. The final conclusions must be reserved until more data are obtained in the laboratory.

5. REFERENCES

1. Alexander, T. A., R. L. Bessey, and E. R. Lawler, Jr. Research for Ocular Effects of Thermal Radiation. Final Report on Contract AF41(609)-2464.

2. Alexander, T. A., E. R. Lawler, Jr., P. W. Wilson, Jr., and R. I. McDonald. High D.C. Power Solid State Switch for Pulsing an Arc Lamp. Review of Scientific Instruments, Vol. 36, No. 12, pp. 1707-1709. December 1965.

3. Vassiliadis, A., R. C. Rosan, R. R. Peabody, H. C. Zweng and R. C. Norney. "Investigation of Retinal Damage Using a Q-Switched Ruby Laser." Special Technical Report, Standford Research Institute Project 5571, Contract AF33(615)-3060, Menlo Park, California, August 1966.

III. FLUORESCENCE ANGIOGRAPHY OF CHORIORETINAL LESIONS BY THERMAL RADIATION

by

W. A. Newsom, M.D., Captain USAF, MC*, W. R. Bruce,
R. A. Neish, and K. R. Kay

1. INTRODUCTION

During the course of the retinal burn study conducted by the Life Sciences Division of Technology Incorporated, the burn criterion has been the appearance of a visible lesion in the animal retina. (1, 2) The major portion of the study has been conducted using rabbits as the experimental animals. It is possible that functional damage occurs at a level of irradiance below that required to produce an ophthalmoscopically visible lesion. Preliminary investigations employing fluorescence angiography were undertaken to determine if physiological damage at an exposure level below the 5 minute burn threshold could be readily detected. Dollery et al, (3), Weidenthal and Plotkin (4) have demonstrated vascular leakage of fluorescein into areas of lesions.

2. EQUIPMENT

The Zeiss photocoagulator modified and calibrated by Bessey and Allen (2) was used to produce chorioretinal lesions. A modified

*Ophthalmology Branch USAF School of Aerospace Medicine
Aerospace Medical Division (AFSC) Brooks Air Force Base, Texas

Zeiss Fundus camera, instrumented according to the methods of Allen et al. (5) was used for fluorescence photography. A Kodak 47A fluorescein exciting filter was inserted in the light beam and a Kodak 15 filter was placed at the film plane. A fast recharge unit paralleled with the Zeiss power supply gave adequate light for rapid sequence photographs. Polaroid photographs were taken using the Vertex adapter and Polaroid 3000 film packs.

3. EXPERIMENTAL PROCEDURES

Both eyes of twelve mixed breed, pigmented rabbits were used in these experiments. A No. 19 intracath was introduced in an ear vein and each rabbit was anesthesized with thiopental sodium (sodium pentothal), relaxed with gallamine triethiodide (flaxedil). Respiration was maintained via a tracheotomy and a Bird Mark 7 respirator. Cyclopentolate hydrochloride (cyclogyl) 1% and penylephrine hydrochloride (neosynephrine) 10% were used for pupillary dilation.

Using the photocoagulator, burns were made inferior to the myelinated nerve fibers of the rabbit's fundus. A large lesion, 1.0 mm dia., was produced by an irradiance of 27.3 cal/cm^2-sec for 2 seconds, which is approximately eight times the energy necessary to produce a minimal lesion. A cluster of small burns placed to the left were 0.18 mm in diameter, and were produced by various levels of irradiance from 21.1 to 27.3 cal/cm^2-sec for thirty seconds. An irradiance

of 20.3 cal/cm^2-sec for thirty seconds in the same area did not produce an ophthalmoscopically detectable lesior.

Baseline photographs were taken of the fundus. One quarter of a cubic centimeter of 5% fluorescein was injected via the intracath and photographs were taken every two to four seconds.

4. RESULTS AND DISCUSSION

4.1 Rabbit Studies

Figures 21 through 26 show the typical fluorescence patterns obtained in rabbit retinas. It should be emphasized that both Figures 25 and 26 were taken after completion of the normal fluorescein cycle and represent residual fluorescein staining not usually found with this technique.

The primary purpose of this work was to determine if any retinal or choroidal changes could be observed by fluorescence angiography in areas that received insufficient energy to produce an opthalmoscopically visible lesion. The authors were unable to demonstrate any such changes in the rabbits. The studies do demonstrate the effect of chorioretinal lesions on the choroidal circulation of the rabbit and some characteristics of the lesions.

Both large and small lesions interrupt the distal choroidal

Figure 21

Four seconds post first injection showing arterial phase of the choroidal circulation. The 1.0 mm lesion being white, reflected considerably more excitation light than the remainder of the retina. There is no filling in the area of the 1.0 mm lesion or the cluster of 0.18 mm burns.

Figure 22

Seven seconds post first injection shows a combined arterial venous phase. Two of the 0.18 mm lesions are now fluorescing as well as the outline of the 1.0 mm lesion, and distal to the 0.18 mm lesions have not received any blood containing fluorescein.

Figure 23

Nine seconds post first injection shows a venous phase. Two more of the 0.18 mm lesions now fluorescing and the area distal to all four of these lesions are now perfused with blood containing fluorescein. More fluorescein has now accumulated around the edge of the 1.0 mm lesion and the area distal to it.

Figure 24

Thirteen seconds post first injection shows a late venous phase. A slight increase in fluorescein accumulation can be seen in the 0.18 mm lesions. A further accumulation of fluorescein in the 1.0 mm lesion is much more prominent and the distal area has decreased in size.

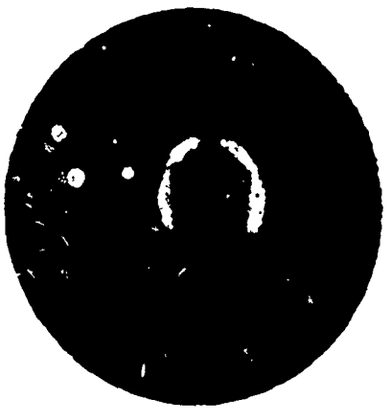

Figure 25

Two minutes, twenty-three seconds post first injection. The four 0.18 mm lesions are still fluorescing. There appears to be some diffusion of fluorescein into the 1.0 mm lesion as well as the rim, with little change in the area distal to it.

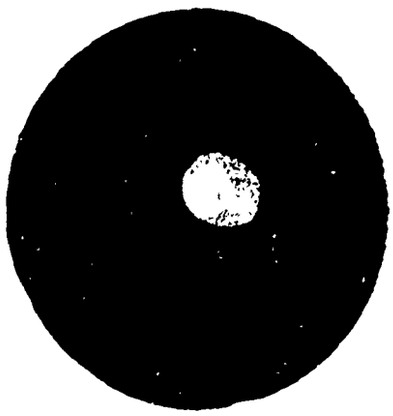

Figure 26

Forty-one minutes post first injection. This shows residual fluorescein staining of the lesions with the rim completely encircling the 1.0 mm lesion. No subminimal irradiated areas can be observed.

circulation by stopping the direct flow of blood through it thus the distal area receives blood supply by collateral circulation. The early fluorescein staining around small lesions and at the rim of the large burns is interpreted as the result of an increase of capillary permeability allowing the fluorescein to leak into these areas.

4.2 Rhesus Monkey and Cat Studies

Preliminary fluorescence angiography was completed using one rhesus monkey and one cat, because of the close similarity to the retinal vascular patterns of man. The irradiance was decreased in steps until the final irradiance level was at least a factor of six below that necessary to produce a visible lesion. It was found fluorescing of the irradiated area occured at a factor of approximately 2 below the level of a minimal visible lesion.

Experiments are in progress using the rhesus monkey to determine the validity of the preliminary studies. If the preliminary findings are valid, fluorescence angiography may be important in detecting subminimal lesions in primates.

5. REFERENCES

1. Ham, William T., Jr., H. Weisinger, Dupont Guerry III, F. H. Schmidt, R. C. Williams, R. S. Ruffin and M. C. Shaffer. Experimental Production of Flash Burns in the Rabbit Retina. Am. J. Ophth. 43:711, 1957.

2. Alexander, T. A., R. G. Allen, Jr., R. L. Bessey, W. R. Bruce, E. R. Lawler, Jr., and C. A. Polaski. Research on Ocular Effects Produced by Thermal Radiation. Progress Report, Contract AF41(609)-2906, Life Sciences Division, Technology Inc., July 1966.

3. Dollery, C. T., E. M. Kohner, J. W. Paterson and P. S. Romaloho. Immediate and Delayed Retinal Vascular Changes Following Exposure to High Intensity Light. Presented at the 17th Meeting of the Aerospace Medical Panel of the Advisory Group for Aerospace Research and Development (NATO) 17-20 April 1961, Lisbon, Portugal. (Dept. of Medicine, Postrgraduate Medical School, Ducane Road, London, W.12)

4. Weidenthal, Daniel and Jack Plotkin. A Fluorescein Study of Fundus Photocoagulation in the Rabbit. A.M.A. Arch. Ophth. 76:7;6. 1966.

5. Allen, Lee, W. H. Kirkendall, W. B. Snyder, and O. Frazier. Instant Positive Photographs and Sterograms of Ocular Fundus Fluorescence. A.M.A. Arch. Ophth. 75:192, 1966.

IV. DEVELOPMENT OF A LASER SYSTEM FOR THE STUDY OF CHORIORETINAL BURNS

by

Charles A. Polaski

1. INTRODUCTION

A maser Optics Model 868 Ruby Laser was adapted for use in the study of retinal burns. This laser is capable of a nominal output of 100 j in a half inch diameter beam. The modifications and additions performed to adapt the laser for retinal burns consisted of the design and construction of a lens system to control and direct the light, control circuit modifications and additions to provide an over-temperature cut-out and remote control of the laser, and construction of a water cooling and treatment system. A system to provide Q-switched operation of the laser was also designed and developed. Investigation of a system to provide light pulses in the region from 1 msec to 100 nsec was carried out with promising results. The finished system was calibrated and preliminary studies of chorioretinal burns produced with the system were conducted.

2. SYSTEM DESIGN

The laser purchased was a general research type and extensive modifications were necessary to adapt the laser for use in producing

retinal burns. As purchased, there was no control of beam size and energy could be varied only with the charging voltage. Also, the parallel beam introduced into the eye would be focused to a very small spot on the retina. A system was therefore designed with the laser as the light source. Requirements of this system were reproducible, independent control of retinal spot size, exposure, and spot positioning. The control system was also modified extensively to provide safer and easier control of the laser.

A Q-switching system was designed and built by Technology Incorporated to provide light pulses in the nanosecond region and the possibility of obtaining pulses or pulse trains in the region from 1 millisecond to 100 nanoseconds was investigated. The results of this investigation were very encouraging.

2.1 Optical System

The optical system shown schematically in Figure 27 provides independent control of the retinal exposure and the diameter of the retinal spot size. The aperture selects a portion of the laser beam which then strikes the first lens. The diverging portion of the beam is intercepted by the exposure control lens and, depending on the lens position, is rendered more or less diverging. Approximately 1.5 meters away, the Spot Size Control iris diaphragm selects a portion of the beam. This controls the size beam presented to the eye piece lens and thus the

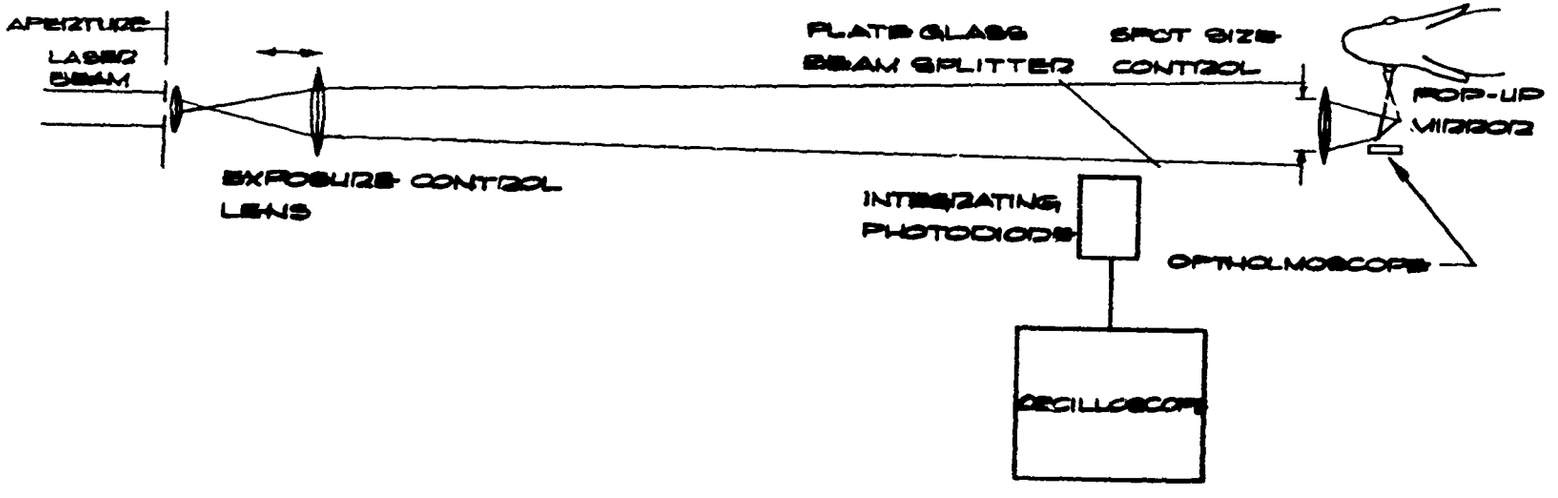

Figure 27

Schematic diagram of lens system

cone angle of the output beam. Controlling the cone angle provides a control of the spot formed on the retina by the eye lens. The plate glass beam splitter reflects about 10% of the beam into a permanently mounted photodiode to monitor each laser pulse. The photodiode output is integrated electronically and the integrator output is proportional to the total energy density in the beam. A beam positioning device is mounted on the end of the lens tube following the last lens. This device consists of a modified ophthalmoscope head geared to a solenoid operated pop-up mirror. The ophthalmoscope reticle is used to locate the burn position on the retina. When the "Fire" button is pressed, the mirror pops up and actuates the laser, deflecting the laser beam into the eye. Very good alignment of the locating light and laser beam has been obtained. The entire laser head and lens system is mounted rigidly to a machined seven inch "I" beam to provide a stable mount for the light system.

2.2 Control Circuit Modification

The laser control circuit modifications provide a more usable and safer system by placing the control switches within easy reach of the operator and preventing recharging of the laser after a shot is fired. Several other safety features were also added including coincidence fire switches to prevent accidental firing of the laser by "bumping" a switch, an audible tone to warn laboratory personnel when the laser is

ready to fire and an electric shutter to prevent the light from a sporadic discharge from leaving the laser head. The control circuit modifications are shown schematically in Figure 28. The Auxiliary Start, Stop and Fire switches are located in the Auxiliary Control Box, normally placed on the end of the "I" beam near the operator. The ophthalmoscope head and foot switch cables plug directly into the Auxiliary Control Box. Thus, from the operators position, the laser can be charged, fired with or without the pop-up mirror, or the energy dumped without firing the laser.

2.3 Water Treatment System

The water cooling and treatment system supplies recirculated water to the ruby and the two xenon flash lamps. The system, shown schematically in Figure 29, consists of a reservoir, a positive displacement pump, a Cuno particulate filter, a mixed bed demineralizer, a water chiller, and an electronic thermometer shown in Figure 30, that provides a temperature indication and prevents unintentional operation of the laser above a set temperature. The filter and demineralizer keep the cooling water clean and free of minerals which would collect in the flash lamp and ruby water jackets causing a decrease in light pump efficiency and lamp life. The cooler maintains the water at approximately 34°F. This increases the laser output by about 30% over the output at room temperature. This also results in extended flash

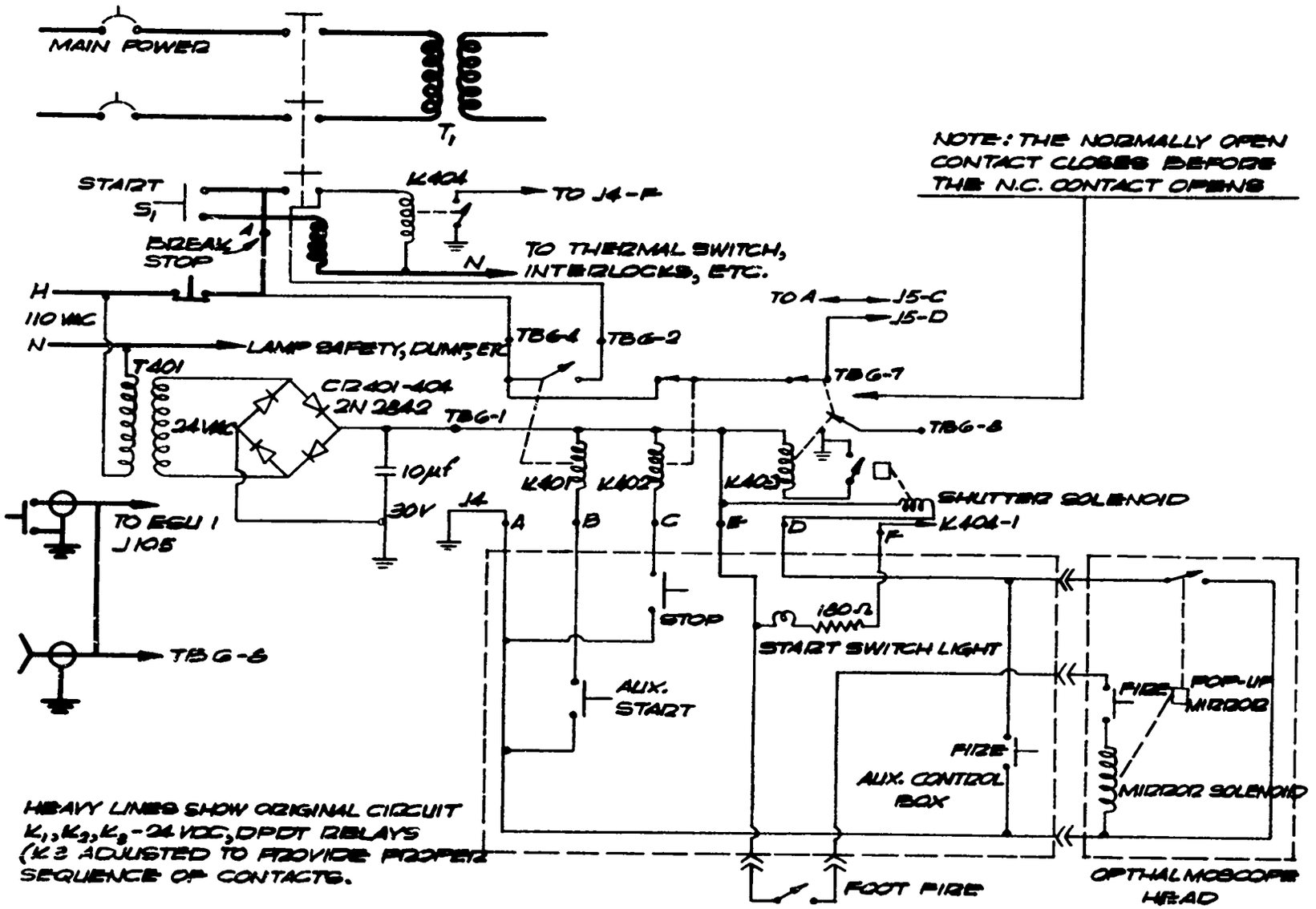

Figure 28

Schematic diagram of control circuit modifications

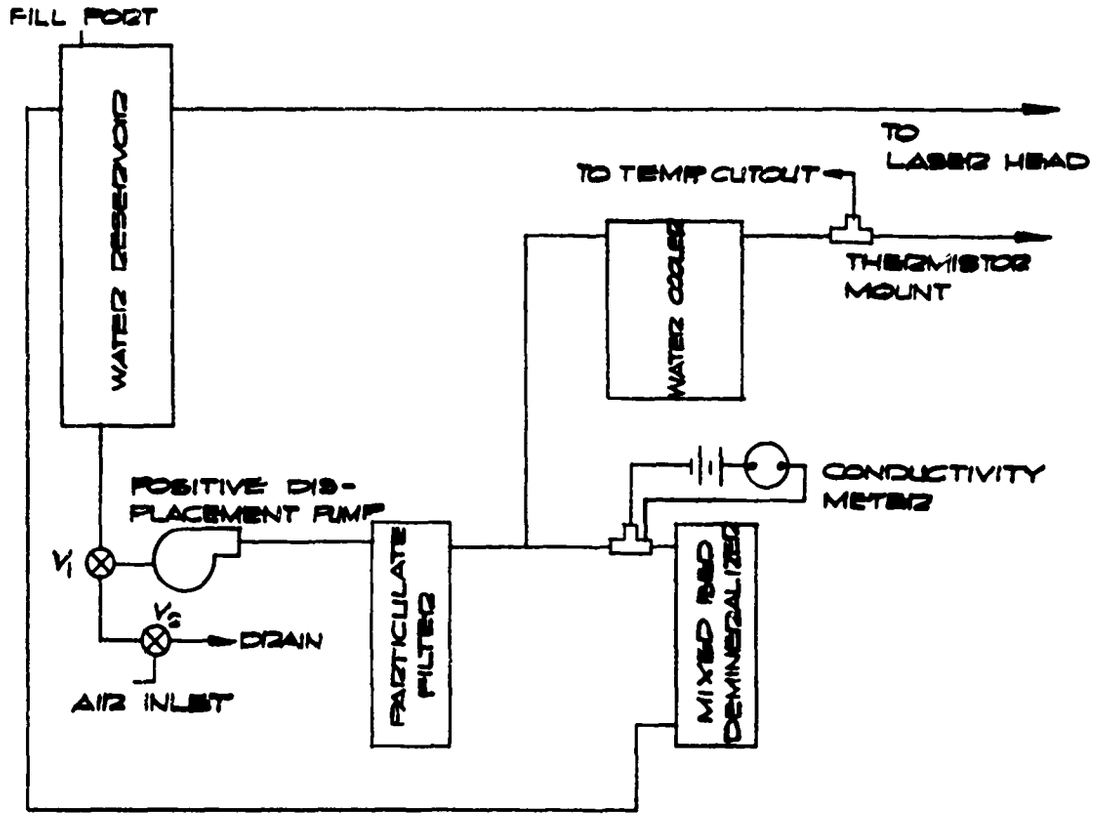

Figure 29

Schematic diagram of Water Treatment System

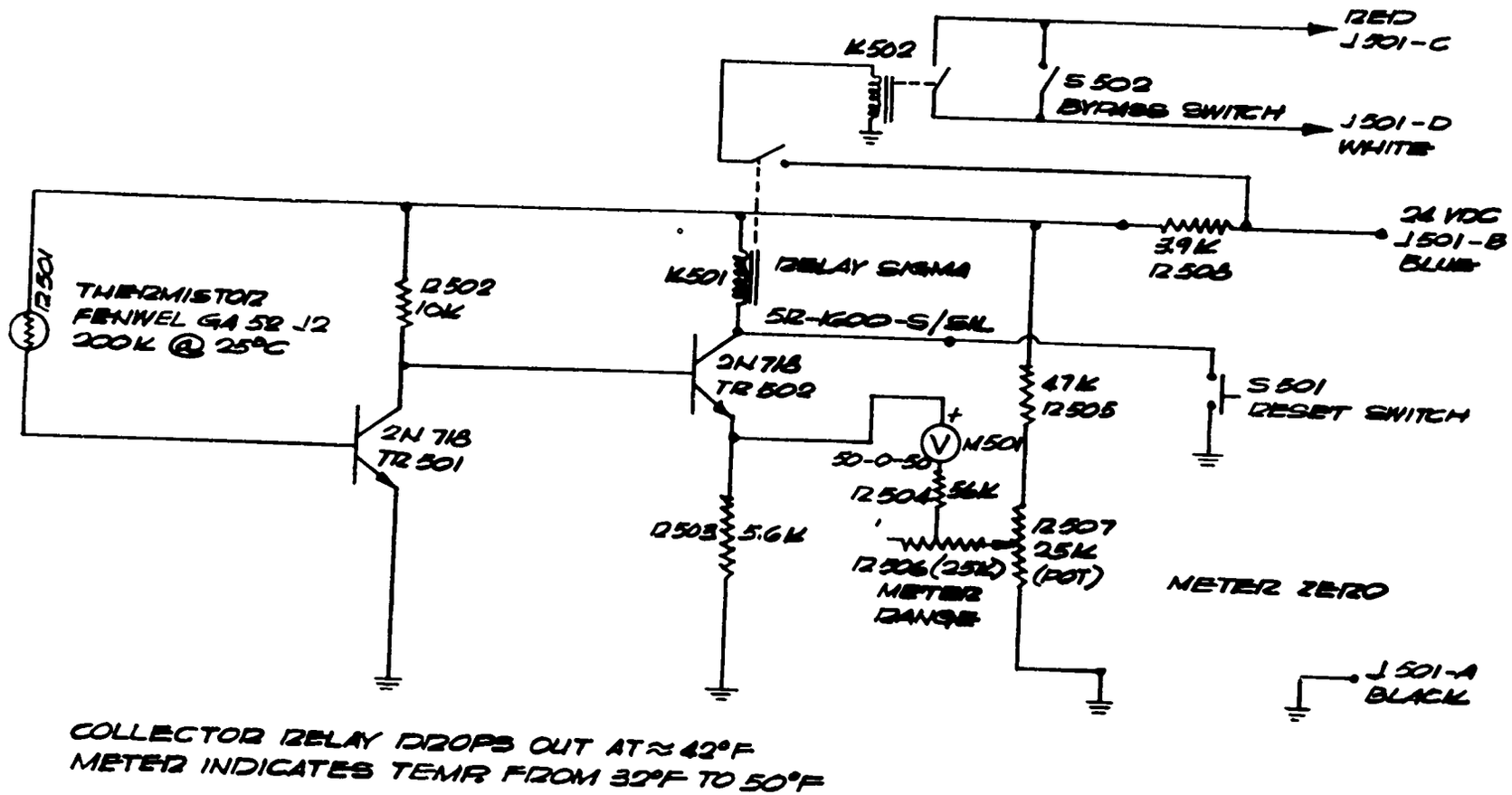

Figure 30

Schematic diagram of Water Temperature Indicator and Cutout Circuit

lamp life and the constant temperature stabilizes the output energy for a given capacitor charging voltage.

2.4 Q-Switched Laser Design

The laser was supplied to operate in the normal lasing mode with an output pulse train width of approximately 2 milliseconds. For this type of operation the mirrors forming the resonant cavity--multilayer dielectric coatings--were applied directly to the ruby ends. The deterioration of these coatings gave a great deal of trouble for about half of the contract period. The last coating applied, while now in need of recoating, has performed quite well.

Operation of the laser in the Q-switched (1) mode was also required to produce exposure times in the nanosecond region but this option was not purchased with the laser. Various methods of Q-switching were investigated and a decision was made to evaluate the passive systems (2) before proceeding to the more costly and complex electro-optical shutter devices. An entire Q-switch laser system is shown in Figure 31. The front reflector is an uncoated Pellicle or membrane beam splitter mounted in a two axis gimble mount. The rear reflector is a TIR prism also mounted in a two axis gimble mount. The switch consists of a bleachable dye--cryptocyanine dissolved in menthanol--contained in a cell with quartz flats on each end.

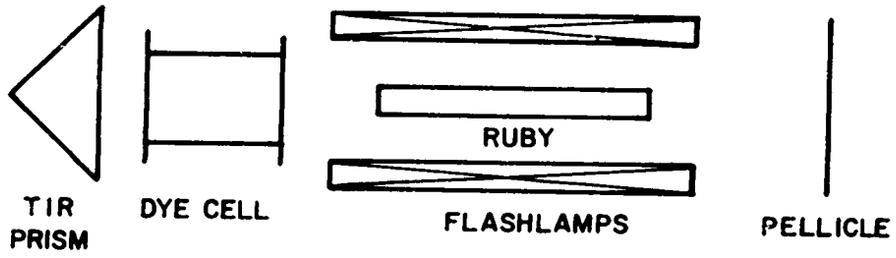

FIGURE 31. Q-switching System

In the normal mode of laser operation, the atomic states of the chromium in the ruby host are elevated by the pump light. After elevation, the atoms decay to a metastable state with no light emitted and then to ground state with the characteristic 6943 Å red light emitted. Until the number of excited atoms is equal to the number of ground state atoms--the threshold level--the dominant action of the system is absorption and little or no light leaves the ruby. When the threshold level is reached, amplification is predominant and "lasing" begins. The light leaving the ruby ends strikes the mirrors and is reflected back into the ruby, stimulating still more atoms to decay in a sort of avalanche. This continues until the pump energy can no longer maintain the atomic population inversion.

In Q-switched operation, the pump cycle is identical to normal lasing but a fast switch or shutter is placed between the ruby and one of the mirrors. The light that escapes the end of the ruby is absorbed by the switch and there is no reflected light to stimulate lasing. When a large number of atoms are excited, the switch is closed and the Q of the cavity is suddenly increased--the Q is switched--allowing the light to be reflected back into the ruby. When the timing of the switch is correct, all of the atoms are stimulated to decay to ground at once producing a single pulse that can be as short as a few nanoseconds. Although the energy is low in Q-switched operation--usually less than 10 joules--the short pulse width yields peak powers in the gigawatt

range (3, 4).

The bleachable dye switch contains a solution that is normally opaque to the laser light. The dye absorbs the photons until a threshold is reached and then very quickly turns transparent.[2] The recovery time of the dye is also very short--several microseconds--making it an ideal light switch for lasers.

Using the system in Figure 31 we have obtained single pulse output 30 nanoseconds wide containing 5 joules or an average power of 166 megawatts. A drawing of the pulse as observed on a Tektronix 519 Oscilloscope is shown in Figure 32.

2.5 Semi-Q-Switched Laser Investigation

A single Q-switched pulse is emitted from the laser when the switch threshold is such that an optimum number of chromium atoms are excited. The switch threshold depends on the dye concentration in the solution. It is thus possible to proceed from normal lasing with no dye in the solution to a sort of semi-Q-switching--several narrow pulses or groups of pulses--with a sub-critical concentration and on to true Q-switching with critical concentration. Concentrations past critical never bleach and all lasing is prevented.

Preliminary tests with sub-critical concentrations of dye indicate it may be possible to obtain pulse trains of shorter width than the

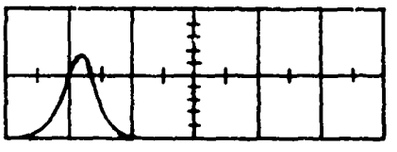

50 NANOSECONDS PER CM.
9.3 VOLTS PER CM.

Figure 32

Oscilloscope trace of Q-switched pulse

millisecond range. The first rod tested was coated anti-reflecting on one end and 40% reflecting on the other. Sub-critical dye concentration with this rod indicated the switch held off lasing for a given time and then bleached allowing normal lasing for the remainder of the pump pulse. The second rod tested was coated anti-reflecting on both ends and the front mirror was the uncoated pellicle. Sub-critical dye concentrations for this rod produced several Q-switched pulses for each pump cycle. These pulses, shown in Figure 33, were very narrow--less than 1 microsecond wide--separated by several hundred microseconds, spread more or less evenly over the pump cycle. Further investigation of this technique may prove successful in producing light pulse widths in the region between 1 millisecond and 100 nanoseconds.

3. LASER CALIBRATION

A cone calorimeter is the laser calibration standard. The calorimeter has been calibrated at National Bureau of Standards, Denver, and is periodically cross calibrated with a Barnes Engineering Thermopile using a standard lamp as the light source. A third method of calibration--probably a liquid calorimeter--will be added at a later date.

In the laser calibration, the calorimeter is positioned so that it collects the entire beam reflected by the pop-up mirror. Thus the total energy of the beam incident on the cornea during the experiment is measured. For a given iris diaphragm setting, the beam cone angle is known

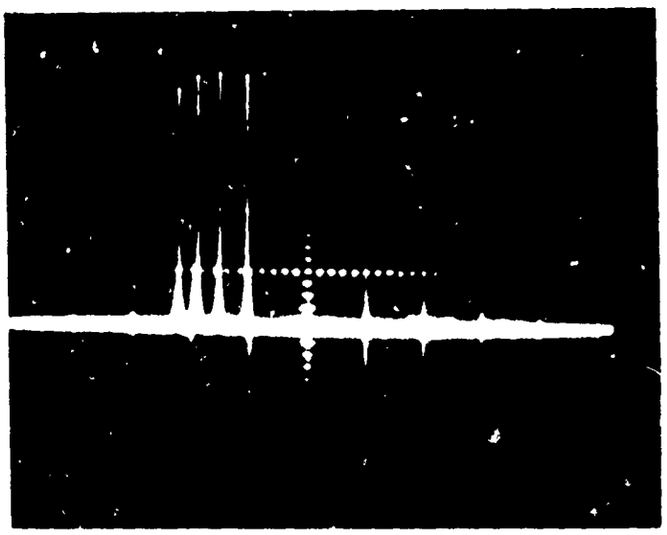

.5 msec/cm

Figure 33

Semi-Q-switched pulse

and the retinal spot can be calculated. Correcting the data for the transmission of the clear media of the eye yields the energy density on the retina.

Because the laser is not an extremely stable device, some method of measuring the energy of each shot during the experiment is necessary. To sample the beam, a plate glass beam splitter and silicon photodiode were installed in the lens tube. Due to the nature of the laser output, it is necessary to electronically integrate the output of the photodiode to obtain an output proportional to the beam energy density.

The calibration compares the measured output energy density with the output of the integrating photodiode. This necessitates two experiments--the measurement of beam cone angle versus the iris diaphragm setting and the measurement of output energy versus the energy density control setting.

3.1 Spot Size Control

In this calibration the beam cone angle versus the diameter of the iris diaphragm controlling the cone angle is measured. The retinal image diameter versus iris diaphragm diameter is then calculated. Equipment necessary for this calibration is:

1. Polaroid Oscilloscope camera back equipped with dark slide
2. Polaroid camera

3. White light field with one inch grid and 1/4 inch tick marks
4. Support for camera back
5. Thin plate glass beam splitter and assortment of neutral density filters.

Figure 34 illustrates the experimental arrangement for this calibration.

1. The plateglass beam splitter is set at 45° to the beam with the beam splitter intercepting the entire beam diameter.
2. The film plane of the Polaroid camera back, with dark slide in place, is set at a distance approximately 20 cm from the end of the lens tube.
3. The laser charging voltage is set to slightly above lasing threshold.
4. Filters are placed in the beam to control the film exposure when the laser is fired. The energy density control is used as a fine adjustment.
5. With the iris opened to maximum diameter, the room is darkened and the film exposed by the laser beam.
6. Step 5 is repeated for various diameters of the iris diaphragm. The spot diameter is recorded for each setting under distance D_1.
7. The film plane is then set at a distance D_2, approximately 30 cm from the end of the lens tube.
8. Steps 5 and 6 are repeated and the diameter of each spot is

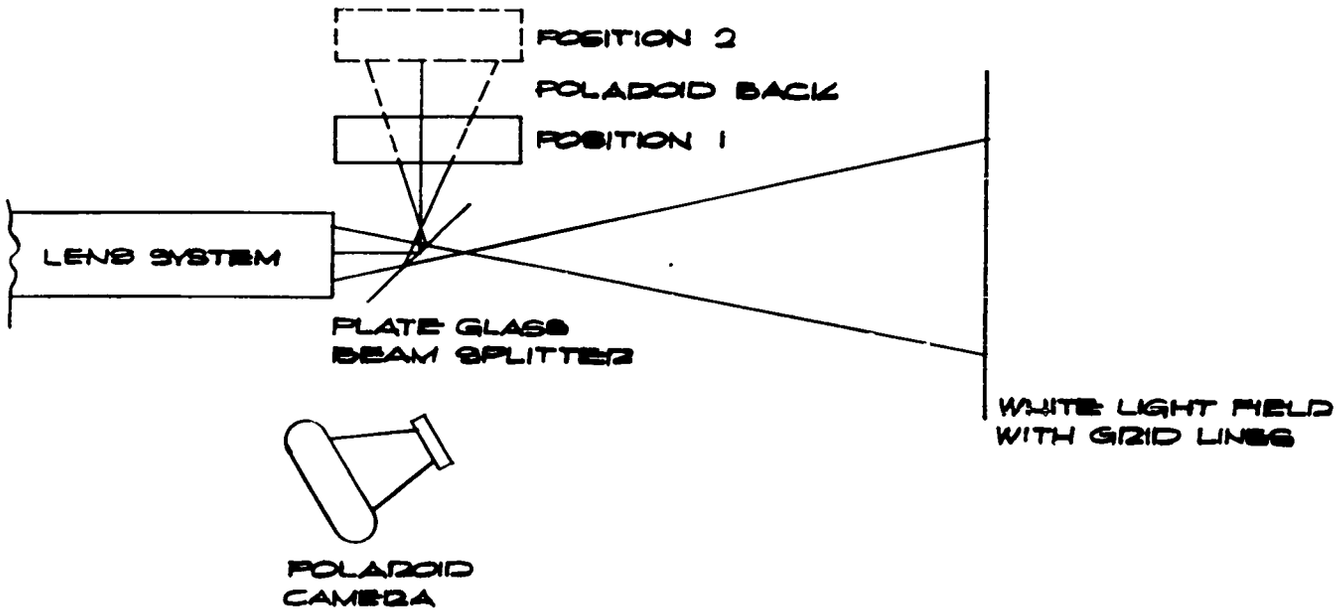

Figure 34

Schematic diagram of equipment arrangement for beam cone angle calibration

recorded under distance D_2.

9. The beam splitter is removed and the white light field placed directly in front of, and approximately 85 cm from the end of the lens tube.

10. A polaroid camera is now used to photograph the laser spot on the light field and the grid marks are used to measure the spot size.

11. Spot photographs are taken for the various iris openings used in the above steps and the spot diameters recorded under distance D_3.

12. Using only the data for the maximum iris opening, the half-angle of the beam is calculated using the equation

$$\theta = \tan^{-1} \frac{d_2 - d_1}{2(D_2 - D_1)}$$

where

d_2 = spot diameter at distance D_2.

d_1 = spot diameter at distance D_1.

θ = beam half angle.

13. Step 12 is repeated for each of the iris diameters.

14. Steps 12 and 13 are repeated for spot diameters at D_1 and D_3, and at D_2 and D_3.

15. Using the average angle, θ, for each iris diameter, the retinal spot diameter is calculated using the equation

$$d = 2f \tan \theta$$

where d is the retinal spot diameter in mm and f is the effective focal length of the eye in mm. We have arbitrarily taken f to be 10 mm.

3.2 Beam Energy Density

With a calibration of the iris diaphragm, the retinal energy density calibration of the integrating photodiode circuit versus position of the lens controlling the energy density may be performed. The calibration assumes that the output beam is homogeneous. In the region of most interest, the beam homogeneity appears to be very good as determined photographically. By making energy measurements for several iris diaphragm settings at the same energy density setting, the energy density measured varies by less than 10% also indicating good homogeneity. Equipment necessary for this calibration is:

1. Oscilloscope equipped with Polaroid camera
2. Calorimeter
3. Microvoltmeter

Figure 35 illustrates the experimental arrangement for this calibration.

1. Using the opthalmoscope light and cross hair, the calorimeter is placed so that the light beam reflected by the pop-up mirror will strike the center of the cone.
2. With the laser charging voltage at the normal operation

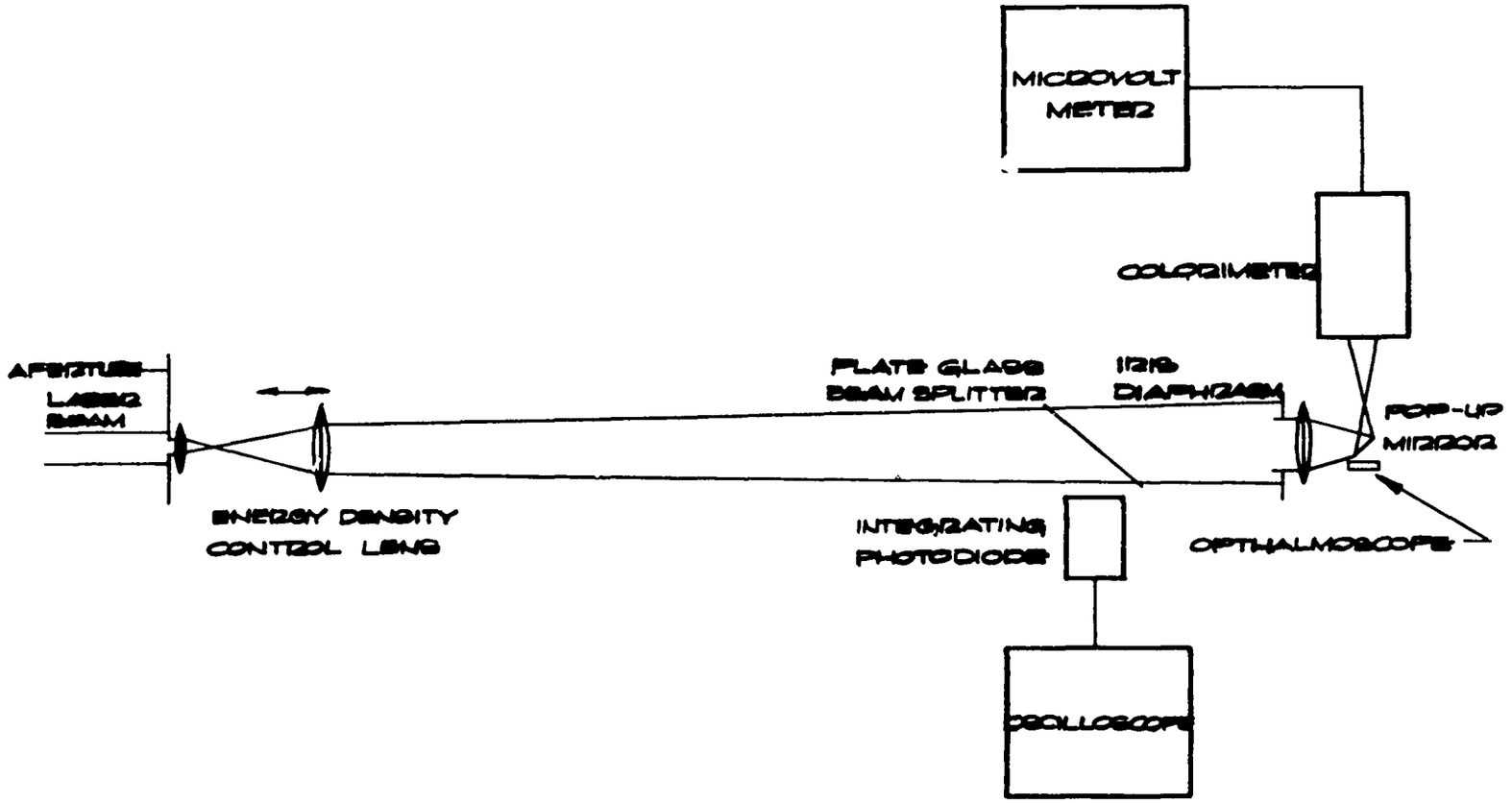

Figure 35

Schematic diagram of equipment arrangement for energy density calibration

position, energy density control at maximum, and iris diaphragm at maximum, the laser is fired and the outputs of the calorimeter and photodiode recorded simulatneously. The peak microvolt reading and the peak integrated photodiode output from the oscilloscope photograph are used.

3. The calibration point of the photodiode for the maximum energy density setting is then given by

$$K_{max} = .9 \frac{V_{cal} C}{A_{max} V_{pd}}$$

where

K_{max} = photodiode calibration constant at maximum energy density settings in $\frac{\text{joules}}{\text{cm}^2 V_{pd}}$ on the retina.

.9 = transmission of clear media of eye at 6943 Å

V_{cal} = peak voltage from microvoltmeter in millivolts

C = calorimeter constant in joules/mv

A_3 = retinal spot area for a Spot Size of 3

V_{pd} = peak integrated photodiode output in volts

4. Steps 2 and 3 are repeated for various other energy density control settings.

5. From this data, the normalized photodiode output, normalized calorimeter output and the photodiode calibration constant K, are plotted versus energy density control settings from maximum to zero.

6. For daily check of the calibration, spot checks at several energy density control settings are made using the above procedure.

4. PRELIMINARY LASER BURN STUDIES

Minimal five minute burns were obtained with the laser system operating in the normal mode. The effective pulse width as shown in Figure 36 was two milliseconds and burns of 1, 0.5, 0.26, and 0.1 mm diameter were studied. These sizes were chosen to permit direct comparison with data from the light coagulator experiments. The same experimental procedures were used with the laser as were used in the light coagulator experiments as described in Part I of this report.

4.1 Results and Discussion

The threshold irradiances are listed by trial in Tables XIV-B and XV-B. The average threshold irradiances as a function of image diameter are shown in Table XIX. This data is plotted in Figure 37 with the best-fit curves from the photocoagulator experiments.

This is reported only as preliminary data due to the small number of data points; however, it is interesting to note that the thresholds do not appear to be size dependent as is the case with the white light from the coagulator.

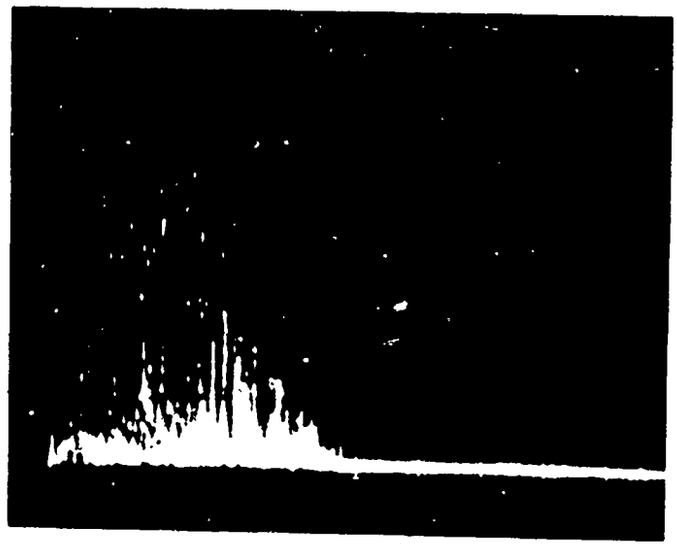

0. 5 milliseconds/cm

Figure 36

Normal lasing pulse

TABLE XIX

Average Laser Burn Thresholds

Retinal Image Diameter mm	$\bar{Q}_r$ J/cm^2	σQ_r	$\bar{H}_r$ $\frac{cal}{cm^2\text{-sec}}$	σH_r
1.0	1.54	.285	192.5	37.1
0.53	1.73	.465	216.5	57
0.26	1.69	.228	212	28.5
0.10	1.81	.40	227	49.4

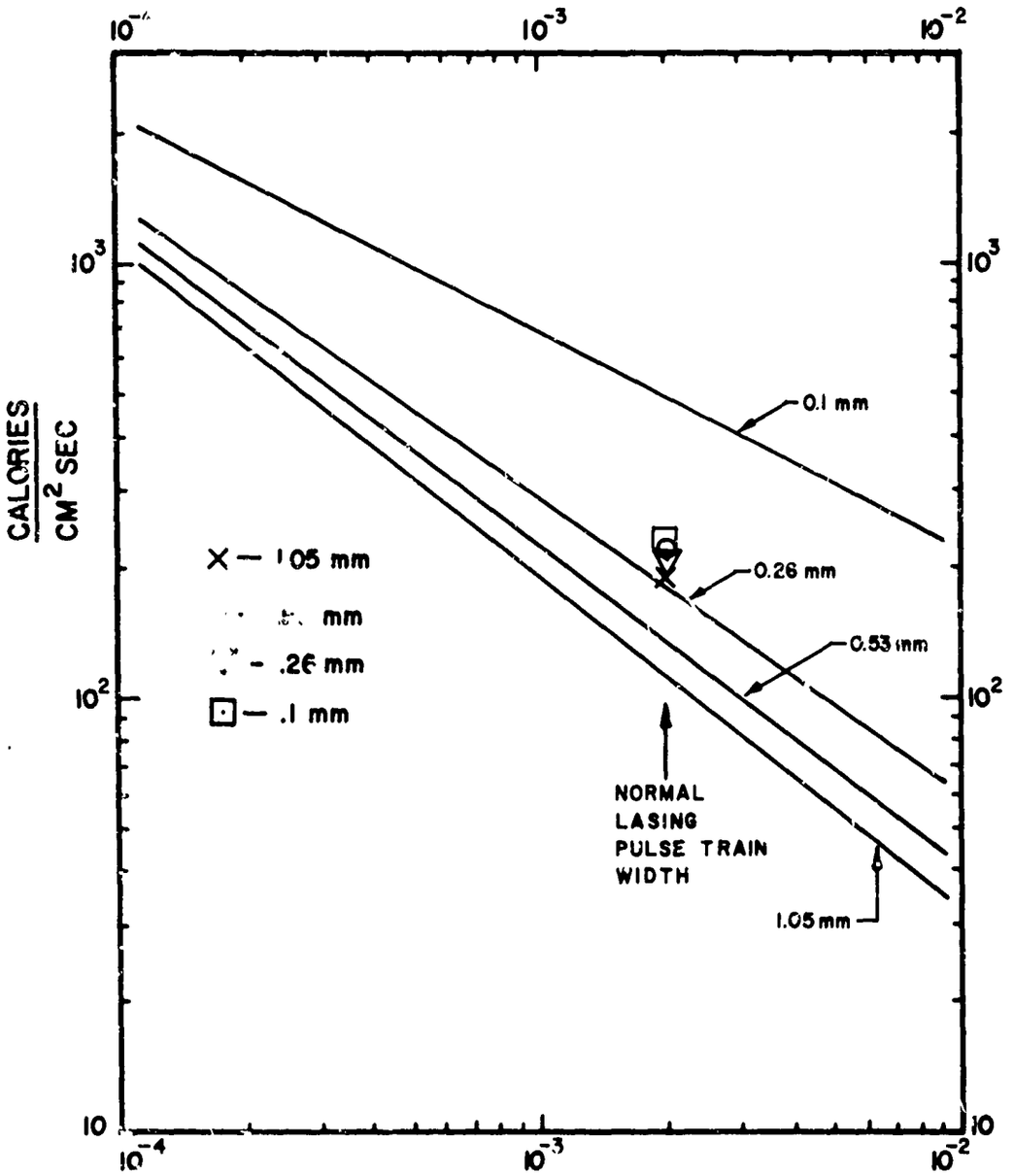

Figure 37

Average threshold irradiances ($\bar{H}_r$) for normal mode laser radiation compared with best fit curves for white light rabbit thresholds

5. REFERENCES

1. Hellwarth, R. W. Advances in Quantum Electronics., J. R. Singer, Ed. (Columbia Univ. Press, New York, 1961) p. 334.

2. Hull, D. Combination Laser Q-Switch Using a Spinning Mirror and Saturable Dye Applied Optics, Vol. 5, No. 8, August 1966.

3. Schawlow, A. L. Lasers. Science, Vol. 149, No. 3679. July 1965.

4. De Maria, A. J., et al. Ultra Short Light Pulses. Science, Vol. 156, No. 3782. June 1967.

V. CONSTRUCTION OF A FLASHBLINDNESS TESTING APPARATUS

by

Larry K. Morrison and Ransom A. Richards

1. INTRODUCTION

The hazard presented by exposure to unusually high luminance flashes of light, such as those produced by nuclear weapons and lasers, has indicated the need for precise knowledge of the maximum safe energy levels for the visual system (1, 2). Two different levels of damage need to be investigated: (1) permanent damage resulting in loss of function in the retinal area exposed, and (2) temporary damage exhibited by an elevated contrast threshold or reduced sensitivity for visual tasks immediately following the flashes. The first type of damage has been studied with experimental animals to determine the energy levels associated with threshold burns (3). The second type can be investigated through controlled experiments with human subjects. The important parameter in the flashblindness, or temporary damage range, is the time required to perform specified visual tasks after receiving a flash exposure (4-7).

The work covered by this report was directed toward the design and construction of a flashblindness test apparatus for the investigation of visual recovery following high intensity light flashes. The apparatus design allows controlled flashes of various durations and luminances to be delivered either monocularly or binocularly. A variety of visual

tasks can be presented over a range of luminance levels for testing the recovery time following the flashes. Provision has been made for a full range of preadaptation levels prior to the flashes. The apparatus has been fully automated to record both flash conditions and recovery time measurements for 10 luminance levels for each exposure.

2. DESIGN AND CONSTRUCTION OF EQUIPMENT

2.1 Optical System

The test equipment was designed to present 10° flash field in maxwellian view for variable exposure durations between 10° and 1 second at luminances from 1.8×10^9 cd/cm^2 to 1.8×10^5 cd/cm^2 respectively at the source. The source is a xenon short-arc lamp supplied by Vitro Laboratories. The power supply for the lamp is rechargeable batteries for pulse lengths from 10 msec to 1 sec and a capacitor bank for durations between 10 μsec and 10 msec. For the long durations the pulse shape is square; while for the shorter durations, it has the shape of a half sine wave.

Durations can also be controlled by a rotating mirror. This system consists of a Lourdes 16,500 RPM centrifuge motor, a 6" cylindrical aluminum mirror table, slotted to receive a 1/2 inch stainless steel mirror. The centrifuge motor is able to turn the mirror up to 11,000 RPM.

Auxiliary elements of the optical system provide a fixation target and/or an adaptation light source, and a visual task system which presents various visual tasks at different luminance levels. A photograph of the system is shown in Figure 38.

The 5' x 6' x 7' subject booth was constructed of plywood, fiber board, and insulation to minimize extraneous noise to the subject. Minimal openings were then made in the booth to allow the light beam and optic bench to enter. The optic bench was made from 6" steel H-beams, welded to fit the optic paths. Both top and bottom surfaces were ground parallel and were given a No. 63 finish. The optic bench rests upon a table, having a top of a 5' x 5' x 1/4" steel plate on cross-braced 2" pipe legs and a 3" angle iron framework.

The flashblindness optical system as shown in Figure 39 consists of three main sections containing: 1) the primary light source, 2) the pre-adaptation and fixation light source, and 3) the visual tasks.

The flash source S_1 is focused on the entrance aperture A_1 with a short focal length lens such that it completely fills the aperture. Aperture A_1 is then the uniformly bright object for anastigmat L_1, which collimates the light for reflection from the rotating mirror M_1, through a second identical anastigmat L_2 which focuses the beam onto the second aperture A_2 with unity magnification.

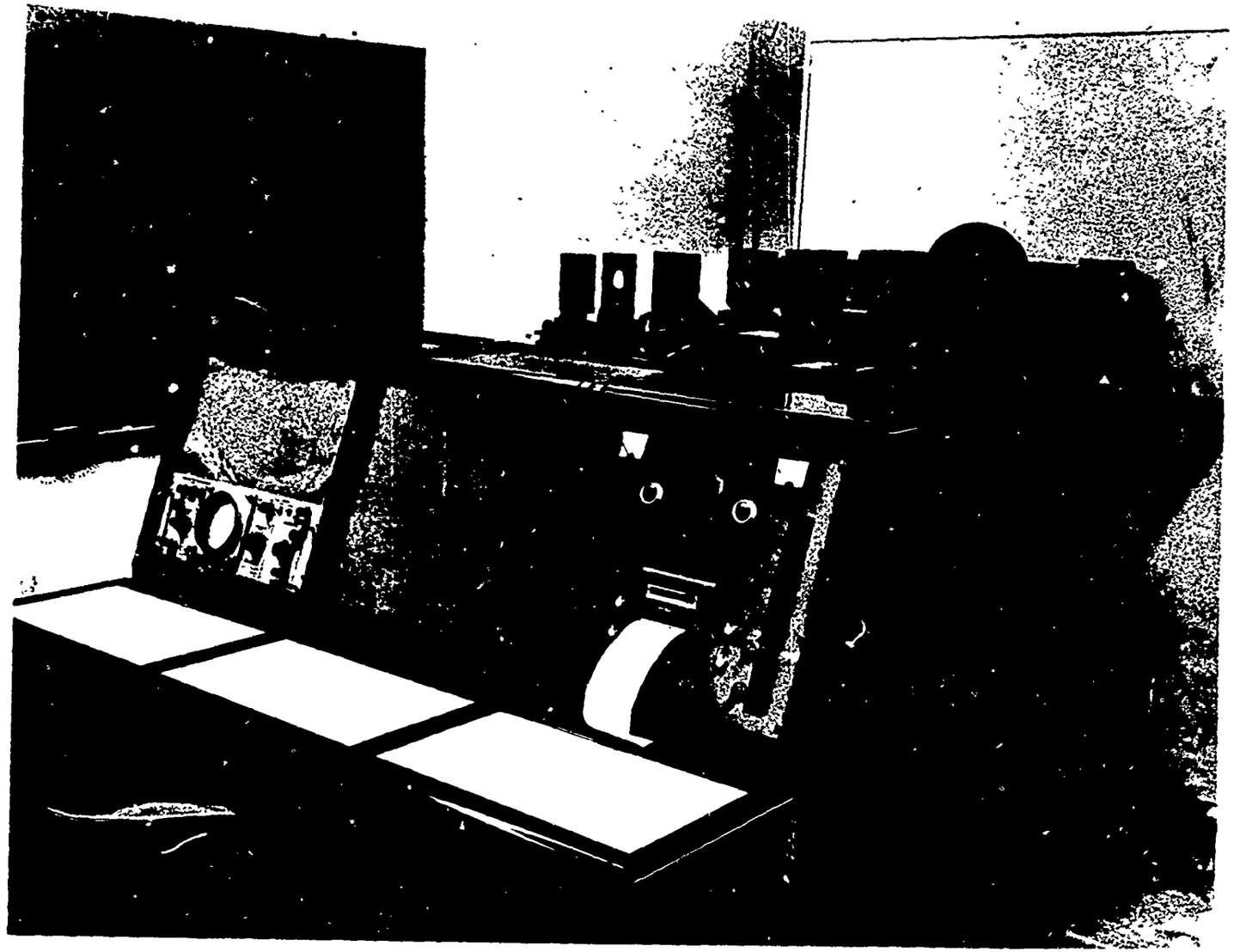

Figure 38 - Photograph of flashblindness system

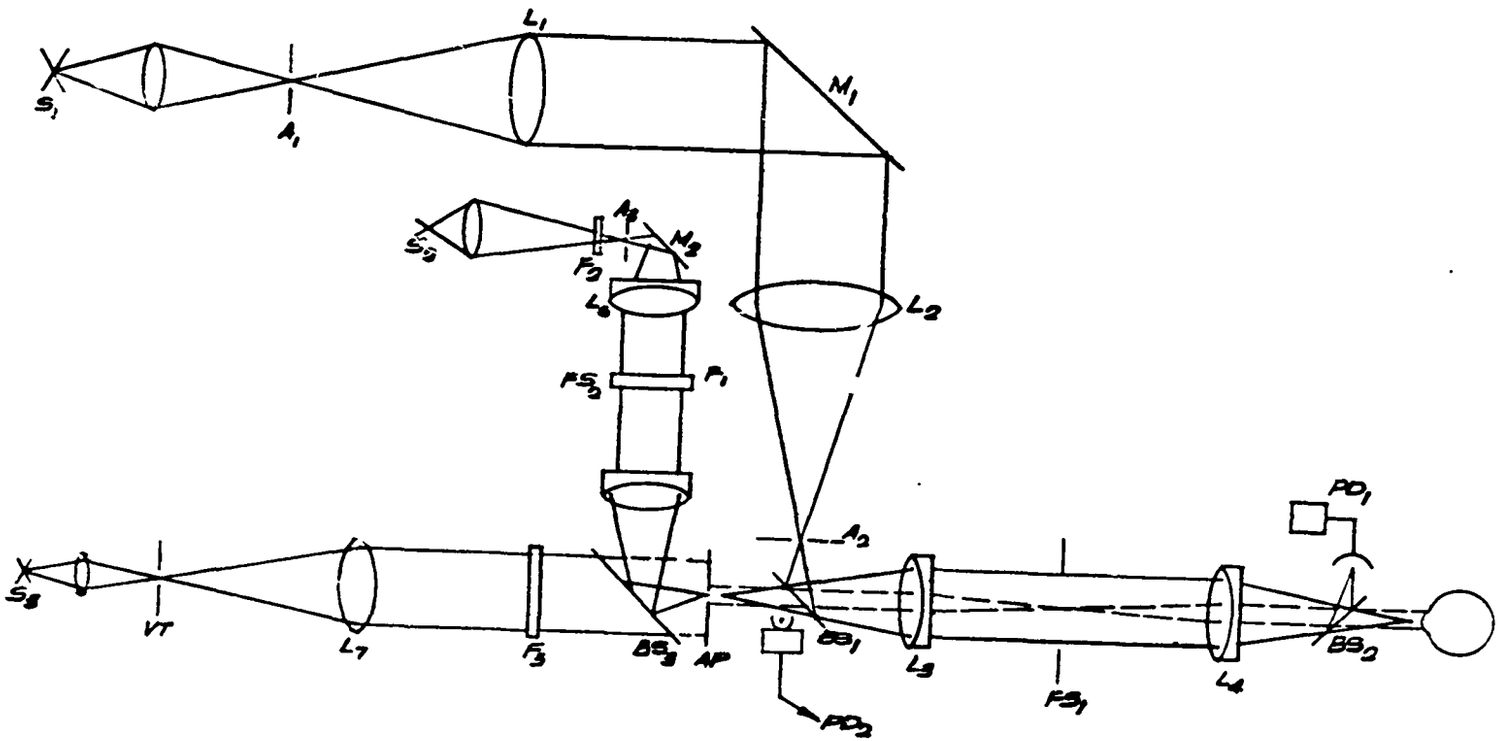

$S_{1,2,3}$ — LIGHT SOURCES
$A_{1,2,3}$ — APERATURES
$L_{1,2,3,4,5,6,7}$ — LENSES
$BS_{1,2,3}$ — BEAMSPLITERS
$FS_{1,2}$ — FIELD STOPS

$F_{1,2,3}$ — FILTERS
$M_{1,2}$ — MIRRORS
VT — VISUAL TASK
AP — ARTIFICIAL PUPIL
$PD_{1,2}$ — PHOTODIODES

Figure 39

Schematic drawing of the flashblindness optical system

Aperture A_2 is the object of a maxwellian view system consisting of two achromats and a field stop. Light from the aperture is reflected from 82% reflectance beam splitter BS_1 and collimated by the first achromat L_3 passing through a field stop FS_2, into the second achromat L_4, and is brought to focus at the entrance pupil of the subject's eye, with unity magnification. Correct alignment of the head is maintained by a biteplate and forehead rest. Head adjustments can be made in three mutually perpendicular directions.

Pre-flash subject orientation is accomplished by aligning the head such that the maxwelliam view system in the fixation element L_5, FS_2, L_6, presents a 10° field of view and appears uniform. The primary flash is then presented simultaneously with the visual task.

The visual task element consists of transilluminated letters, Z, H, K, R, N, C, imaged at a 2:1 reduction in the field stop FS_1, of the maxwellian system. The anastigmat L_7 collimates the light beam after which it passes through a 40% transmission beam splitter BS_2, a 9 mm artificial pupil and focused by lens L_3. The subject then views the image at infinity through lens L_4. The letters are held in a 80-slide carousel holder arranged in a random, but pre-determined order. Each letter is presented to the subject for 0.5 seconds. The luminance of the test letters is controlled by inconel neutral density filters arranged around the circumference of a filter wheel. These filter

densities were 0.0, 1.0, 1.50, 2.0, 2.25, 2.50, 2.75, and 3.0. Filters are selected by using a geneva gear to rotate the filter wheel.

2.2 Automation System

The operating circuit for the automatic control of the filter wheel, timers, and print out is shown in Figure 40. At the conclusion of the flash, the Run Relay K12 is energized from a 24v pulse operated by the shutter and holds through its A contacts the B contacts of the Stop-Print Relay K14. The K12 B contacts feed out through terminals 2 and 3 of TB105 to the projector. This actuates the solid state timer circuits shown in Figure 41. The timer is equipped with speed control to set the display time at .5 seconds viewing and .5 seconds dark. With the timer triggering at the proper speed, a cam operated switch on the projector's main shaft energizes K19 (Figure 40) at the proper time to pulse the 80 position selector switch. Random code wiring to the six identification push buttons then feed out to the flip-flop latching relay K20 which alternately selects either K21 or K22. When a correct identification is made, one of these two is energized and holds through its holding circuit for 2 seconds. If a second correct identification is made in sequence, K20 will have switched over to the other relay, and it will be energized along with the first. The contacts of K21 B and K22 B are wired in series so that when both are closed (indicating two correct identifications in sequence), a 24v pulse will be fed to terminal #1 of

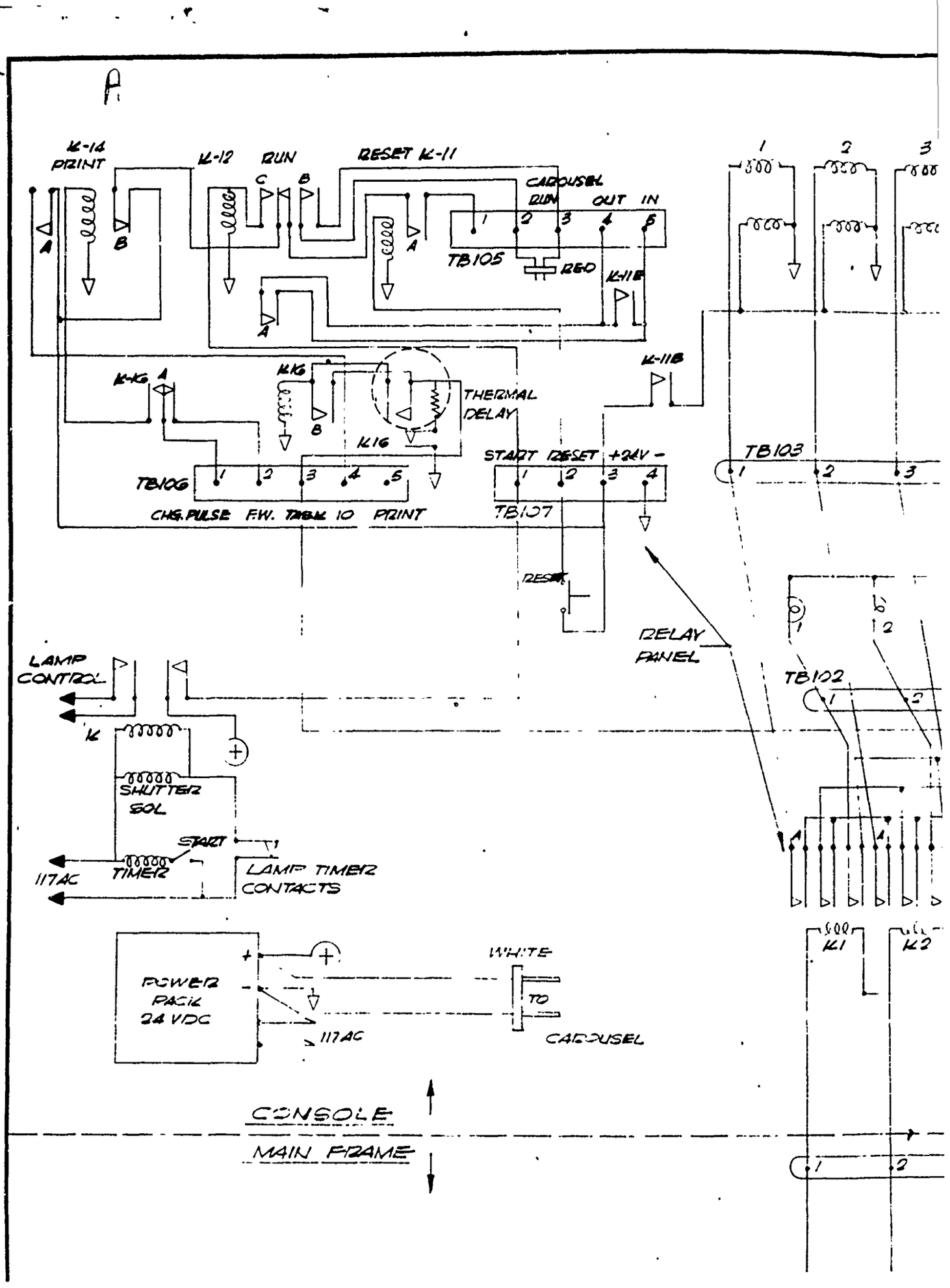
A
K-14
PRINT
K-12
RUN
RESET K-11
CAROUSEL
RUN
OUT
IN
TB105
RED
K-11B
K-16 A
K16
THERMAL
DELAY
K-11B
TB106
CHG. PULSE F.W. TRIG. IO PRINT
START
RESET
+24V -
TB107
TB103
RESET
RELAY
PANEL
TB102
LAMP
CONTROL
K
SHUTTER
SOL
START
TIMER
117AC
LAMP TIMER
CONTACTS
POWER
PACK
24 VDC
117AC
WHITE
TO
CAROUSEL
K1
K2
CONSOLE
MAIN FRAME

12

TASK CLOCKS

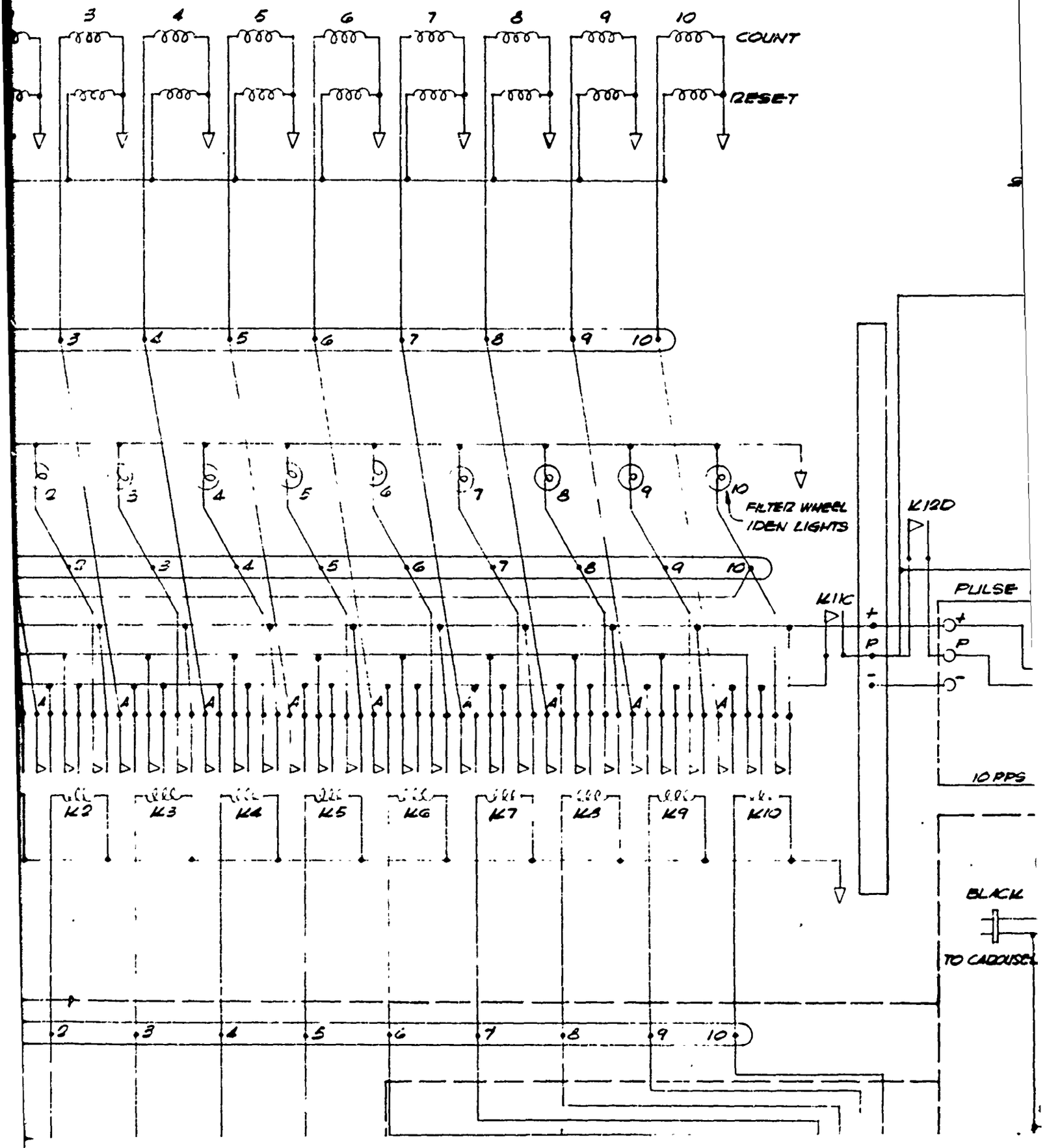

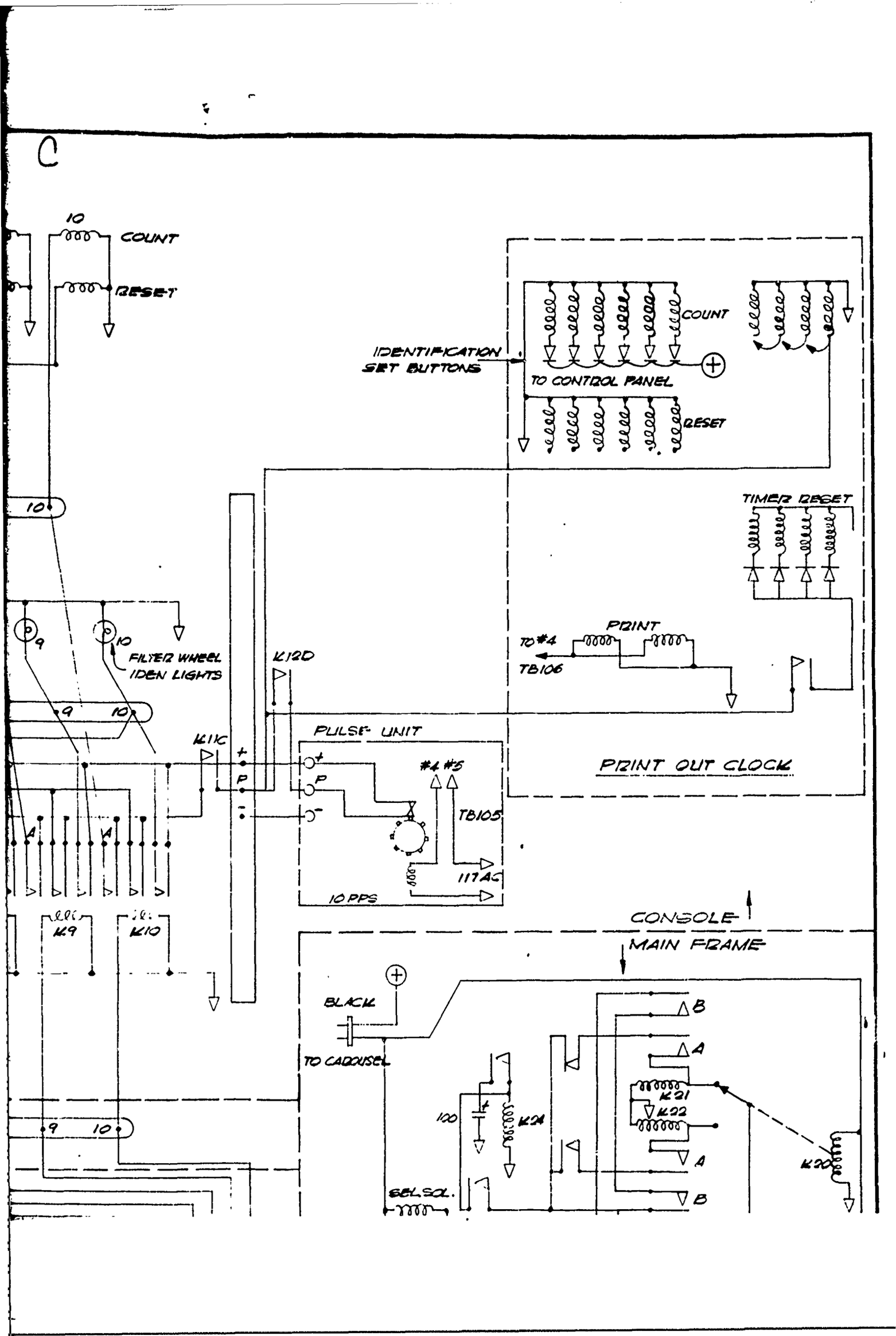
C
10
COUNT
RESET
IDENTIFICATION SET BUTTONS
COUNT
TO CONTROL PANEL
RESET
TIMER RESET
PRINT
TO #4
TB106
PRINT OUT CLOCK
9
10
FILTER WHEEL IDEN LIGHTS
K12D
K11C
PULSE UNIT
#4 #5
TB105
117AC
10 PPS
K9
K10
CONSOLE
MAIN FRAME
BLACK
TO CAROUSEL
100
K21
K22
K20
SELSOL.
A
B

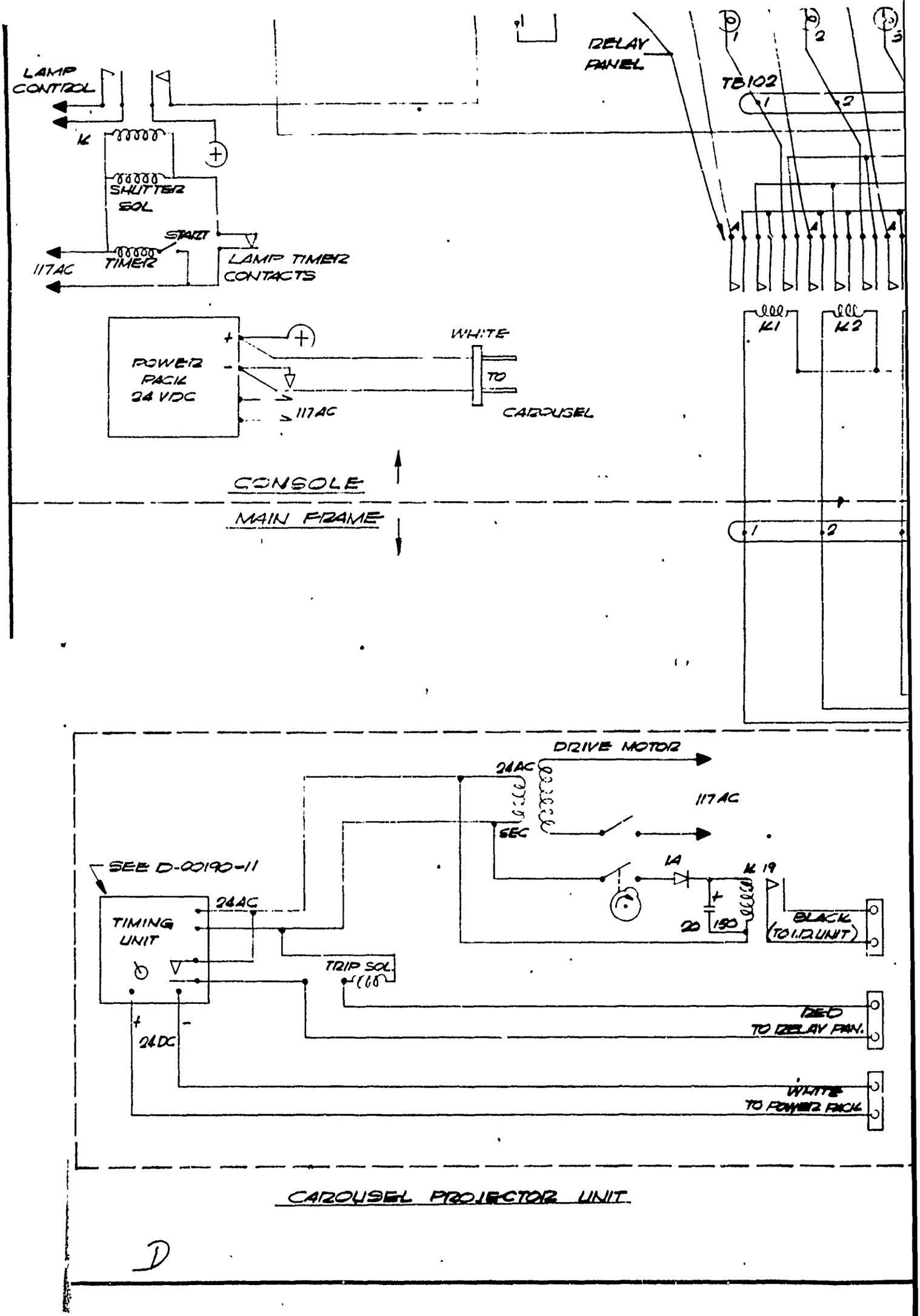

CAROUSEL PROJECTOR UNIT

D

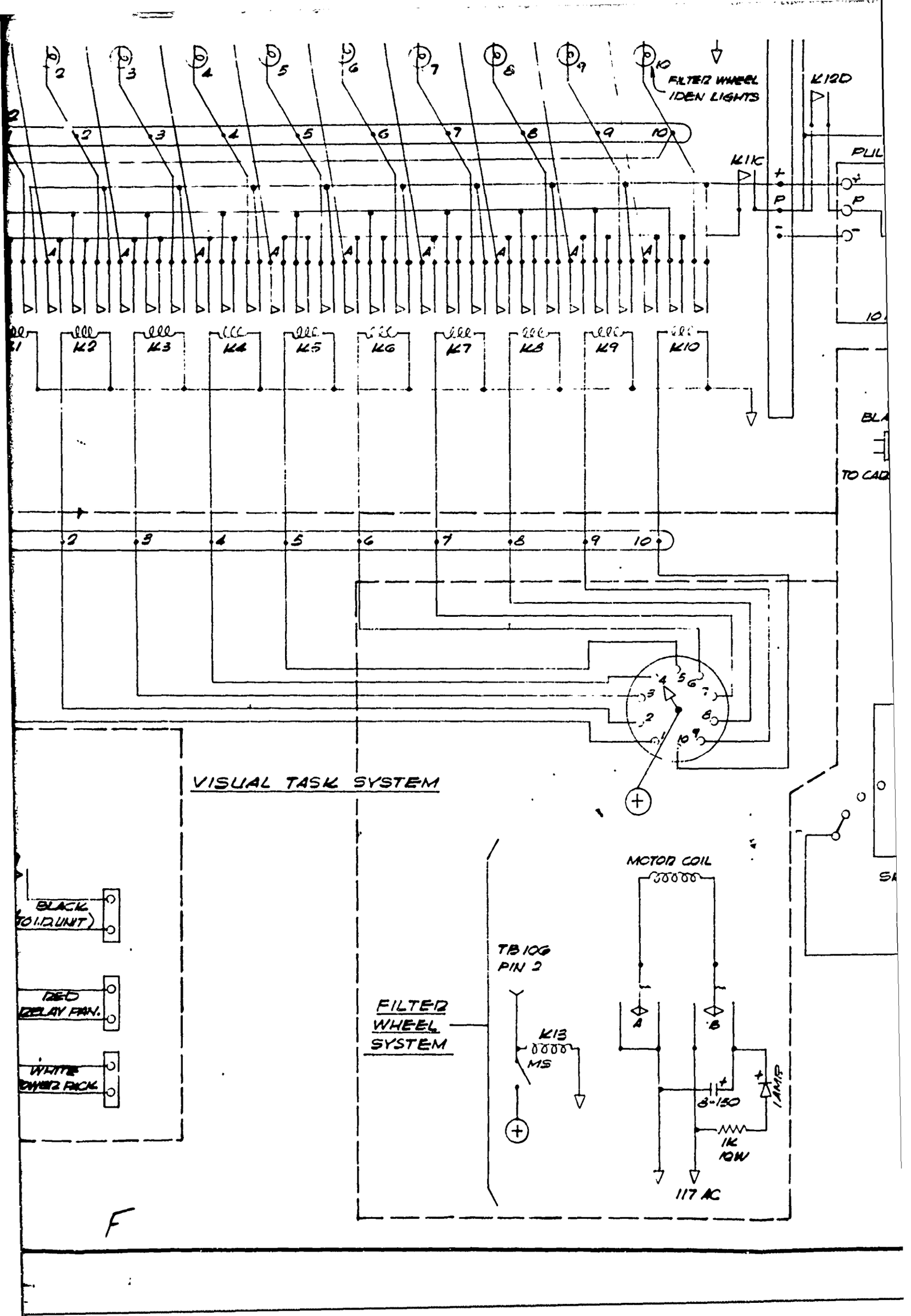
FILTER WHEEL IDEN LIGHTS
K12D
K11C
K1
K2
K3
K4
K5
K6
K7
K8
K9
K10
TO CAR
VISUAL TASK SYSTEM
BLACK (TO I.D. UNIT)
RED (DELAY PAN.)
WHITE (PWR PACK)
FILTER WHEEL SYSTEM
TB 10G PIN 2
K13
MS
MOTOR COIL
A
B
8-150
1AMP
1K 10W
117 AC

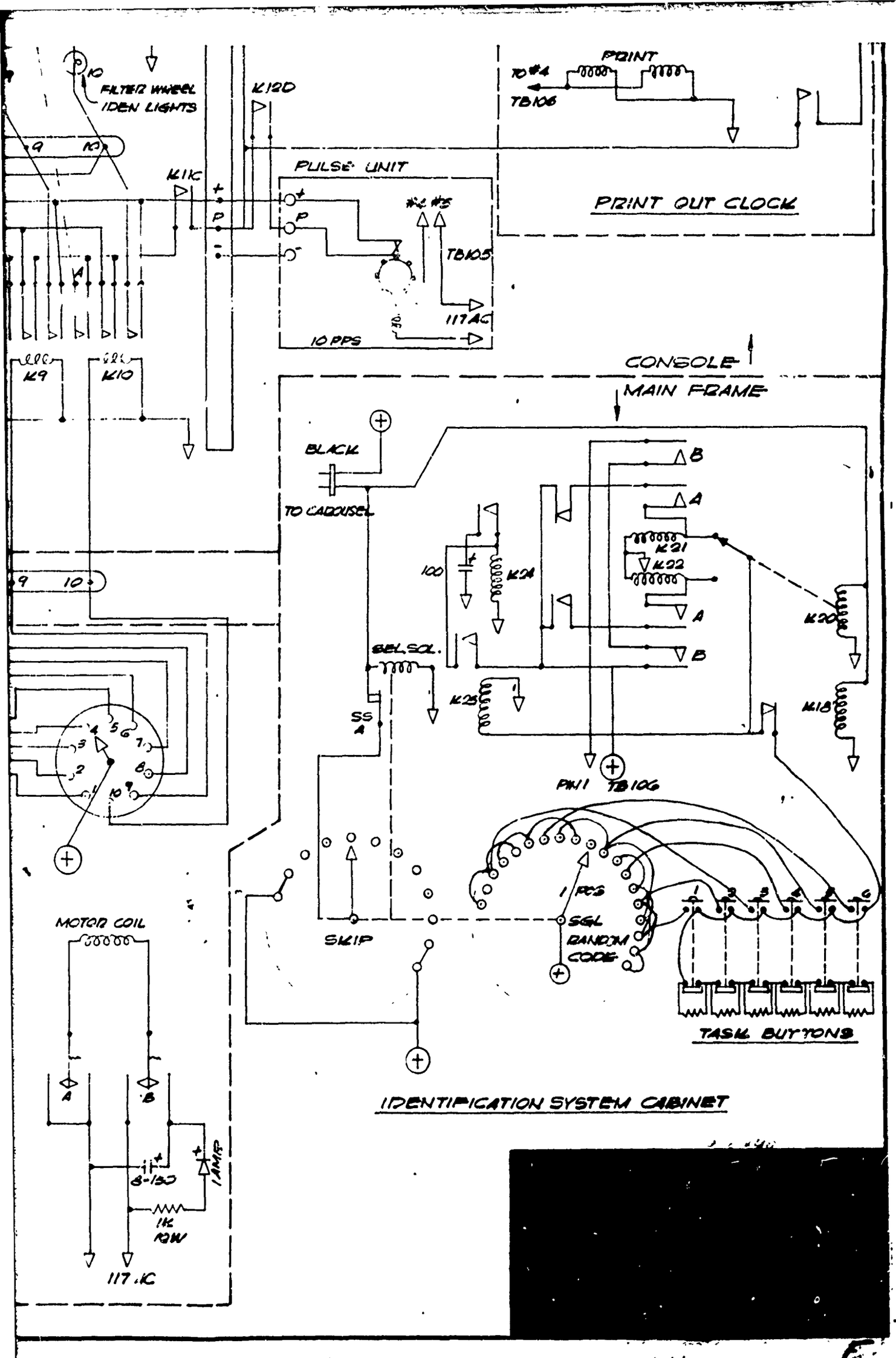
FILTER WHEEL IDEN LIGHTS
K12D
PRINT
TO #4
TB106
PRINT OUT CLOCK
PULSE UNIT
K11C
TB105
117 AC
10 PPS
K9
K10
CONSOLE
MAIN FRAME
BLACK
TO CAROUSEL
K21
K22
K20
K24
100
SEL SOL.
K25
K18
SS A
PIN 1 TB106
1 PPS
SGL RANDOM CODE
SKIP
TASK BUTTONS
MOTOR COIL
B-150
1 AMP
1K 10W
117 AC
IDENTIFICATION SYSTEM CABINET

[redacted]

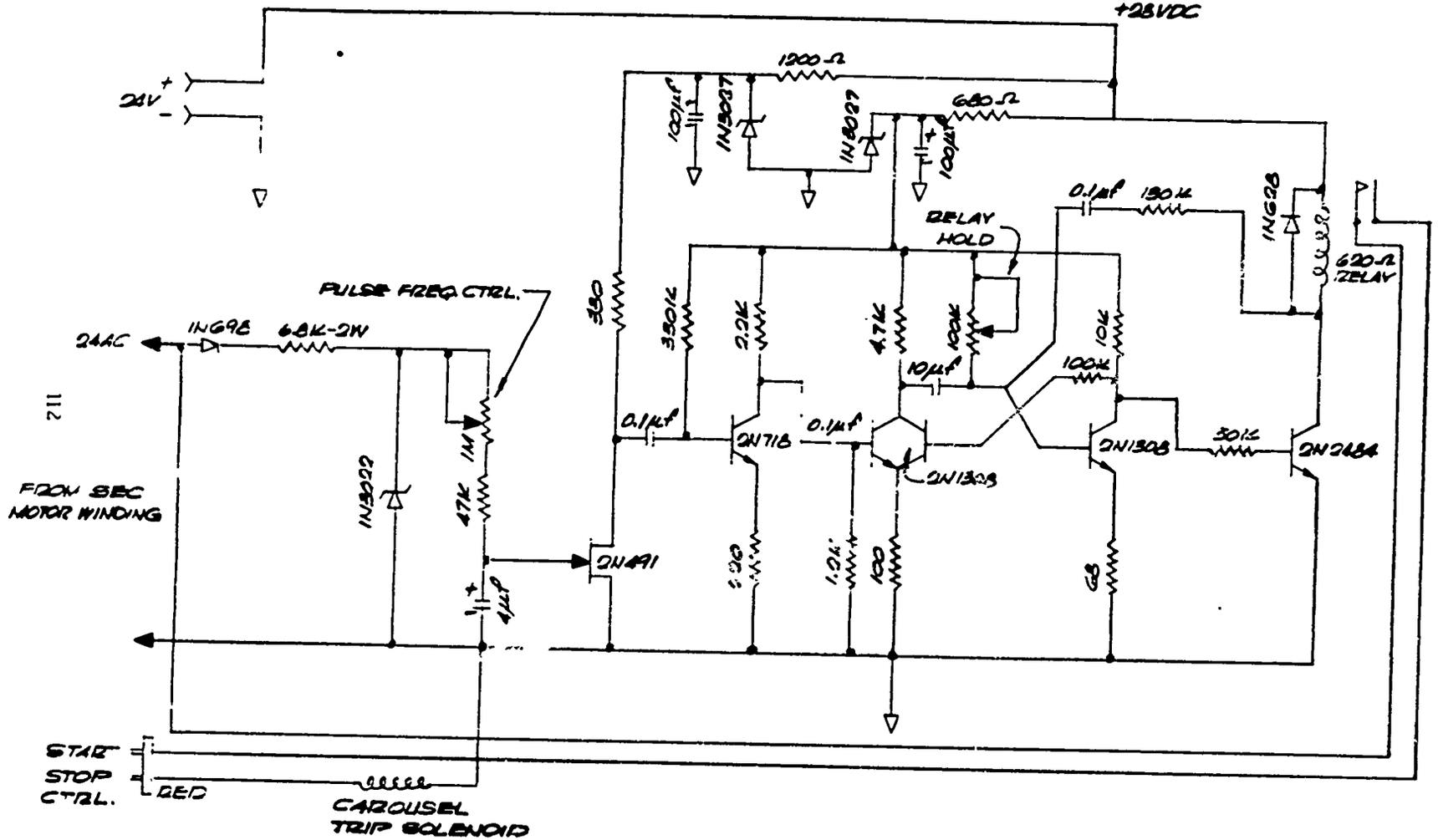

Figure 41

Carousel Timing & Control System

TB106 on the main relay panel. Then, as long as the test has not reached the tenth or final luminance position, this pulse will feed back out the #2 terminal of TB106 to energize K13 in the filter wheel box. K13 A and B will transfer, applying 117 AC to the filter wheel drive motor. As the filter wheel starts to turn, the microswitch on the main shaft closes and holds power on the drive motor until a cycle has been completed. When the microswitch opens, it drops out K13 and the normally closed contacts apply approximately 8 volts of DC to the motor coil to act as a brake to stop any coasting action. The filter wheel is thus pulsed until all ten positions have been presented to the subject. A ten position rotary contact shown above the filter wheel motor coil feeds 24 volts AC to relays 1 through 10 successively. At each position of the switch, the proper relay is energized to both apply a 10-cycle-per-second-24 DC pulse to the proper task counter; the total timer, and to light an identification lamp on the panel to show the filter position. After the completion of the ninth task, the filter wheel will move to the 10th position and its control circuit will be shifted as follows: 24v DC from the position 10 relay energizes the Delay Relay K17 which, in approximately one second, picks up the Shift Relay K16 which holds up as long as the filter wheel is in the 10th position. Contacts K16 A transfer so that when a sequence of two correct identifications occur, this pulse energizes the Stop-Print Relay K14. K14 B drops out the Run Relay K12, opening all pulse and timing circuits. K14A energizes the

print magnets in the main clock timer to print out the total elapsed time.

3. ENERGY CALIBRATION AND MONITORING

The calibration of the light sources is accomplished by comparison with a National Bureau of Standards, GE DXW-120v 1000w tungsten-filament, quartz-iodide envelope lamp, at a distance of 50 cm from a Jarrel-Ash 0.25 meter Ebert Monochromator. The exit slit width of the monochromator was set at 1.0 mm which provided a 3.3 nm bandwidth and an adequate signal for the photomultipliers. Two photomultipliers were used in the calibration. An RCA 1P28 whose maximum sensitivity was at 3000A and an RCA 7102 which had a maximum at 8000A. Thus, it was possible to cover the visible spectrum with some overlap. Voltage readings were taken with an Epsco digital voltmeter.

Careful measurements were taken at 50 nm intervals from 350 nm to 800 nm. The N.B.S. standard lamp was then replaced with the tungsten ribbon filament lamp and the measurements repeated. The ratio of the unknown lamp voltage V_x to the standard lamp voltage V_s times the calibration factor H (λ) and the relative photopic spectral sensitivity V (λ) of the eye for each of the intervals were summed. The result was multiplied by 680 watt and divided by the original calibrations of the N.B.S. standard. This figure represents the number of lumens/sr

being emitted by the unknown lamp. Dividing the result by the area of the test source gives the number of candles being emitted per unit area A_x of the unknown filament; i.e., the luminance. In mathematical notation, the above calibration would be:

$$L = \frac{680}{A_x W_s} \int_{350}^{700} \frac{V_x}{V_s} \cdot H(\lambda) \cdot V(\lambda)\, d\lambda$$

The measured luminance of five 108W bulbs operated at 18.0 amps was 1187 cd/cm^2 with a variation of less than 5% in the measured values.

4. PRELIMINARY DATA

Preliminary data has been taken in an experiment whose primary purpose was to check out the test equipment. The test consisted of exposing the eye for 10 seconds to a tungsten ribbon filament lamp in maxwellian view. The intensity of the lamp was reduced by various inconel neutral density filters. The time required by two subjects to identify letters subtending 45 minutes of arc was measured for various luminances of the target. The equipment proved to be reliable and adequate for testing small differences in flash exposures.

5. REFERENCES

1. Buettner, K., and H. W. Rose. Eye Hazards from an Atomic Bomb. Sight Saving Rev. 23, 1. 1953.

2. Whiteside, T. C. D., The Observation and Luminance of a Nuclear Explosion. Air Ministry Flying Personnel Research Committee. FPRC 1075.1. March, 1960.

3. Ham, W. T., et. al. Flash Burns in the Rabbit Retina as a Means of Evaluating the Retinal Hazards from Nuclear Weapons. USAF School of Aviation Medicine. Contract AF18(600)-1272, 1958.

4. Chisum G. T., and H. H. Hill. Flashblindness Recovery Time Following Exposure to High Intensity, Short Duration Flashes. U.S. Naval Air Development Center, NADC-MA-6142, November, 1961.

5. Brown, J. L. Flashblindness. Am. J. Ophth. 60/3 505-520. September, 1965.

6. Metcalf, R. D. and R. E. Horn. Visual Recovery Times from High Intensity Flashes of Light. WADC Technical Report 58-232, October, 1958.

7. Miller, N. D. Visual Recovery from Brief Exposures to Very High Luminance Levals. USAF Schooi of Aerospace Medicine SAM-TDR-64-36, August, 1964.

APPENDIX A

DESCRIPTION OF COMPONENTS

The components necessary for operation and calibration of the system (Figure 1) are listed below:

For Operation

Manufacturer	Equipment
Tektronix, Incorporated	Waveform Generator, Type 162
	Power Supply Type 160A
	Two pulse generators, Type 161
Carl Zeiss	Coagulator
Beckman Instruments, Inc.	Eput / Timer, Model 6144
Kepco, Incorporated	Power Supply, Type KM255
Lambda Electronics Corp.	Power Supply, Model 150
Technology Incorporated	Capacitor bank
	D. C. contactor
	Sequential control
	SCR pulse switch
Keeler Optical Products, Inc.	Ophthalmoscope, modified by addition of a control handle and moveable mirror

For Calibration

Manufacturer	Equipment
Edgerton, Germeshausen & Grier, Incorporated	Photodiode SD-100
Tektronix, Incorporated	Oscilloscope, Type 551
	Oscilloscope Camera, Type C-12
Eppley Laboratory, Inc.	16 Junction Bismuth-silver thermopile
Hewlett-Packard	D.C. VTVM, Model 412A

Power Requirements

External power: (a) 115 VAC, single phase, 30 amperes

(b) 240 VAC, 3 phase Wye, 60 amperes and

(c) Aircraft nickel - cadmium batteries (8), 48 V DC, 200 amperes.

APPENDIX B

TABLES

TABLE I-B

Irradiance as a Function of Sampling Position for the

6.20° Cone of the Zeiss Coagulator

Vertical		Horizontal		Vertical		Horizontal	
Position*	H†	Position*	H†	Position*	H†	Position*	H†
-47	.18	-47	.21	+ 8	1.02	+ 2	.98
-44	.85	-43	.32	+12	1.02	+ 5	.98
-39	1.00	-40	.43	+16	1.04	+ 9	.98
-35	1.02	-34	.68	+20	1.04	+12	.93
-31	1.02	-30	.75	+24	1.07	+15	.86
-27	1.02	-27	.80	+28	1.07	+18	.77
-23	1.02	-24	.80	+32	1.09	+22	.71
-19	1.00	-21	.80	+36	1.11	+25	.69
-15	.99	-17	.93	+40	1.18	+28	.54
-11	.99	-14	.96	+44	1.18	+31	.45
- 7	.99	-11	.98	+48	1.18	+38	.25
- 3	1.00	- 8	.98	+50	.14	+44	.14
0	1.00	- 4	1.00			+48	.07
+ 4	1.00	- 1	1.00				

*Arbitrary units

†Relative to center of beam

TABLE II-B

Irradiance as a Function of Sampling Position for the 3.07° Cone of the Zeiss Photocoagulator

Vertical		Horizontal	
Position*	H†	Position*	H†
-44	.07	-49	0.10
-43	.47	-44	.73
-36	.88	-38	.79
-29	.91	-32	.83
-22	.91	-26	.5
-15	.93	-20	.89
-8	.93	-14	.90
-1	.99	-8	.96
+4	.99	-1	1.00
+13	.95	+5	1.00
+19	.98	+11	.98
+26	.98	+17	.96
+33	.98	+23	.94
+40	1.00	+29	.90
+47	.75	+35	.87
+49	.70	+41	.83
		+47	.77

*Arbitrary units

†Relative to center of beam

TABLE III-B

Retinal Irradiance for the Production of 5 Minute Minimal Burns in Rabbits

A. 6.20° light cone angle (1.08 mm calculated image diameter)

H_r (cal/cm^2-sec)

Rabbit	Exposure Time (msec)						
No.	.165	.400	1	10	40	100	250
G-79			242		10.5		4.80
Q-15			211			7.73	5.00
N-03			211			9.88	5.40
L-78			176			8.45	6.11
Q-21		328		41.7		8.99	5.32
Q-39	1010	302		32.6		7.40	4.38
Q-43	590	324		33.6		9.52	5.78
S-96		374		36.5		8.66	5.27
T-16		367		39.6	15.4	8.81	5.37
T-18	797	287		37.7		8.05	4.76
6C-3L					14.42		
6C-3R					14.95		
5B-8					13.56	7.01	5.05
5C-9				36.1	13.89	7.09	4.85
$\bar{H}_r$	799	330	210	36.8	13.8	8.33	5.17
$\sigma(H_r)$	210	34.6	27.0	3.19	1.75	0.96	0.47
$\bar{Q}_r$	0.13	0.13	0.21	0.37	0.55	0.83	1.29

TABLE IV-B

Retinal Irradiance for the Production of 5 Minute Minimal Burns in Rabbits

B. 3.07° light cone angle (0.54 mm calculated image diameter)

H_r (cal/cm^2-sec)

Rabbit	Exposure Time (msec)						
No.	.165	.400	1	10	40	100	250
G-79			306		15.8		8.43
P-97		482	179	27.9	12.0	5.78	5.78
Q-15			220	54.9		10.6	7.73
N-03			219			12.2	7.16
L-78						12.4	9.70
Q-21		454		49.6		10.5	7.60
Q-39	86[a]					8.66	6.25
Q-43	760	380		47.3		12.0	8.12
S-96		483		57.0		10.9	7.40
T-16		506		58.0	19.6	9.97	6.36
T-18		313		58.9		11.9	8.05
$\bar{H}_r$	815	436	231	50.2	15.8	10.5	7.51
$\sigma(H_r)$	77.1	74.6	53.5	10.8	3.8	2.02	1.11
$\bar{Q}_r$	0.13	0.17	0.23	0.50	0.63	1.05	1.88

TABLE V-B

Retinal Irradiance for the Production of 5 Minute Minimal Burns in Rabbits

C. 1.47° light cone angle (0.26 mm calculated image diameter)

H_r (cal/cm^2-sec)

Rabbit	Exposure Time (msec)						
No.	.165	.400	1	10	40	100	250
G-79		979	357	70.8	28.9	18.2	12.1
G-79			363				13.9
P-97		564	190	41.7	18.2	9.5	6.9
Q-15			220			21.4	16.7
N-03			534		54.8	29.0	22.0
Q-21	792	429		55.6		16.6	15.0
Q-39	603	292		46.9	25.4	16.2	13.7
Q-43		502		41.8	27.5	23.1	18.2
Q-43						21.8	
S-96		376		63.2	30.0	26.8	20.2
T-16		473		71.9	34.1	24.6	21.5
T-18	603	268		44.1	25.1	19.8	16.9
K-37		520				22.8	
M-10		537		63.2	30.6		21.3
Q-23	952	593		76.1	36.0		
Q-27						24.7	22.7
Q-17				55.7	39.3	29.2	
Q-47						31.0	
Q-51						37.8	
$\bar{H}_r$	738	503	333	57.4	31.8	23.3	17.0
$\sigma(H_r)$	168.5	190.3	137.0	12.6	9.54	6.74	4.64
$\bar{Q}_r$	0.12	0.20	0.33	0.57	1.28	2.33	4.25

TABLE VI-B

Retinal Irradiance for the Production of 5 Minute Minimal Burns in Rabbits

D. 1.05° light cone angle (0.18 mm calculated image diameter)

H_r (cal/cm^2-sec)

Rabbit	Exposure Time (msec)						
No.	.165	.400	1	10	40	100	250
G-79			697		41.0		31.4
P-97			211	70.0	25.5	18.2	15.0
Q-15			239			49.0	65.0
Q-21		808		74.3		30.3	23.5
Q-21		676					
Q-39	670	365		64.8	39.1	28.5	25.4
Q-43		584		48.4	30.9	27.5	21.8
S-96		820		99.7	45.4	33.6	30.0
T-16		753		91.7	41.4	34.1	27.4
T-18	1090	831		79.1	31.2	22.4	22.4
$\bar{H}_r$	880	691	382	75.4	36.4	30.5	29.1
$\sigma(H_r)$	297	169	273	17.0	7.19	9.22	14.3
$\bar{Q}_r$	.15	.28	.38	.75	1.46	3.05	7.28

TABLE VII-B

Retinal Irradiance for the Production of 5 Minute Minimal Burns in Rabbits

E. 0.52° light cone angle (0.09 mm calculated image diameter)

H_r (cal/cm^2-sec)

Rabbit	Exposure Time (msec)							
No.	.165	.400	1	4	10	40	100	250
G-79						102		65
P-97						76	80	70
P-97						130		
Q-21					181		150	103
Q-21					177		76	55
Q-39		1160			173	89	74	69
Q-43		1150				87	68	48
S-9[illegible]						190	94	84
T-16						155	108	92
T-18					376	216	109	79
Q-93		1010	726	431	230	131	117	
Q-93		1110	619	447	222	119	89	
R-03		883	740	411	230	117	90	59
R-03	1030	985	490	423	209	85	63	50
R-17	1150	1240	486	472	217	105	82	62
R-17	1330	1110	690	438	275	142	93	78
R-31	1240	1280	666		343	201	149	126
R-31	1280							98
W-07	1610							
W-07	1610							116
6B-0				404	218.3	121.6	94.4	74
$\bar{H}_r$	1321	1100	645	432	238	129	96	79
$\sigma(H_r)$	219.6	125.8	87.8	22.98	63.74	42.29	25.53	21.80
$\bar{Q}_r$	.218	.440	.645	1.75	2.39	5.16	9.60	19.8

TABLE VIII-B

Retinal Irradiance for the Production of 5 Minute Minimal Burns in Rabbits

F. 0.45° light cone angle (0.067 mm calculated image diameter)

H_r (cal/cm^2-sec)

Rabbit	Exposure Time (msec)					
No.	4	10	20	40	100	250
9B1				122	103	88
8E8L	426	258	172	134	101	88
8E8R	418	258	172	134	92	85
9E0R	421	261	177	124	99	93
9E0L	421	261	182	124	102	90
9E4R	426	256	183	126	99	93
9E4L	426	261	187	126	99	90
5C7R	426	251	179	126	89	84
5C7L	434	251	184	126	93	84
9J4L	426	257	189	122	100	88
9J4R	426	257	184	126	93	84
$\bar{H}_r$	425	257	181	126	97	88
$\sigma(H_r)$	$\pm$3.56	$\pm$3.56	$\pm$5.92	$\pm$3.99	$\pm$4.64	$\pm$3.50
$\bar{Q}_r$	1.70	2.57	3.62	5.05	9.74	21.98

TABLE IX-B

Retinal Irradiance for the Production of 5 Minute Minimal Burns in Rabbits

G. 0.33° light cone angle (0.053 mm calculated image diameter)

H_r (cal/cm^2-sec)

Rabbit	Exposure Time (msec)						
No.	1	4	10	20	40	100	250
6B8			329	268	187	131	102
7B8	1230	424	315	270	196	131	103
7B8	1270	440	278	234	169	130	110
1A1	1230	440	278	234	180	130	100
1A1	1270	440	264	247	190	130	110
6B0		431	298	250	186	129	101
7B0		434	302	250	186	132	115
7B0		450	313	273	196	132	124
7B2		451	279	279	192	139	117
7B2		438	266	279	181	129	107
6B2		466	290	263	190	134	116
6B2		455	290	261	196	139	114
$\bar{H}_r$	1250	442	292	259	187	132	110
$\sigma(H_r)$	23.1	11.9	20.2	15.9	7.95	3.49	7.54
$\bar{Q}_r$	1.25	1.77	2.92	5.18	7.52	13.2	27.5

TABLE X-B

Retinal Irradiance for the Production of 5 Minute Minimal Burns in Rabbits

	6.2° cone angle (1.08 mm image diam.)			3.1° cone angle (0.54 mm image diam.)		
Rabbit No.	Exposure Time (sec) 1	4	10	1	4	10
S-15	4.05	3.36	2.78	8.01	7.15	6.28
X-18	4.45	3.11	2.55	7.00	5.25	4.59
S-25	4.13	3.43	3.01	7.70	6.79	6.42
S-23R	4.13	3.48	2.29	6.79	5.80	5.16
S-23L	4.17	3.38	2.29	6.79	5.80	5.16
S-79	4.35	3.30	2.71	7.40	6.00	5.15
S-51	3.67	3.34	2.78	6.59	5.99	5.30
S-35	3.28	2.61	2.07	5.88	4.95	4.22
S-17	3.49	2.59	2.01			
S-43				6.27	4.90	4.07
OA-1	3.26	2.43	2.43	5.85	4.62	3.84
5B-8	4.01	3.11	2.47	5.76	5.58	4.70
OA-7				7.14	4.79	4.30
$\bar{H}_r$	3.91	3.10	2.49	6.77	5.64	4.93
$\sigma(H_r)$	0.42	0.38	0.31	0.734	0.789	0.816
$\bar{Q}_r$	3.91	12.4	24.9	6.77	22.6	49.3

TABLE XI-B

Retinal Irradiance for the Production of 5 Minute Minimal Burns in Rabbits

1.05° cone angle (0.18 mm image diameter)

Rabbit	Exposure Time (sec)				
No.	1	4	10	30	100
S-15	24.9	22.5	21.2		
X-18	23.2	20.5	18.3		
S-25	21.1	18.2	18.3		
S-79	23.2	20.2	18.9		
S-51	24.5	22.2	23.4		
S-35	21.8	19.8	20.3	20.7	20.7
S-43	21.6	17.9	17.9	18.0	18.0
S-17	21.1	17.9	16.8	17.1	17.1
OA-7	20.68	19.17	17.40	17.70	17.76
OA-1	21.73	18.47	16.91	16.05	16.05
5B-8	23.02	20.72	18.81	17.78	17.78
$\bar{H}_r$	22.4	19.8	18.9	17.9	17.9
$\sigma(H_r)$	1.42	1.63	2.00	1.55	1.55
$\bar{Q}_r$	22.4	79.2	189	539	1790

TABLE XII-B

Retinal Irradiance for the Production of 5 Minute Minimal Burns in Rabbits

	1.47° cone angle (0.26 mm image diam.)			0.52° cone angle (0.09 mm image diam.)		
Rabbit No.	Exposure Time (sec) 1	4	10	1	4	10
S-15	17.8	17.5	16.8	68.6	68.9	68.3
X-18	16.6	13.7	13.2	69.5	60.3	57.7
S-25	16.6	14.2	14.4			
S-23	15.1	12.6	11.3	68.9	66.1	64.9
S-79	16.7	16.0	14.8	69.7	71.1	69.2
S-51	17.6	14.5	15.2	67.1	64.7	68.8
S-35	17.0	15.7	14.6	68.9	64.0	61.4
S-43	14.0	12.7	11.4	69.0	59.1	57.6
S-17	13.8	12.7	11.4	67.44	62.64	58.88
OA-7	15.92	13.86	12.45	65.50	60.37	58.52
OA-1	15.56	13.26	12.01			
5B-8	16.66	14.86	13.47	69.57	63.37	61.44
$\overline{H}_r$	16.1	14.3	13.4	68.4	64.1	62.1
$\sigma(H_r)$	1.28	1.51	1.77	1.34	3.83	4.85
$\overline{Q}_r$	15.1	57.2	134	68.4	256	62.1

TABLE XIII-B

Calculated Constants for the Equations for Threshold Retinal Irradiance Versus Time ($\bar{H}_r = At^B + C$)

Cone	A(cal/cm^2-sec^{B+1})	B	C(cal/cm^2-sec)
1. 6.20°	0.91	-0.770	2.68
2. 3.07°	0.96	-0.783	5.01
3. 1.47°	1.68	-0.733	12.79
4. 1.05°	1.98	-0.736	18.57
5. 0.52°	11.6	-0.566	55.24
6. 0.45°	12.3	-0.591	63.39
7. 0.33°	17.8	-0.559	73.86

t = sec

TABLE XIV-B

Laser Exposure Thresholds

Retinal Exposure, Q_r, J/cm^2

Retinal Image Diameter mm	Trial Number 1	2	3	4	5	6	7	8	9	Q_r	σ
1.0	1.57	1.48	1.3	1.18	1.85	1.75	1.15	1.46	2.11	1.54	.285
0.53	1.65	1.65	1.63	1.49	1.10	2.36	2.46	1.55		1.73	.465
0.26	1.65	1.58	1.54	1.54	1.72	2.15				1.69	.228
0.10	1.56	2.46	1.67	1.79	1.56					1.81	.40

TABLE XV-B

Laser Irradiance Thresholds

Retinal Irradiance, H_r, $\frac{cal}{cm^2\text{-}sec}$

Retinal Image Diameter mm	Trial Number 1	2	3	4	5	6	7	8	9	$\bar{H}_r$	σ
1.0	196	185	163	147	232	218	144	184	264	192.5	37.1
0.57	205	205	204	106	140	294	309	194		216.5	57
0.26	205	198	192	192	215	240				212	28.5
0.10	195	310	209	222	194					227	49.4

UNCLASSIFIED
Security Classification

DOCUMENT CONTROL DATA - R&D

(Security classification of title, body of abstract and indexing annotation must be entered when the overall report is classified)

1. ORIGINATING ACTIVITY (Corporate author)	2a. REPORT SECURITY CLASSIFICATION
Technology Inc 8531 No. New Braunfels Ave. San Antonio, Texas 78209	UNCLASSIFIED 2b GROUP

3. REPORT TITLE

Research on Ocular Effects Produced by Thermal Radiation

4. DESCRIPTIVE NOTES (Type of report and inclusive dates)

Final Report - July 1966 - June 1967

5. AUTHOR(S) (Last name, first name, initial)

Allen, R. G. Jr., Bruce, W. R., Kay, K. R., Morrison, L. K., Neish, R. A. Polaski, C. A., Richards, R. A.

6. REPORT DATE	7a. TOTAL NO. OF PAGES	7b. NO. OF REFS
July 1967	134	22

8a. CONTRACT OR GRANT NO.	9a. ORIGINATOR'S REPORT NUMBER(S)
AF41(609)-3099 b. PROJECT NO. 6301 Task 630103 c. Work Unit 6301 03 023 d.	9b. OTHER REPORT NO(S) (Any other numbers that may be assigned this report)

10. AVAILABILITY/LIMITATION NOTICES

Distribution of this document is unlimited

11. SUPPLEMENTARY NOTES	12. SPONSORING MILITARY ACTIVITY
	Defense Atomic Support Agency Washington D. C. 20305

13. ABSTRACT

Chorioretinal burn thresholds for rabbits have been determined for 66 various combinations of exposure durations and retinal image diameters. The criterion for burn damage was the appearance of an ophthalmoscopically visible lesion 5 minutes after the flash exposure. Exposure durations ranged from 165 μsec to 100 sec and the range of image diameters was from 0.053 mm to 1.08 mm. The thresholds were based on an average of 9 eyes per condition.

The same Zeiss photocoagulator that was used in the rabbit burn study was used for determining burn thresholds for rhesus monkeys. Exposure durations from 4 to 250 msec and image diameters from 0.11 to 1.30 mm were employed for the threshold determinations. Fluorescein angiographs were investigated as a means for the detection of chorioretinal damage below the level of the ophthalmoscopically visible lesion. In an area of moderate damage there is rapid fluorescence which was interpreted to be the result of an increase in capillary permeability.

Two new pieces of apparatus were constructed for research on the ocular effects from high intensity visible radiation. A ruby laser was adapted for further studies on chorioretinal burns in rabbits and primates. And a flashblindness testing apparatus for measuring visual recovery times for human subjects has been constructed and tested.

DD FORM 1 JAN 64 1473

UNCLASSIFIED
Security Classification

UNCLASSIFIED
Security Classification

14. KEY WORDS	LINK A		LINK B		LINK C	
	ROLE	WT	ROLE	WT	ROLE	WT
Vision Flashblindness Retinal burns Laser system Fluorescein angiography						

INSTRUCTIONS

1. ORIGINATING ACTIVITY: Enter the name and address of the contractor, subcontractor, grantee, Department of Defense activity or other organization *(corporate author)* issuing the report.

2a. REPORT SECURITY CLASSIFICATION: Enter the overall security classification of the report. Indicate whether "Restricted Data" is included. Marking is to be in accordance with appropriate security regulations.

2b. GROUP: Automatic downgrading is specified in DoD Directive 5200.10 and Armed Forces Industrial Manual. Enter the group number. Also, when applicable, show that optional markings have been used for Group 3 and Group 4 as authorized.

3. REPORT TITLE: Enter the complete report title in all capital letters. Titles in all cases should be unclassified. If a meaningful title cannot be selected without classification, show title classification in all capitals in parenthesis immediately following the title.

4. DESCRIPTIVE NOTES: If appropriate, enter the type of report, e.g., interim, progress, summary, annual, or final. Give the inclusive dates when a specific reporting period is covered.

5. AUTHOR(S): Enter the name(s) of author(s) as shown on or in the report. Enter last name, first name, middle initial. If military, show rank and branch of service. The name of the principal author is an absolute minimum requirement.

6. REPORT DATE: Enter the date of the report as day, month, year; or month, year. If more than one date appears on the report, use date of publication.

7a. TOTAL NUMBER OF PAGES: The total page count should follow normal pagination procedures, i.e., enter the number of pages containing information.

7b. NUMBER OF REFERENCES: Enter the total number of references cited in the report.

8a. CONTRACT OR GRANT NUMBER: If appropriate, enter the applicable number of the contract or grant under which the report was written.

8b, 8c, & 8d. PROJECT NUMBER: Enter the appropriate military department identification, such as project number, subproject number, system numbers, task number, etc.

9a. ORIGINATOR'S REPORT NUMBER(S): Enter the official report number by which the document will be identified and controlled by the originating activity. This number must be unique to this report.

9b. OTHER REPORT NUMBER(S): If the report has been assigned any other report numbers *(either by the originator or by the sponsor)*, also enter this number(s).

10. AVAILABILITY/LIMITATION NOTICES: Enter any limitations on further dissemination of the report, other than those imposed by security classification, using standard statements such as:

(1) "Qualified requesters may obtain copies of this report from DDC."

(2) "Foreign announcement and dissemination of this report by DDC is not authorized."

(3) "U. S. Government agencies may obtain copies of this report directly from DDC. Other qualified DDC users shall request through _____."

(4) "U. S. military agencies may obtain copies of this report directly from DDC. Other qualified users shall request through _____."

(5) "All distribution of this report is controlled. Qualified DDC users shall request through _____."

If the report has been furnished to the Office of Technical Services, Department of Commerce, for sale to the public, indicate this fact and enter the price, if known.

11. SUPPLEMENTARY NOTES: Use for additional explanatory notes.

12. SPONSORING MILITARY ACTIVITY: Enter the name of the departmental project office or laboratory sponsoring *(paying for)* the research and development. Include address.

13. ABSTRACT: Enter an abstract giving a brief and factual summary of the document indicative of the report, even though it may also appear elsewhere in the body of the technical report. If additional space is required, a continuation sheet shall be attached.

It is highly desirable that the abstract of classified reports be unclassified. Each paragraph of the abstract shall end with an indication of the military security classification of the information in the paragraph, represented as *(TS), (S), (C), or (U)*.

There is no limitation on the length of the abstract. However, the suggested length is from 150 to 225 words.

14. KEY WORDS: Key words are technically meaningful terms or short phrases that characterize a report and may be used as index entries for cataloging the report. Key words must be selected so that no security classification is required. Identifiers, such as equipment model designation, trade name, military project code name, geographic location, may be used as key words but will be followed by an indication of technical context. The assignment of links, rules, and weights is optional.

GPO 886-551

UNCLASSIFIED
Security Classification